RECLAMATION

Managing Water in the West

Hydraulic Laboratory Report HL-2015-01

Helix Design for Downstream Fish Passage at Cle Elum Dam

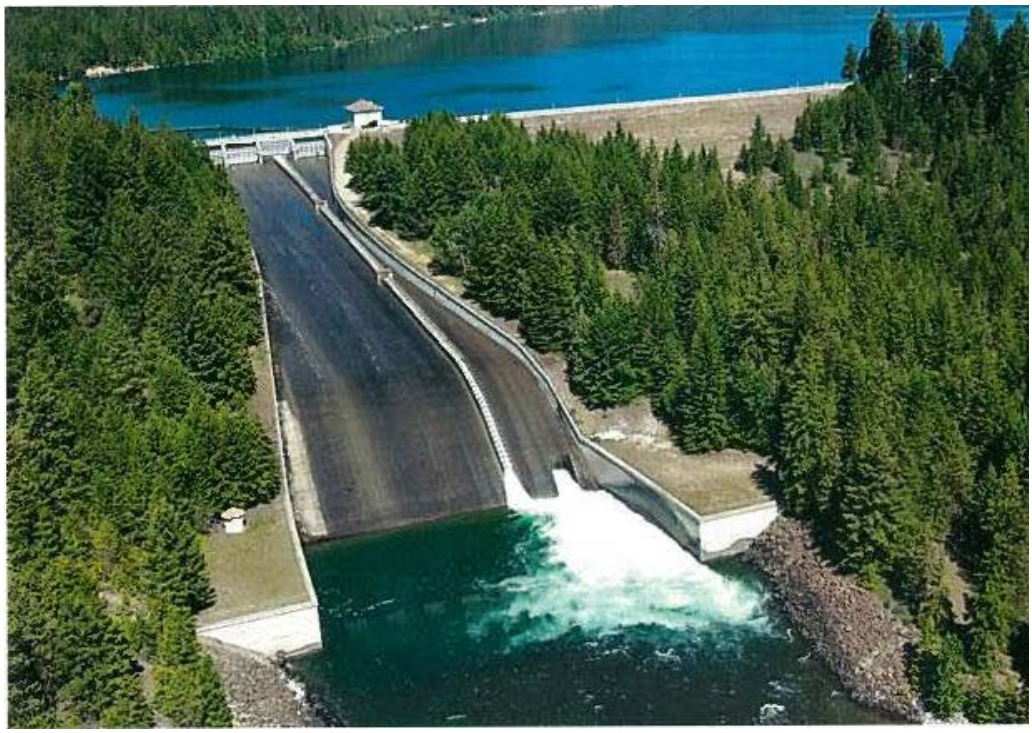

U.S. Department of the Interior
Bureau of Reclamation
Technical Service Center
Hydraulic Investigations and Laboratory Services Group
Denver, Colorado

April 2016

REPORT DOCUMENTATION PAGE

Form Approved
OMB No. 0704-0188

PLEASE DO NOT RETURN YOUR FORM TO THE ABOVE ADDRESS.

1. REPORT DATE *(DD-MM-YYYY)*	**2. REPORT TYPE**	**3. DATES COVERED** *(From - To)*
11-13-2015	Technical	May 2013 – Jan 2015

4. TITLE AND SUBTITLE

Helix Design for Downstream Fish Passage at Cle Elum Dam

5a. CONTRACT NUMBER

5b. GRANT NUMBER

5c. PROGRAM ELEMENT NUMBER

6. AUTHOR(S)
Leslie J. Hanna
Jim Higgs
Brent Mefford
Jason Wagner

5d. PROJECT NUMBER

5e. TASK NUMBER

5f. WORK UNIT NUMBER

7. PERFORMING ORGANIZATION NAME(S) AND ADDRESS(ES)
U.S. Dept. of the Interior, Bureau of Reclamation
Technical Service Center, 86-68460
Denver, CO 80225

8. PERFORMING ORGANIZATION REPORT NUMBER

HL-2012-01

9. SPONSORING/MONITORING AGENCY NAME(S) AND ADDRESS(ES)
U.S. Department of the Interior, Bureau of Reclamation
Research and Development Office, 86-69000
P.O. Box 25007
Denver, CO 80225

10. SPONSOR/MONITOR'S ACRONYM(S)

11. SPONSOR/MONITOR'S REPORT NUMBER(S)

12. DISTRIBUTION/AVAILABILITY STATEMENT
National Technical Information Service, 5285 Port Royal Road, Springfield, VA 22161
http://www.ntis.gov

13. SUPPLEMENTARY NOTES

14. ABSTRACT Reclamation's Hydraulics Laboratory in Denver, Colorado conducted numerical and physical hydraulic model studies to support development of a downstream fish passage system design for Cle Elum Dam. A helical open channel was used to extend the length and flatten the slope of the fishway. This report addresses only the development of the helix design and the components that help the flow to transition into and out of the helix. The purpose of this study was to determine helix and transition geometries that would provide optimal hydraulic conditions for continuous safe downstream juvenile fish passage. Both numerical and physical modeling were used to develop and refine the final design.

15. SUBJECT TERMS **Helix, downstream fish passage, hydraulic model, numerical model, high head dam, storage reaservoir fish passage**

16. SECURITY CLASSIFICATION OF:			**17. LIMITATION OF ABSTRACT**	**18. NUMBER OF PAGES**	**19a. NAME OF RESPONSIBLE PERSON**
REPORT	**ABSTRACT**	**THIS PAGE**			Robert F. Einhellig
UU	UU	UU	SAR	128	**19b. TELEPHONE NUMBER** *(Include area code)* 303-445-2142

Hydraulic Laboratory Report HL-2015-01

Helix Design for Downstream Fish Passage at Cle Elum Dam

Prepared by:

Leslie J. Hanna
Hydraulic Engineer, Hydraulic Investigations and Laboratory Services Group, 86-68460

Jim Higgs
Hydraulic Engineer, Hydraulic Investigations and Laboratory Services Group, 86-68460

Brent Mefford. P.E.
Hydraulic Engineer, Hydraulic Investigations and Laboratory Services Group, 86-68460

Jason Wagner. P.E.
Civil Engineer, Water Conveyance Group, 86-68140

Technical Approval:

Robert Einhellig, P.E., Group Manager
Hydraulic Investigations and Laboratory Services Group, 86-68460

Peer Review:

Tony L. Wahl, P.E
Hydraulic Engineer, Hydraulic Investigations and Laboratory Services Group, 86-68460

11/19/15
Date

U.S. Department of the Interior
Bureau of Reclamation
Technical Service Center
Hydraulic Investigations and Laboratory Services Group
Denver, Colorado

November 2015

Mission Statements

The mission of the Department of the Interior is to protect and provide access to our Nation's natural and cultural heritage and honor our trust responsibilities to Indian Tribes and our commitments to island communities.

The mission of the Bureau of Reclamation is to manage, develop, and protect water and related resources in an environmentally and economically sound manner in the interest of the American public.

Acknowledgments

Thanks to the State of Washington and Reclamation's Columbia Cascades Area Office for providing funding on this project. Thanks to the Yakima Storage Dams Fish Passage Core Team (CORE team) for providing invaluable expert guidance on this project. Special thanks to the Hydraulics Laboratory shop staff who constructed the physical hydraulic models: Dane Cheek, Marty Poos, Jimmy Hastings and Jason Black.

Hydraulic Laboratory Reports

The Hydraulic Laboratory Report series is produced by the Bureau of Reclamation's Hydraulic Investigations and Laboratory Services Group (Mail Code 86-68560), PO Box 25007, Denver, Colorado 80225-0007. At the time of publication, this report was also made available online at **http://www.usbr.gov/tsc/hydlab/pubs/**.

Disclaimer

The information provided in this report is believed to be appropriate and accurate for the specific purposes described herein, but users bear all responsibility for exercising sound engineering judgment in its application, especially to situations different from those studied. References to commercial products do not imply endorsement by the Bureau of Reclamation and may not be used for advertising or promotional purposes.

CONTENTS

TABLES

APPENDIX TABLES

FIGURES

APPENDIX FIGURES

GLOSSARY

1. **Average Downstream Velocity:** Reported values used the average velocity perpendicular to the observed slice. In Cartesian coordinate systems it was either x- or y-velocity, depending which quadrant the slice was taken from. In cylindrical coordinate systems, the *theta* (radial) velocity value was used.
2. **Average Vertical Velocity:** Reported values used the average vertical velocity of the observed slice. The z-velocity value was used for both coordinate systems. This value was used to make the Lagrangian adjustment (average fish's perspective) to the flow field.
3. **Core Team:** Short for Yakima Storage Dams Fish Passage Core Team. This team provided expert advice and opinions and approved final designs from a fisheries perspective. The team included the following: Walt Larrick and Joel Hubble, Reclamation's Yakima Field Office, Derek Sandison, State of Washington Department of Ecology: Bruce Heiner , Washington Department of Fish and Wildlife (WDFW); Bryan Nordland/Jeff Brown (NOAA); Mark Jonston (Yakama Nation); David Child and John McKern (Yakima Joint Board); Pat Monk (USFWS), Scott Revell (Roza Irrigation District): Steve Montague Reclamation's Pacific NW Regional office.
4. **Free Surface channel:** Non-pressurized open surface flow.
5. **Maximum Downstream Velocity:** Reported values used the maximum velocity perpendicular to the observed slice. In Cartesian coordinate systems it was the x- or y-velocity, depending which quadrant the slice was taken from. In cylindrical coordinate systems, the *theta* (radial) velocity value was used.
6. **Maximum Relative Vertical Velocity:** Maximum vertical velocity adjusted by the average vertical velocity.
7. **Maximum Vertical Velocity:** Reported values used the maximum vertical velocity of the observed slice. The z-velocity value was used for both coordinate systems. This value was almost always upwards and near the inside wall.
8. **Minimum Vertical Velocity:** Reported values used the minimum vertical velocity of the observed slice. The z-velocity value was used for both coordinate systems. This value was almost always downwards and near the outside wall.
9. **Minimum Relative Vertical Velocity:** Minimum vertical velocity adjusted by the Average vertical velocity.
10. **Roll Over Parameter:** The difference between the maximum vertical velocity and the minimum vertical velocity. The distance between the

locations of maximum vertical velocity and minimum vertical velocity was generally near 4 feet since these values were almost always found to be near the side walls. This value was used as a relative indication of roll-over strength to compare simulations.

11. **Secondary Velocity:** Velocities shown in cross section from a fish's perspective with the vertical component adjusted by the average vertical velocity of that section. This does not include downstream velocity.
12. **Sweeping Velocity:** Maximum component velocity towards the inside wall in a vertical cross sectional slice. In Cartesian coordinate systems component velocity was the either x- or y-velocity, depending which quadrant the slice was taken from. In cylindrical coordinate systems, the r-velocity value was used. The sweeping velocity is illustrated in Figure A-4.
13. **Sweet Spot:** The area with secondary velocities less than 1 ft/s in a vertical cross sectional view.
14. **Tumbling Roll-Over:** Term used to describe a flow condition where banked flow is so extreme that a portion of the flow separates and curls over the main body of flow.

Executive Summary

The U.S. Bureau of Reclamation (Reclamation) is actively pursuing the development and construction of a downstream fish passage system at Cle Elum Dam. The system consists of a series of structures that will allow fish (primarily juvenile sockeye salmon, *Oncorhynchus nerka*) to self-guide into a structure that carries them around the dam and into the downstream river channel. This design includes an intake structure, helical fish passage, tunnel, and outfall. The helical fish passage (Helix) represents a groundbreaking design intended to fit a long, gradually sloped channel into a very compact physical space in order to produce a system that is both technically and economically feasible.

Reclamation's Hydraulics Laboratory in Denver, Colorado conducted numerical and physical hydraulic model studies to support development of the fish passage system design. This report addresses only the development of the helix design and the components that help the flow to transition into and out of the helix.

The purpose of this study was to determine helix and transition geometries that would provide optimal hydraulic conditions for continuous safe downstream juvenile fish passage. Both numerical and physical modeling were used to develop and refine the final designs. The helix structure will be located between a multilevel fish inlet structure in Cle Elum Reservoir and a tunnel that goes from the helix, through the right abutment of the spillway, to the juvenile outfall near the downstream end of the spillway stilling basin. This study began with a sensitivity analysis using numerical modeling to determine a geometry that would produce acceptable hydraulic flow conditions to provide continuous passage for fish. This analysis determined that by using a rectangular geometry to minimize secondary flow current rotation and cross sectional sweeping flow currents, a large sweet spot could be produced within the body of flow to provide a stable environment for fish. Once an acceptable design was determined from the numerical modeling, the physical model was used to refine and verify the final design. Final results from the model investigations demonstrated that the helix can be used to provide stable and continuous downstream fish passage while dropping fish more than 80 feet in elevation through a sloping rectangular channel at Cle Elum Dam.

The development of the intake structure design is discussed in a companion report, Reclamation's Hydraulic Laboratory report HL-2015-03 [1]. Physical hydraulic modeling was also used to study flow conditions in the Cle Elum River downstream from the dam, focusing on the downstream (juvenile) passage system outfall and the entrance to an accompanying upstream (adult) fish passage system. That study is described in report HL-2015-02 [2].

Background

Cle Elum Dam, located on the Cle Elum River about 8 miles northwest of Cle Elum, Washington, was built in 1933 without fish passage facilities (figures 1 and 2). The dam expanded a natural lake that historically supported populations of three species of salmon (sockeye, coho and spring Chinook), steelhead, Pacific lamprey, bull trout and other resident fish. Lack of passage at the dam blocked access to the lake and upstream habitat for anadromous salmonids and contributed to the extirpation of sockeye salmon runs in the Yakima River basin. The absence of passage has also isolated local populations of bull trout and may have prevented the recolonization of populations. [3]

A fish recovery effort has been underway in the Yakima River basin since the 1980s. Reclamation began studying fish passage at the five Yakima Project Dams in 2002 as a result of commitments made to Washington State and the Yakama Nation related to Safety of Dams (SOD) work in the re-build of Keechelus Dam. In 2003 Reclamation completed an appraisal-level assessment of alternatives for providing fish passage at the five dams and identified Cle Elum and Bumping Lake Dams as the highest priority sites for continued investigation of fish passage feasibility.[4]

In 2004 a temporary fish passage structure was constructed to assess whether reintroduced salmonids would effectively find downstream egress through a surface release near the dam. The "Interim Flume" involved modification of a spillway radial gate, headworks structure, and addition of a wooden flume that ran inside of the main spillway channel. After multiple years of testing, it was determined that juvenile salmonids would locate the passage entrance, and volitionally move downstream. However the Interim Flume was only able to be operated in a 17 foot range between full pool and the spillway crest, which often does not temporally coincide with the optimal juvenile migration period [5].

The relative success of the Interim Flume and its limitations led the Project Team to investigate concepts for a more permanent solution with improved performance over a range of reservoir conditions. A Final planning report was completed in April 2011. The project's purpose and need was "to construct fish passage facilities and to maximize ecosystem integrity by restoring connectivity, biodiversity and natural production of anadromous salmonids." [3]

This collaborative project involves the Bureau of Reclamation (Reclamation), Washington State Department of Ecology (Ecology), Washington State Department of Fish and Wildlife (WDFW), and the Yakama Nation. This project has two components—fish passage facilities design, with Reclamation taking the lead, and a fish reintroduction program developed by the Yakama Nation with assistance from WDFW. Fish species expected to benefit include sockeye, coho and spring chinook salmon, and Pacific Lamprey. The project also benefits the Upper Middle Columbia River Steelhead and Bull Trout, two species listed as threatened under the Endangered Species Act.

Introduction

The U.S. Bureau of Reclamation (Reclamation) has completed the development of a downstream passage design for Cle Elum Dam that consists of a series of structures that will allow fish to self-guide into a structure that carries them around the dam and into the downstream river channel. Downstream fish passage at high head dams has always been difficult. Most high dams with downstream fish passage are hydropower generation facilities with minimal fluctuation in pool elevation. Generally fish passage structures at these facilities consist of manned surface collectors, and trap and haul methods that require high operation and maintenance (O&M) costs. Cle Elum Dam is a storage reservoir, and experiences seasonal swings in reservoir elevation of about 100 feet. Surface collectors are not compatible with such large reservoir fluctuations, so new fish passage concepts were developed and evaluated for use at this site.

During the design phase, several options were modeled by Reclamation's Hydraulic Investigations and Laboratory Services group, including a drop pool structure that was first modeled in 2012. This structure was discussed in a presentation at the National Conference on Engineering and Ecohydrology for Fish Passage at Oregon State University June 25 - 27, 2013 [6]. The basis for this design was NMFS criteria for safe juvenile downstream passage [7] that limits the maximum vertical drop to 10 ft and maximum flow velocity to 25 ft/s. The laboratory investigations demonstrated there were significant fish safety issues with this design. This led researchers to consider concepts that fall outside of previously accepted criteria. In addition, there is evidence to suggest that under controlled conditions fish survival may be good at higher velocities, as long as fish passing through the system are contained within a relatively smooth body of flow and are not exposed to excessive shear stresses. As a result, a new downstream passage concept using a helix configured design was developed for Cle Elum Dam. (Figure 3).

This design includes an intake structure, helical free-surface fish passage channel, tunnel, and outfall (figure 4). Of primary significance is the helical fish passage (helix) which represents a groundbreaking design. Only the development of the helix design and transitions into and out of the helix are discussed within this report. The helix is an energy dissipation device that allows downstream juvenile fish transport from Cle Elum Reservoir while the reservoir water surface ranges from a maximum of about 2243.0 ft to a minimum of about 2180.0 ft based on hydrologic studies [3]. Water exits from the proposed helix around elevation 2137.0 ft into a tunnel that extends over 1200 ft through the right abutment of the spillway to the Cle Elum River. Flow can be introduced into the helix at six different elevations, each vertically separated by 11.75 ft.

One of the major challenges in designing this structure was that flow depths and velocities within the structure must fall within a range that promotes continuous downstream movement, but does not cause injury. This also means that any transitions within the system, i.e., from intake structure conduit into the helix or

from the helix into the downstream conduit (the conduit that carries the fish to the river channel downstream from the dam) must be extremely smooth hydraulically.

Throughout the design process, Reclamation has collaborated with a Technical Yakima Basin Storage Fish Passage Work Group (Core team) of biologists, engineers, and other specialists from Federal, State, Tribal, and local entities to evaluate the effectiveness of the fish passage alternatives and their potential for causing injury to fish.

Figure 1. Cle Elum Dam and spillway (existing).

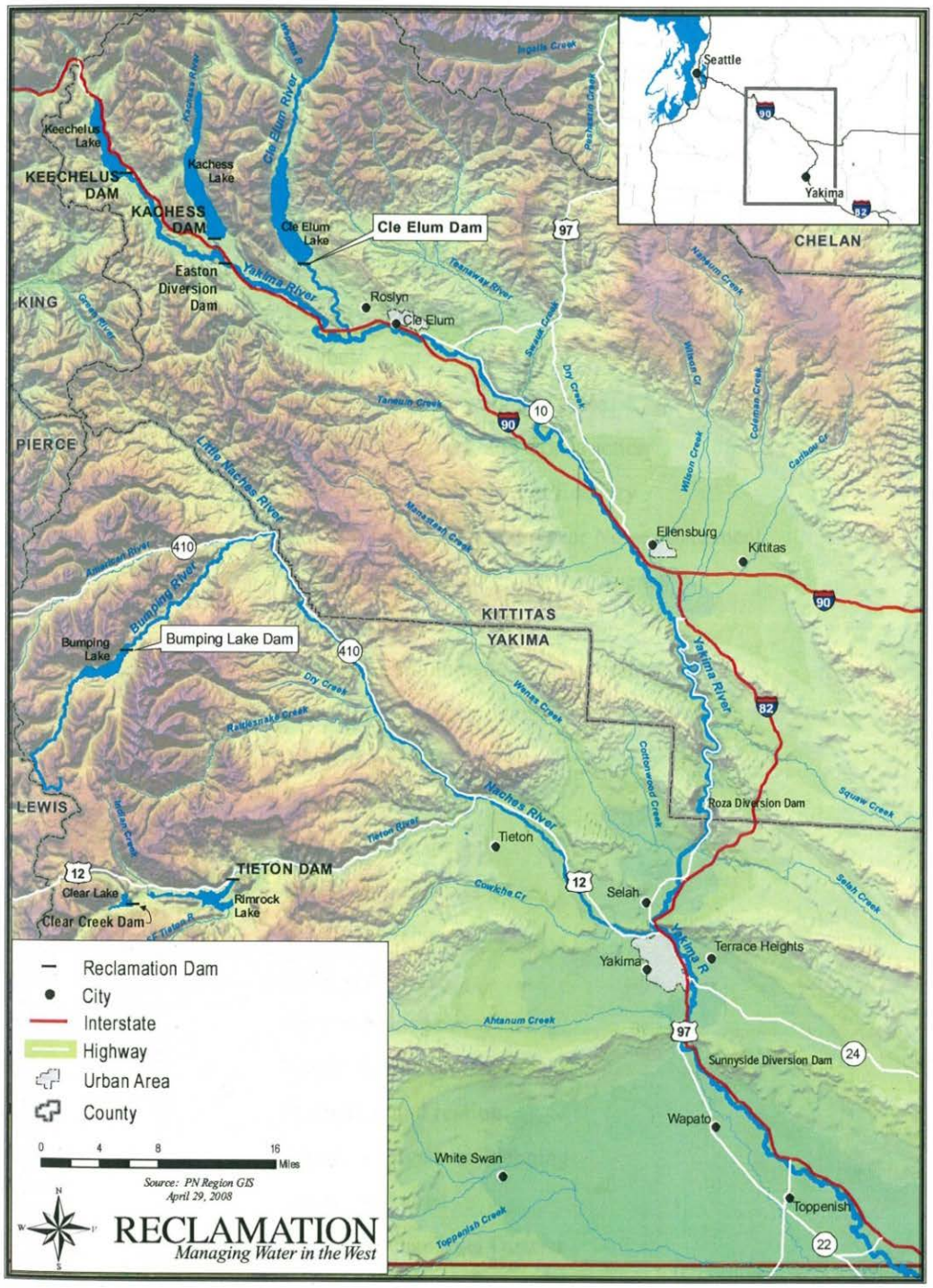

Yakima Project Storage Dams, including Cle Elum and Bumping Lake Dams

Figure 2. Location map for Cle Elum Dam.

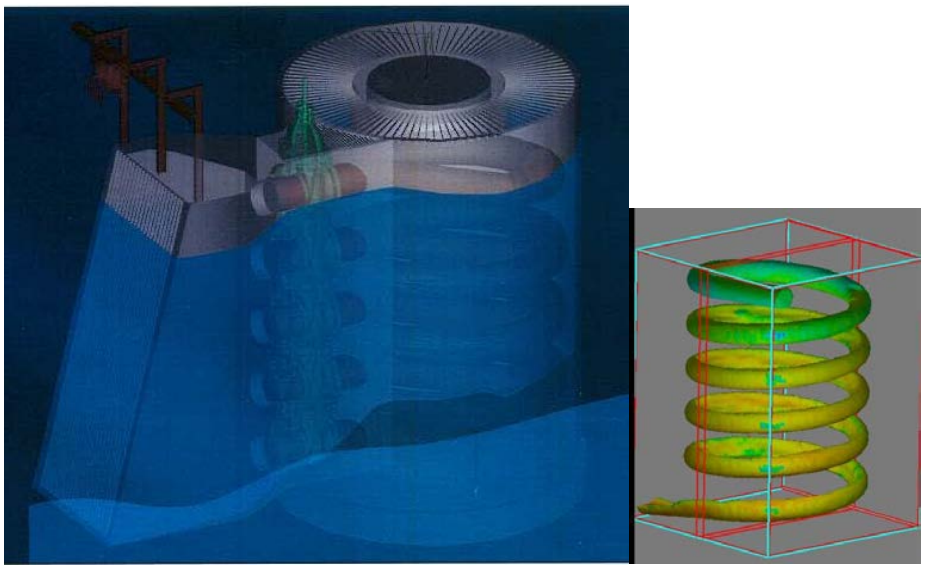

Figure 3. Initial helix design concept with vertical intake tower.

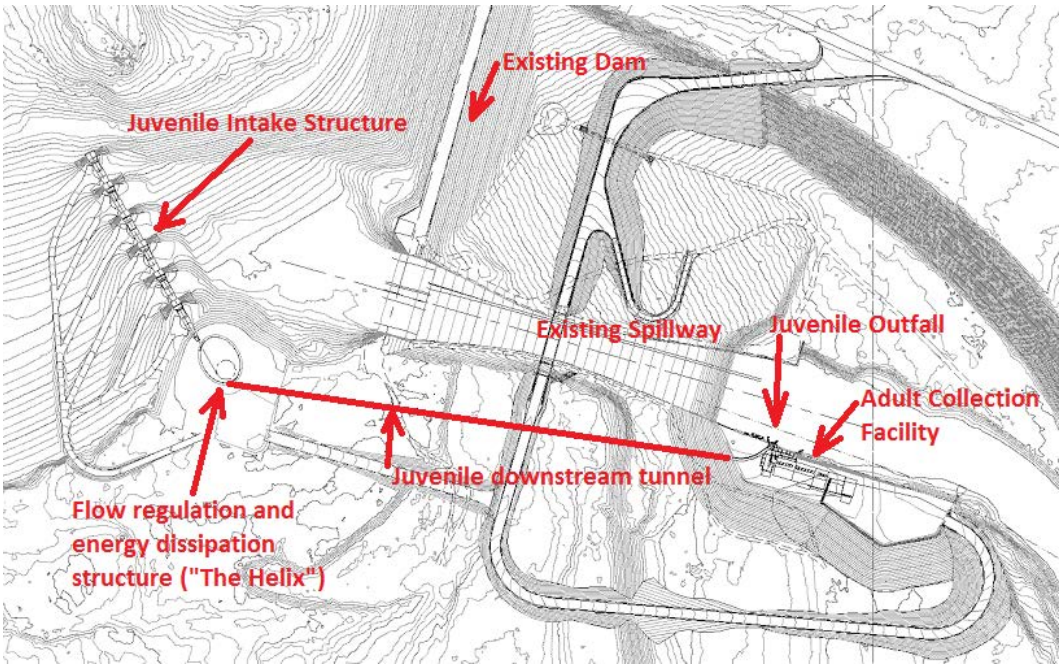

Figure 4. Layout of intake structure, helix and tunnel through right abutment.

Model Objectives

The purpose of this study was to determine helix and transition geometries, for providing optimal hydraulic conditions for continuous safe downstream juvenile passage, primarily for salmon during the downstream juvenile passage season. Both numerical modeling and physical modeling were used to determine, refine, and optimize the final designs. The transitions studied included the transition from the intake structure conduit to the helix, and the transition from the helix to the tunnel. Once a geometry and diameter of the helix structure were determined using numerical modeling, a physical model of the structure was constructed and tested in Reclamation's hydraulics laboratory. The physical model was used to refine and verify the numerical model so that additional information could be extracted and used for determining the final acceptable design.

Helix Numerical Model

Methods and Approach

The helix structure will be located between a multilevel juvenile intake structure in Cle Elum Reservoir and a tunnel that runs from the helix, through the right abutment of the spillway, to the juvenile outfall near the downstream end of the spillway stilling basin. The first step in the process of determining an acceptable design for the helix structure geometry was to conduct a sensitivity analysis to determine a geometry that would produce acceptable hydraulic flow conditions to provide safe passage for fish.

A computational fluid dynamics (CFD) model was created using FLOW-3D (Appendix A) and was used to test alternative designs, varying the overall diameter, slope, and channel geometry for the proposed helix design. FLOW-3D is a finite difference, free surface, transient flow modeling system that solves the Navier-Stokes flow equations in up to three spatial dimensions. The flow equations are solved within an orthogonal coordinate mesh. The model is well-suited to the simulation of flows having a free water surface.

Key parameters of the helical fish passage channel design are the channel shape and section size, the helix diameter, and the rate of elevation drop per helix loop. The helix diameter and drop rate per loop in turn determine a channel slope, which varies between the inside and outside of the channel. In the discussion of designs that follows, the helix diameter is always expressed as the diameter to the outside walls and the channel slope will always be given as determined along the centerline of the channel.

The first design modeled in FLOW-3D consisted of a 6 ft diameter pipe with a helix diameter of 52 ft and 11.75 ft drop between loops. The drop rate was based

on the spacing required to match the intake structure (figure 5). The resulting channel slope was 7.8%. A numerical simulation using FLOW-3D was run for this initial geometry. To help evaluate the flow in the helix chute, tools in FLOW-3D were used to illustrate a stream ribbon produced as the flow made its way down the helix chute (figure 6). This graphic appears to show a high potential for rollover as indicated by the pinch points in the ribbon of flow. The use of ribbons to compare potential for rollover was inadequate as it only demonstrated a single flow path (streamline). Other evaluation methods were used to make performance comparisons for various chute geometries and to evaluate whether flow currents within the chute might cause injury to fish.

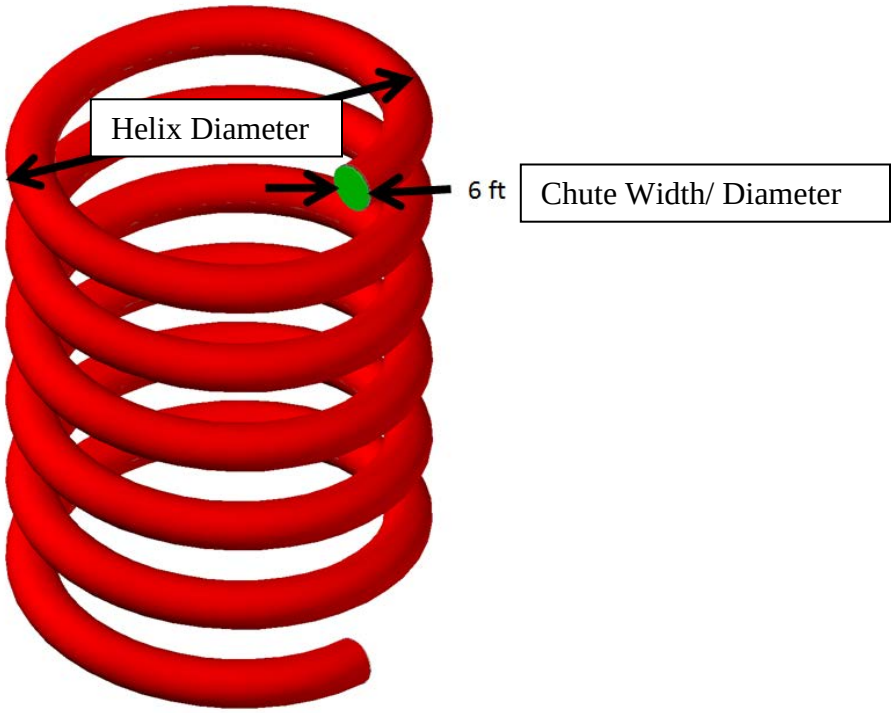

Figure 5. Initial model configuration geometry for numerical modeling simulation.

A cross section extracted once flow had become stabilized, about 2½ loops below where flow entered into the helix, was evaluated by transferring the data into Tecplot 360 (a commercially available CFD post processing analysis and visualization tool). Unfortunately, the average downward velocity in the helix flume (due to the 7.8% channel slope) dominated the velocity map (figure 7). Thus, the decision was made to evaluate the cross section from a fish's perspective to better represent potential cross currents and rotational flows experienced by an "average" fish. To represent this perspective, data from the initial simulation was imported into Tecplot and the vertical velocity was adjusted to remove the average downward velocity, as shown in Figure 8. That is to say

that when the vertical component of the average flow velocity in the helix chute was -2.3 ft/s, the average fish would also have an average vertical velocity of -2.3 ft/s. To view the flow field as the average fish experiences it, 2.3 was added to W. This provided a better understanding of the strength of secondary rotational flows that juvenile fish would need to endure.

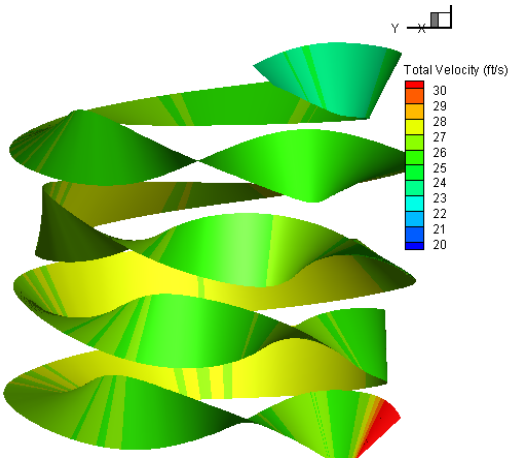

Figure 6. A single streamline of flow in the helix chute at 400 ft^3/s.

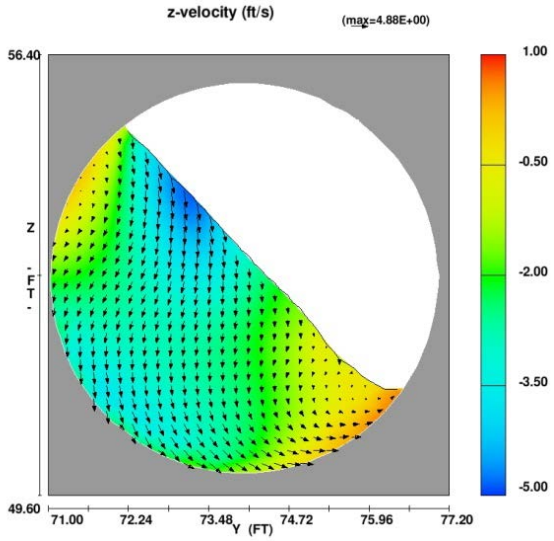

Figure 7. Cross section of flow from a FLOW-3D simulation. The average vertical velocity (z-velocity) in this cross section is -2.3 ft/s (downward). The color contours indicate the vertical velocity simulated. Due to the average vertical velocity being -2.3 ft/s, it is difficult to visually isolate the rotational flow the fish would experience

Since there were no existing guidelines for evaluating cross sections extracted from the helix chute, several parameters were established for comparing designs and determining whether or not secondary flow currents would cause injury to

fish. These key parameters were evaluated and compared among the designs in an effort to fulfill the following objectives:

- Minimizing impingement of flow and fish – This was evaluated based on magnitude of sweeping velocity that could potentially sweep fish into a sidewall

- Smooth flow conditions – This was evaluated based on the percentage area within the cross section where velocity (relative to the fish) was 1.0 ft/s or less. This was determined as the ideal fish location within the body of flow, and was designated as the "sweet spot".

- Minimizing flow rotation that can cause the body of flow to roll-over, potentially leading to injury or disorientation of fish – This was evaluated by subtracting the minimum (downward) velocity from the maximum (upward) velocity at a flow cross section after flow in the helix chute stabilized. This was designated as the Roll Over Potential (ROP) parameter.

- Reduced Secondary flow rotation that can cause fish to rollover - This was evaluated by observation, based on tightness of rotation.

The ROP value for the initial simulation (case A) was 5.06 ft/s and since this case appeared to have a high potential for rollover or rotational secondary flows that may cause injury to fish (as evidenced from the flow ribbon), this became the baseline for comparing to other chute shapes or geometries.

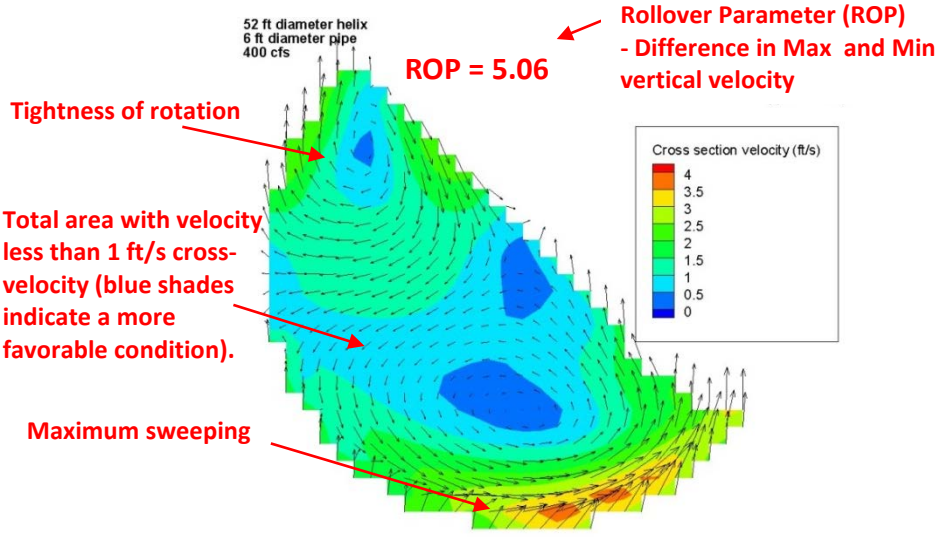

Figure 8. Test Case SA1, 6 ft diameter round pipe, 52 ft helix diameter. Parameters for evaluation and comparison of helix chute geometries using fish's perspective (i.e. vertical component of average flow velocity has been subtracted.) Surface choppiness seen here and in subsequent plots is due to nuances with Tecplot presenting flow edges without smoothing surface cells.

Sensitivity Analysis for Helix Chute

Once parameters were established for comparing helix geometry performance, a sensitivity analysis was conducted to test round and rectangular shapes, and a range of helix diameters to determine combinations that would reduce secondary flow rotation and produce a significant “sweet spot” within the flow regime where fish can ride out relatively high velocities without injury.

The shapes that were evaluated in the Sensitivity analysis are shown in figure 9 and can be described as:

1) Case SA1 - 6 ft diameter round pipe, 52 ft helix diameter
2) Case SA2 - 6 ft diameter round pipe, 40 ft helix diameter
3) Case SA3 - 6 ft diameter round pipe, 80 ft helix diameter
4) Case SA4 - 4 ft wide chamfered rectangular box, 52 ft helix diameter
5) Case SA5 - 4 ft wide rectangular box, 52 ft helix diameter.
6) Case SA6 - 4 ft wide rotated box, 52 ft helix diameter.
7) Case SA7 - 5 ft wide rotated rectangular box, 52 ft helix diameter.
8) Case SA8 - 5 ft wide rectangular box, 52 ft helix diameter.

For each sensitivity analysis test case, the average vertical velocity component in the helix chute was calculated and this value was subtracted to obtain velocities relative to fish moving with the flow. The resulting cross sectional flow patterns (extracted at a location after flow within the helix chute had stabilized) are presented in figures 10-17. In addition the ROP value for each test case was calculated and is presented in the upper right hand corner of each figure.

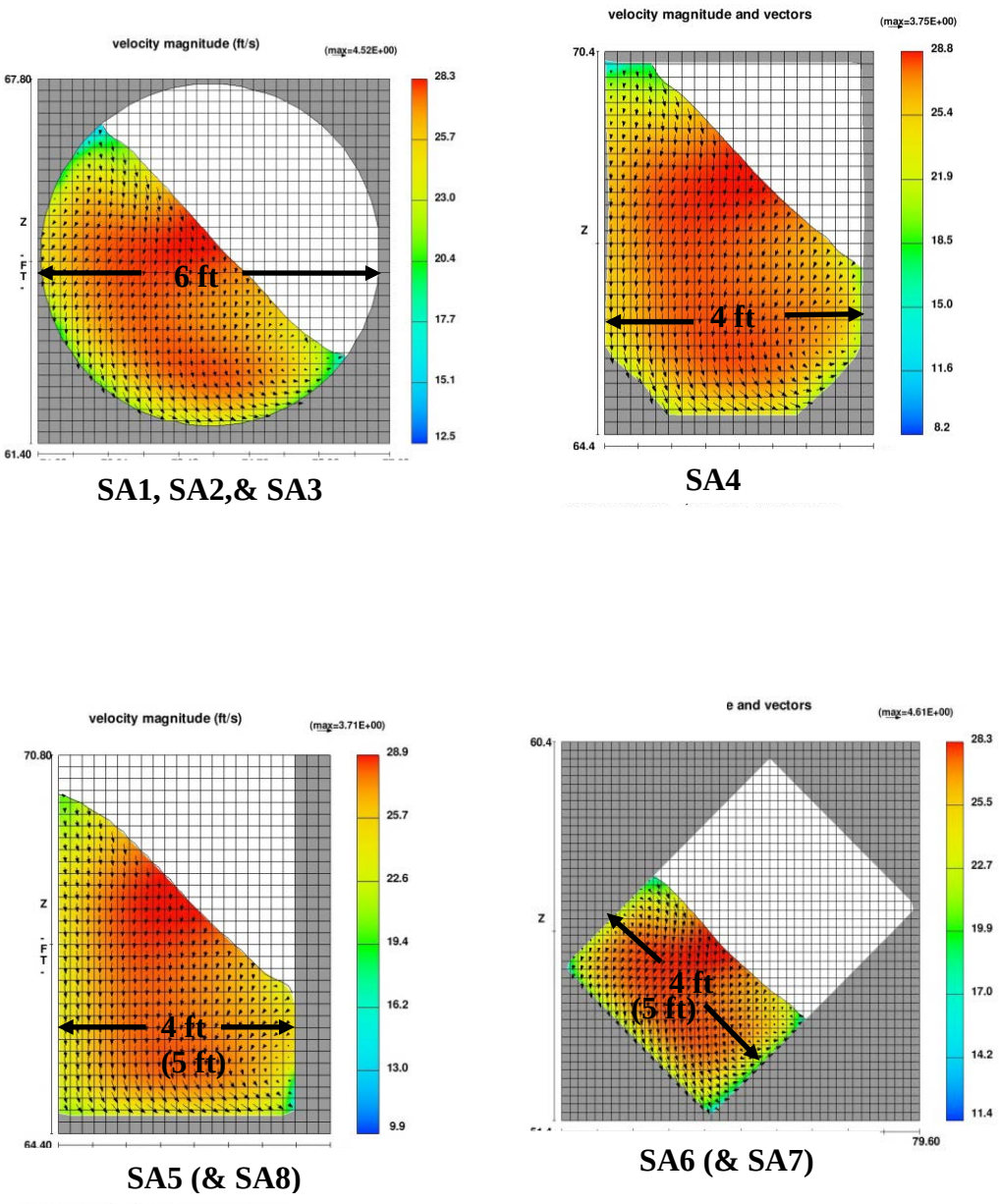

Figure 9. Shapes tested in sensitivity analysis shown in FLOW 3D graphics.

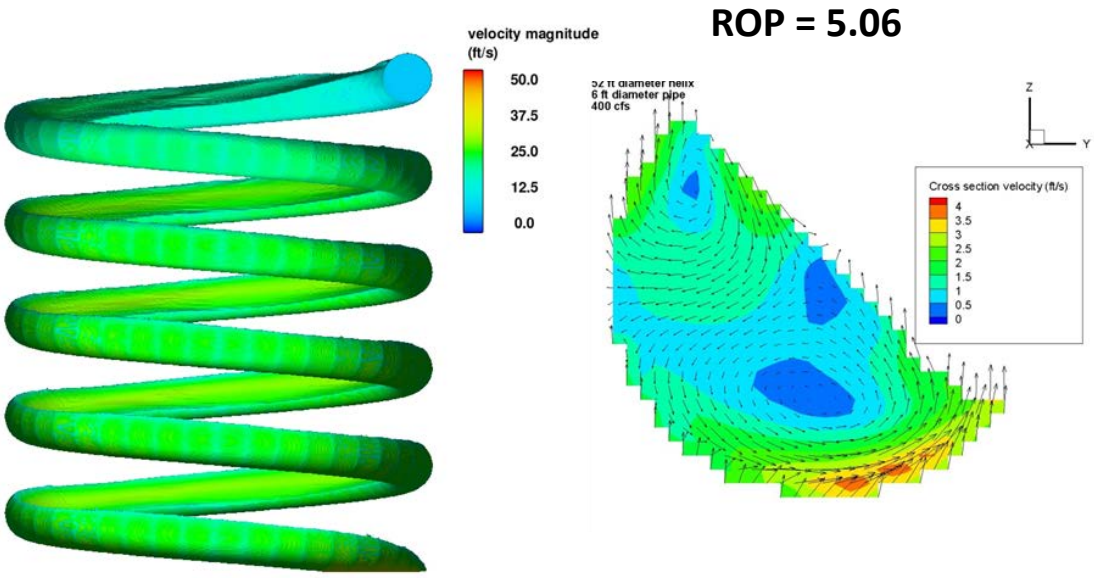

Figure 10. Test Case SA1, 6 ft diameter round pipe, 52 ft helix diameter, adjusted by the average vertical velocity of -2.30 ft/s.

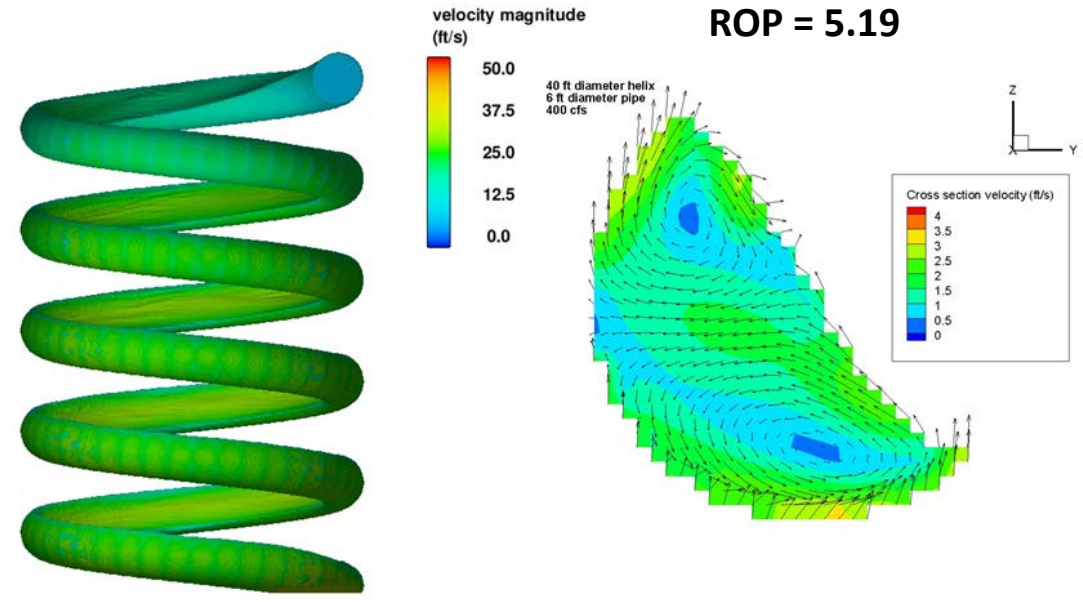

Figure 11. Test Case SA2, 6 ft diameter round pipe, 40 ft helix diameter adjusted by the average vertical velocity of -2.65 ft/s.

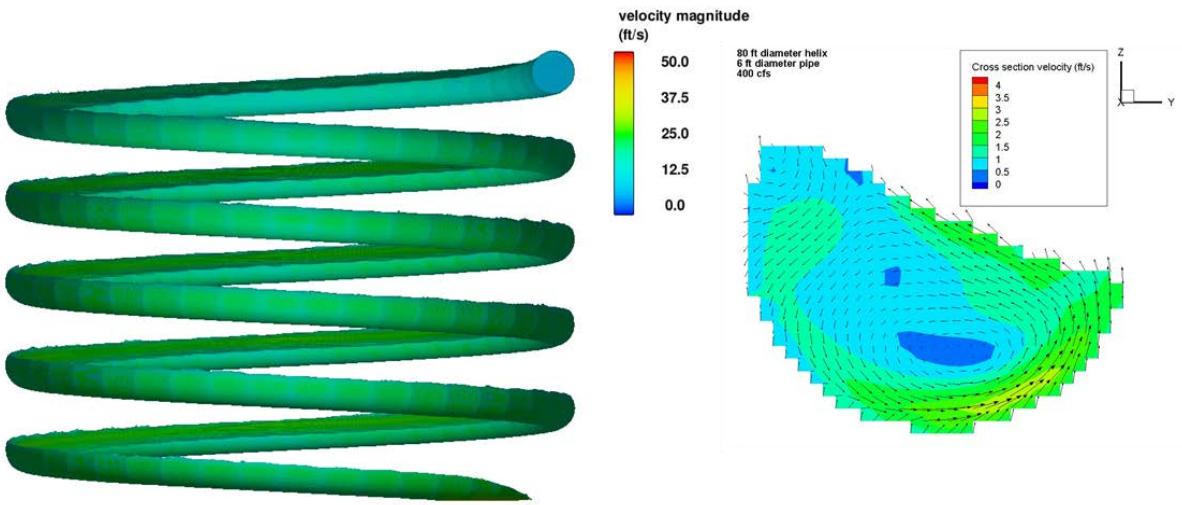

Figure 12. Test Case SA3, 6 ft diameter round pipe, 80 ft helix diameter adjusted by the average vertical velocity of -1.19 ft/s.

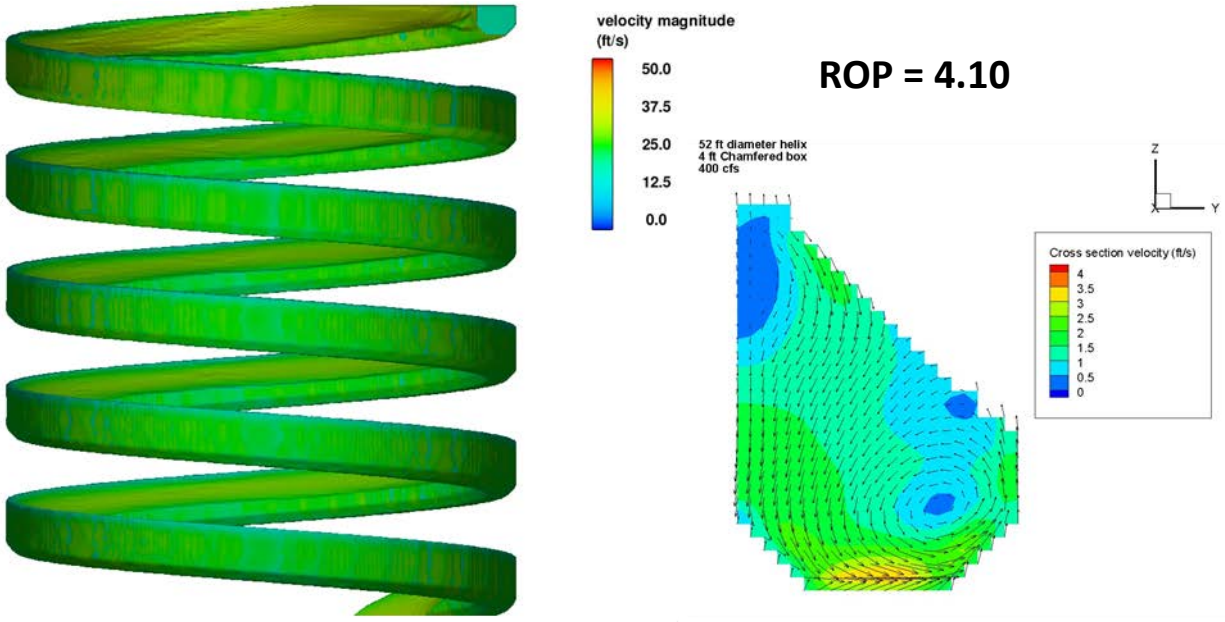

Figure 13. Test Case SA4, 4 ft wide chamfered rectangular box, 52 ft helix diameter, adjusted by the average vertical velocity of -2.05 ft/s.

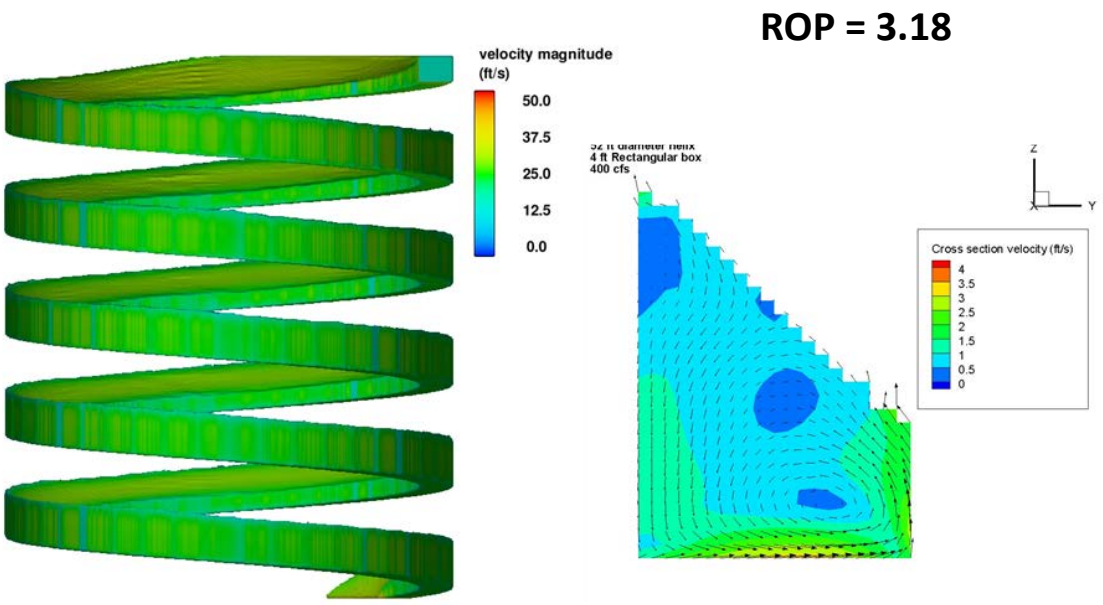

Figure 14. Test case SA5, 4 ft wide rectangular box, 52 ft helix diameter, adjusted by the average vertical velocity of -2.12 ft/s.

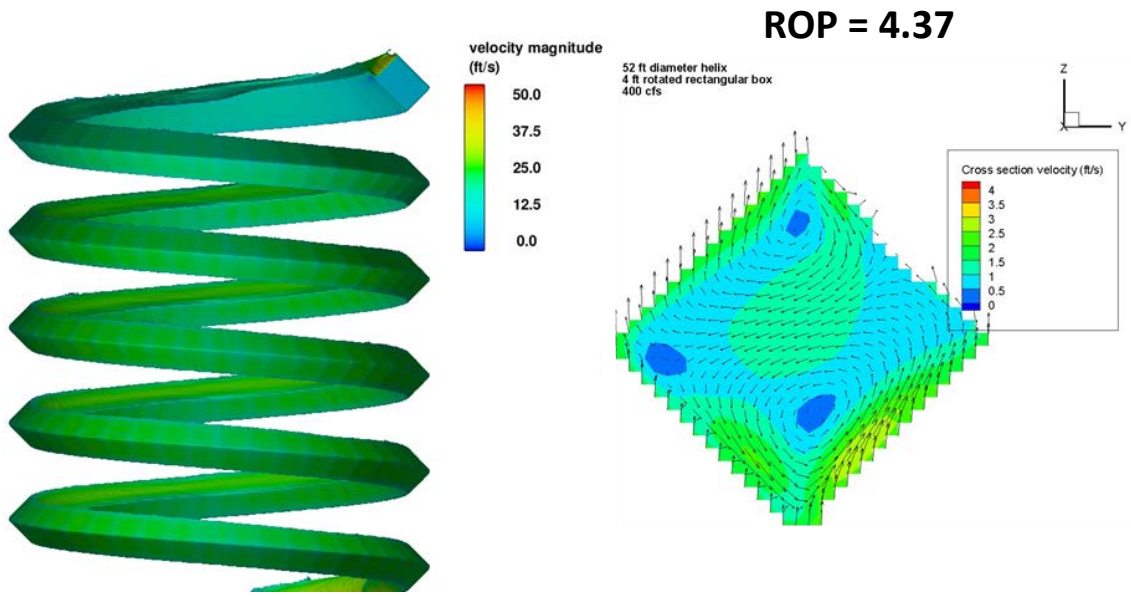

Figure 15. Test case SA6, 4 ft wide rotated rectangular box, 52 ft helix diameter, adjusted by the average vertical velocity of -2.12 ft/s.

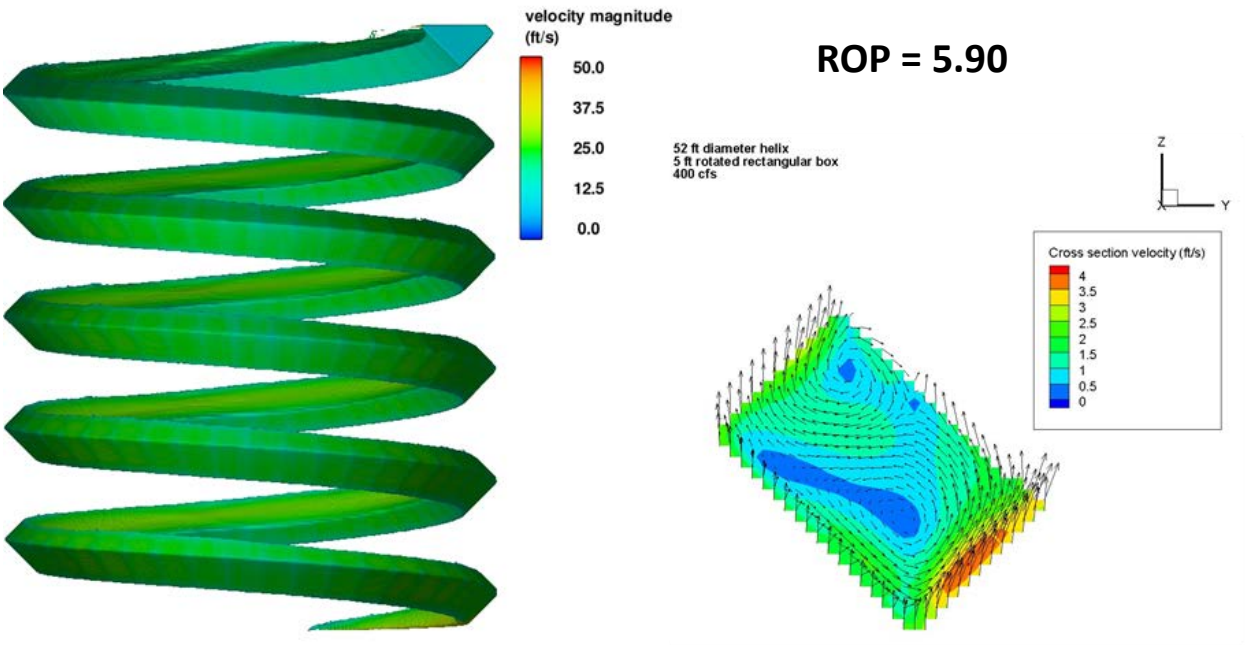

Figure 16. Test case SA7, 5 ft wide rotated rectangular box, 52 ft helix diameter, adjusted by the average vertical velocity of -2.16 ft/s.

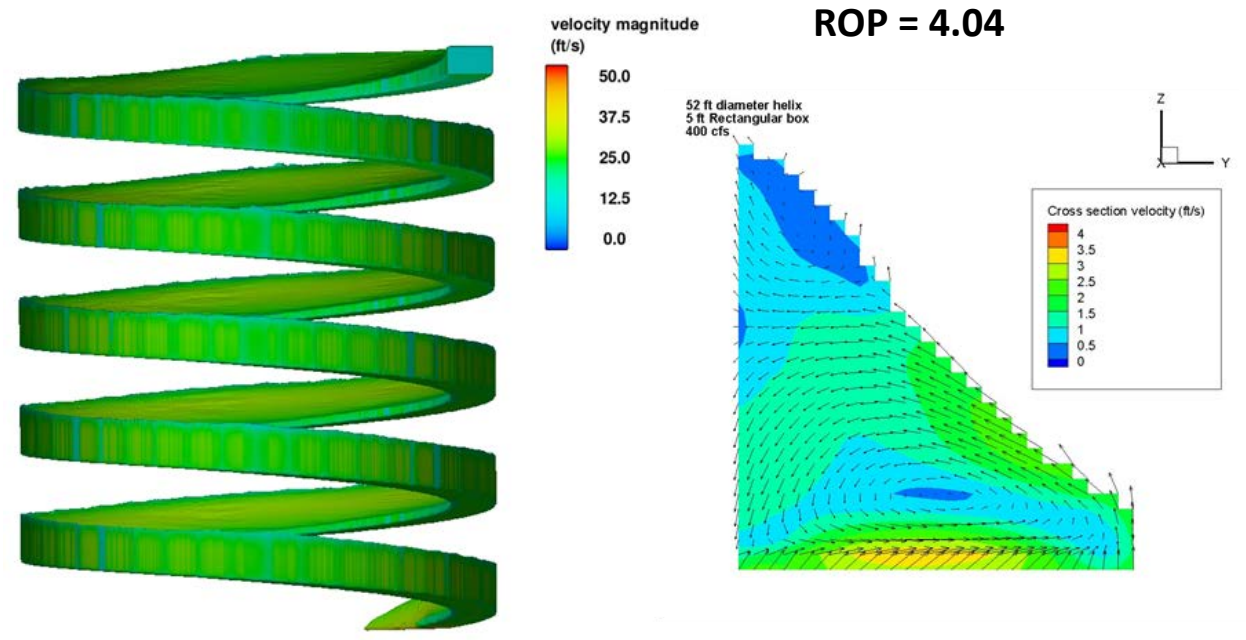

Figure 17. Test case SA8, 5 ft wide rectangular box, 52 ft helix diameter, adjusted by the average vertical velocity of -1.90 ft/s.

Table 1. Each sensitivity test case with corresponding calculated parameters (see glossary for definitions).

Sensitivity Analysis (SA)	Helix chute slope along center line:	Average downstream velocity (ft/s)	Average vertical velocity (ft/s)	Maximum vertical Velocity (ft/s)	Minimum vertical velocity (ft/s)	Maximum Relative Vertical Velocity (ft/s)	Minimum Relative Vertical Velocity (ft/s)	Vertical Velocity difference (ROP) (ft/s)
SA1: 52-Foot-Helix-6-Foot-Diameter-Circular-Pipe Simulation	**7.8%**	**25.81**	**-2.3**	**0.66**	**-4.4**	**2.96**	**-2.1**	**5.06**
SA2: 40-Foot-Helix-6-Foot-Diameter-Circular-Pipe Simulation	**10.4%**	**27.49**	**-2.65**	**0.17**	**-5.02**	**2.82**	**-2.37**	**5.19**
SA3: 80-Foot-Helix-6-Foot-Diameter-Circular-Pipe Simulation	**4.9%**	**23.17**	**-1.19**	**1.00**	**-2.33**	**2.19**	**-1.14**	**3.33**
SA4: 52-Foot-Helix-4-Foot-Bottom-Chamfered-Box Simulation	**7.8%**	**26.28**	**-2.05**	**0.61**	**-3.49**	**2.66**	**-1.44**	**4.1**
SA5: 52-Foot-Helix-4-Foot-Bottom-Box Simulation	**7.8%**	**26.20**	**-2.12**	**0.04**	**-3.14**	**2.16**	**-1.02**	**3.18**
SA6: 52-Foot-Helix-4-Foot-Bottom-Rotated-Box Simulation	**7.8%**	**24.79**	**-2.12**	**0.65**	**-3.72**	**2.77**	**-1.6**	**4.37**
SA7: 52-Foot-Helix-5-Foot-Bottom-Rotated-Box Simulation	**7.8%**	**25.83**	**-2.16**	**1.6**	**-4.3**	**3.76**	**-2.14**	**5.9**
SA8: 52-Foot-Helix-5-Foot-Bottom-Box Simulation	**7.8%**	**27.22**	**-1.9**	**0.18**	**-3.87**	**2.07**	**-1.97**	**4.04**

Throughout all test cases, the average velocity in the helix flume stabilized after about 2½ loops. In general, comparison of the eight test cases (Table 1) showed that performance was improved with a rectangular chute geometry over a round or chamfered design, because it reduced the magnitude of the vertical flow components that could lead to tumbling roll-over within the helix chute. In addition, a milder slope improved performance because it reduced the average chute velocity, thereby reducing the extent of banked flow against the outside wall, and potential for roll-over. Best overall performance based on the parameters stated above occurred with test cases SA3 & SA5 . Test case SA3 shows a slightly lower average velocity of about 23 ft/s compared with test case SA5 at 26 ft/s. Both test cases provided a large “sweet spot” (from observation) for fish to ride within the body of flow moving down the helix chute, and low ROP values indicated minimal rotation within the flow. However based on the additional cost for construction of an 80 ft diameter helix, SA5 (4 ft wide rectangular box with 52 ft helix diameter) was chosen as the preferred design.

This design for the helix chute was accepted by the stakeholders for final design. Figure 18 shows the numerical simulation with the final chute geometry in place.

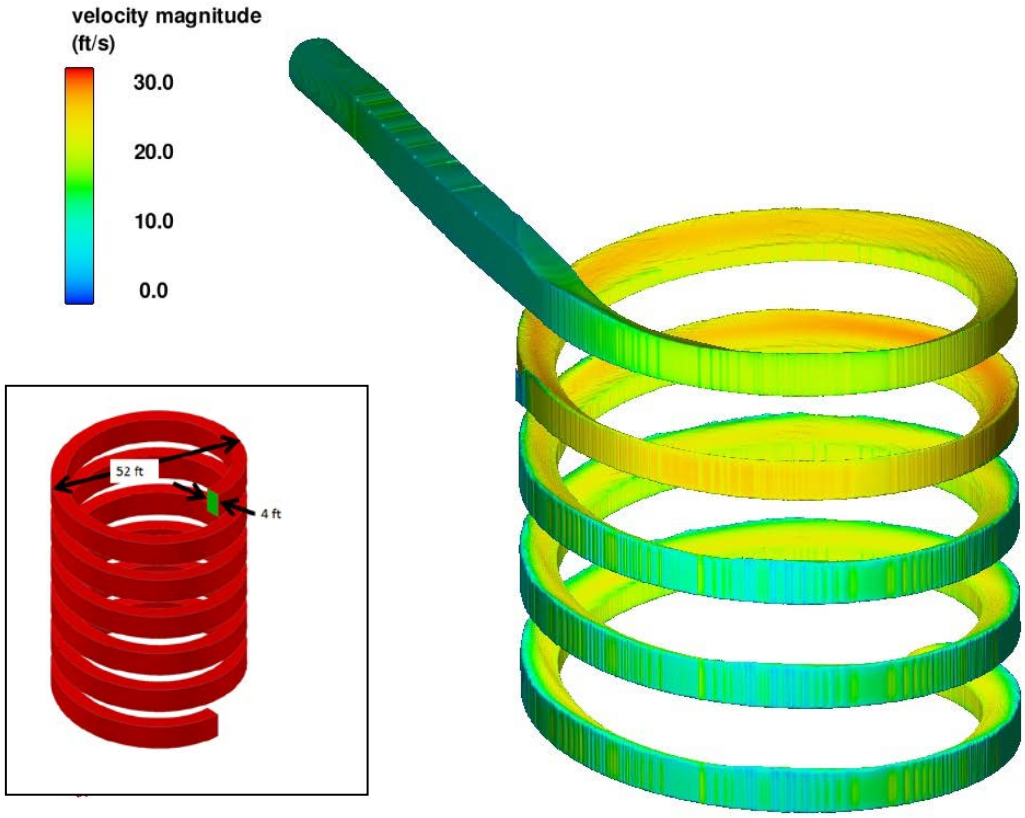

Figure 18. Final helix geometry and numerical simulation of flow in the helix transition and chute simulation

Helix Chute Modeling Refinement

Development of the helix chute geometry consisted of the synthesis of several different analytical and physical modeling processes.

Testing of the physical model (described in the next section of this report) led to the refinement of the numerical model. Average velocities measured in the helix chute in the physical model were significantly higher than the velocities determined with the numerical model (about 30 ft/s versus about 40 ft/s in the physical model at loop #3 at 400 ft^3/s). During the process of constructing the helix numerical model several assumptions were made in defining various parameters. Therefore it was necessary to adjust these parameters and conduct further simulations and analyses to try to match the numerical model more closely with the physical model. This was important so that information could be

extracted from the numerical model that would be difficult to assess with the physical model, such as pressure gradients and rotational flow currents.

This process began by evaluating the assumptions made in the numerical model regarding the roughness coefficient in the flume. However, several new simulations proved this was not the issue. Finally, further analyses determined that using a Cartesian coordinate system to represent the helix produced unrealistic areas of localized turbulence along the sidewall boundaries due to form roughness created by the grid. This turbulence dissipation produced an unrealistic reduction of flow velocity. To resolve this issue, the helix chute was defined using a cylindrical coordinate system with the walls of the 4 foot wide rectangular chute matching the cell boundaries in the CFD model. As a result the CFD model more closely matched the physical model.

Additional simulations were run with the cylindrical coordinate system in place, with results extracted at the four quadrants of the helix shown in Figure 19. The cross section velocity maps and calculated parameters for the for a flow rate of 400 ft^3/s are shown in figures 20-31. The station numbers where each consecutive loop begins are shown in Table 2. Figures 20-28 show flow cross sections in each of 4 quadrants for loops one and two, and then quadrants 2 and 4 for the remaining loops.

The figures demonstrate that the sweet spot within the flow stabilizes by the time the flow reaches the 2^{nd} quadrant of the second loop. Figure 29 shows that at 400 ft^3/s the maximum flow depth along the outside wall is about 5.5 ft with a minimum flow depth of about 0.8 ft. Figure 30 shows that maximum velocity of about 38 ft/s is reached at loop 7 (sta. 9+79.7), but velocity has nearly stabilized at about loop 5 or 6. Maximum rollover potential ranges from about 4.8 where flows enters into the helix, to about 4.0 as flow becomes more stable within the chute (figure 30). The ROP value of 4.8 is not a concern since it is an extremely brief occurrence and the sweet spot at that time is over 70% of the total flow area cross section. Figure 31 shows that the sweet spot stabilizes at a about 60% of the cross section for the remaining loops, and therefore provides a large area for fish to ride out the flow with minimal disturbance.

Cross sectional velocity maps and calculated parameters for 300 ft^3/s, 200 ft^3/s, and 100 ft^3/s are shown in figures 32-67 and show trends similar to the 400 ft^3/s case. The average velocities and flow depths in the flume decrease and the sweet spot percentage increases as flow rate is reduced. In addition, it appears that flow stabilizes more quickly after entering the chute as flow rate is reduced.

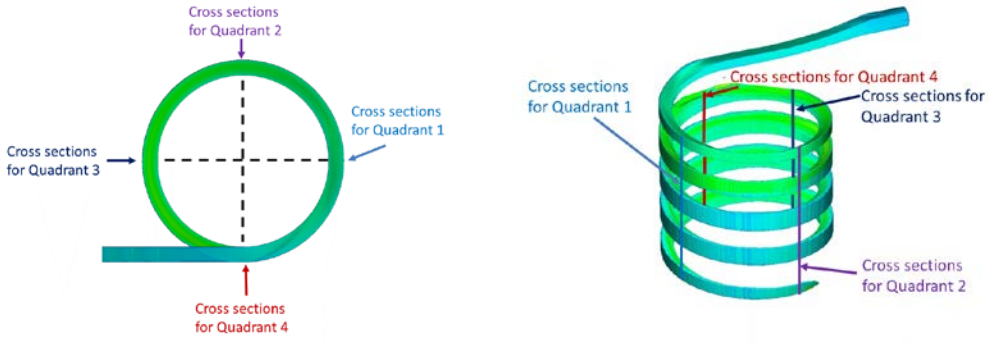

Figure 19. Quadrant locations in helix.

Table 2. Helix station number corresponding to location where each loop begins.

Loop Number	Station # where Loop begins
1	40.8
2	163.4
3	326.6
4	489.8
5	653.1
6	819.4
7	979.6

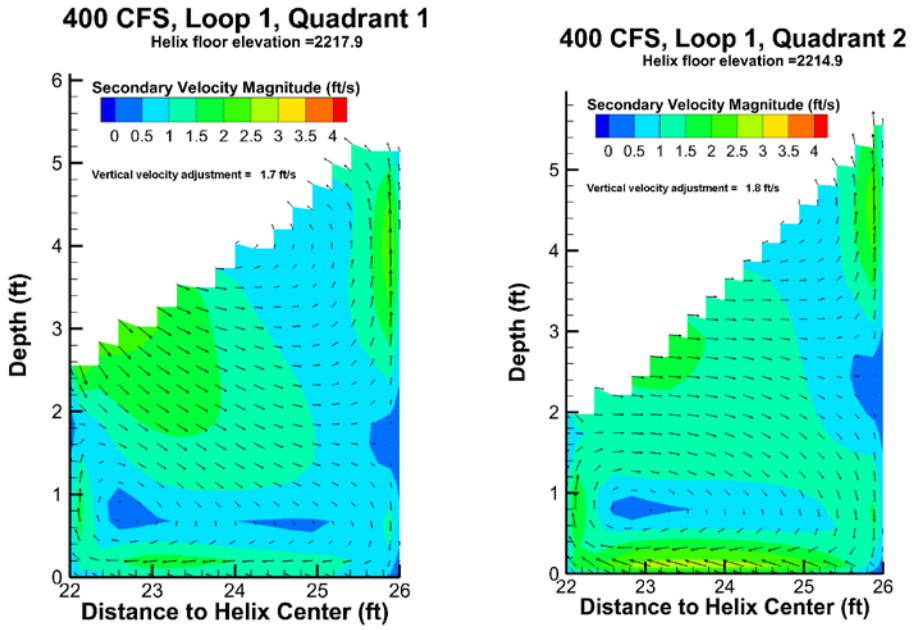

Figure 20. Helix flow cross section (fish's perspective) at 400 ft^3/s, Loop 1, quadrants 1&2

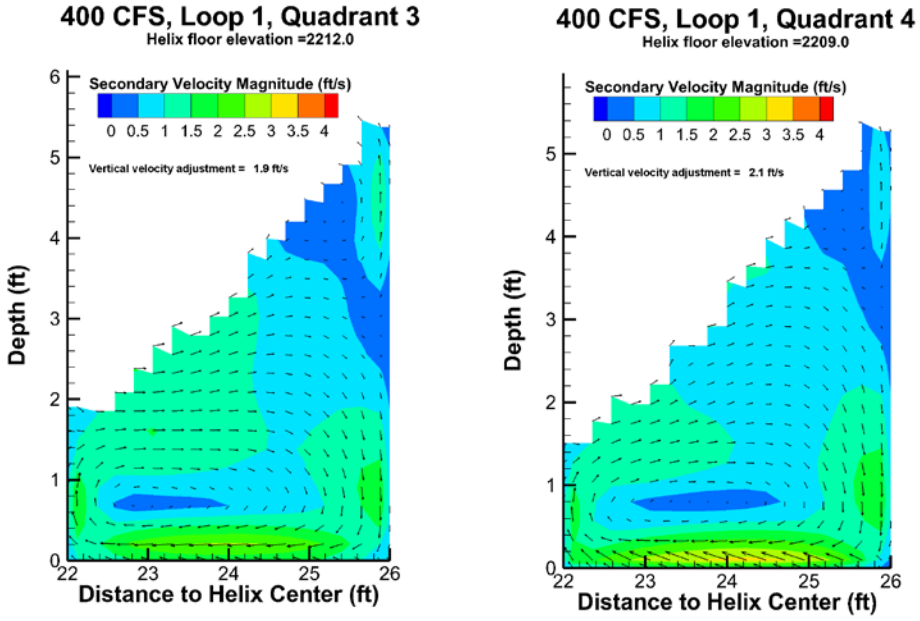

Figure 21. Helix flow cross section (fish's perspective) at 400 ft^3/s, Loop 1, quadrants 3&4

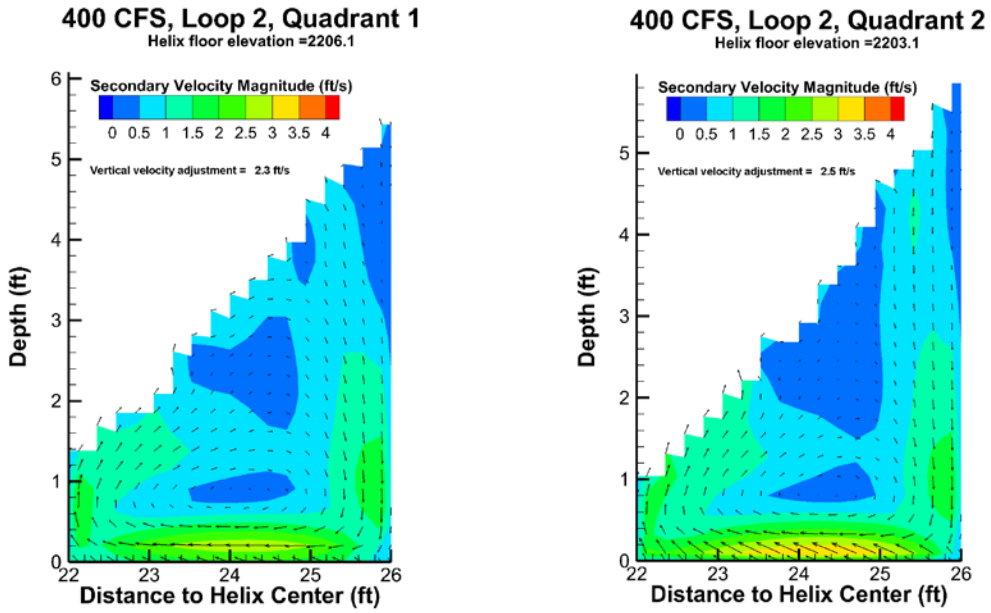

Figure 22. Helix flow cross section (fish's perspective) at 400 ft^3/s, Loop 2, quadrants 1&2

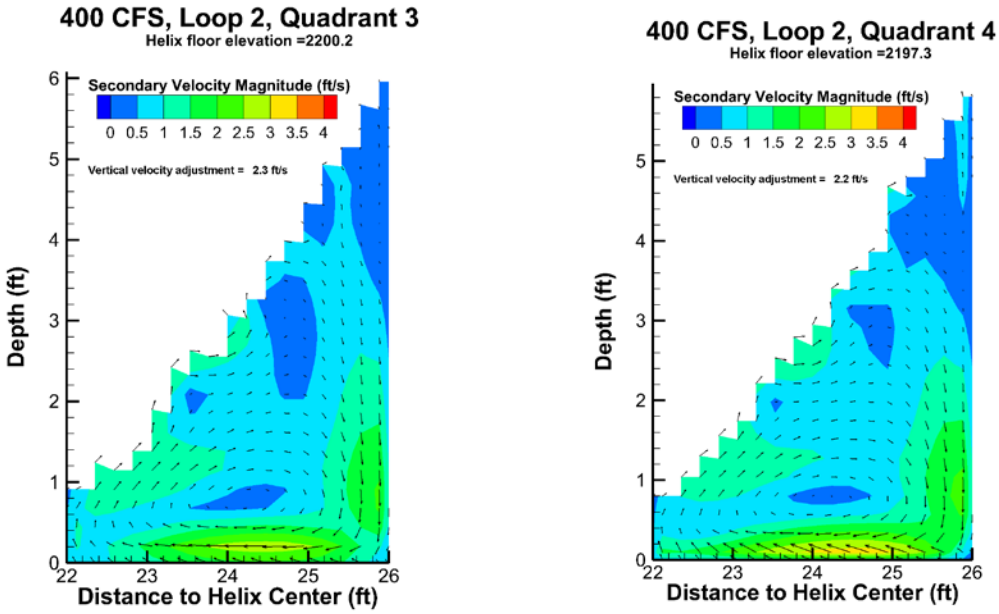

Figure 23. Helix flow cross section (fish's perspective) at 400 ft^3/s, Loop 2, quadrants 3&4

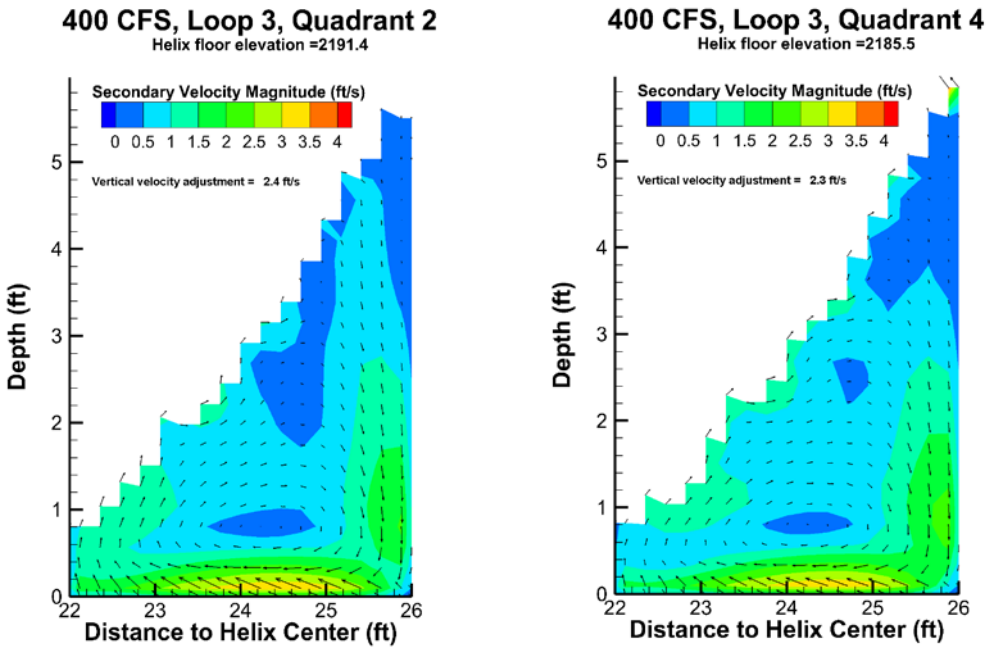

Figure 24. Helix flow cross section (fish's perspective) at 400 ft^3/s, Loop 3, quadrants 2&4

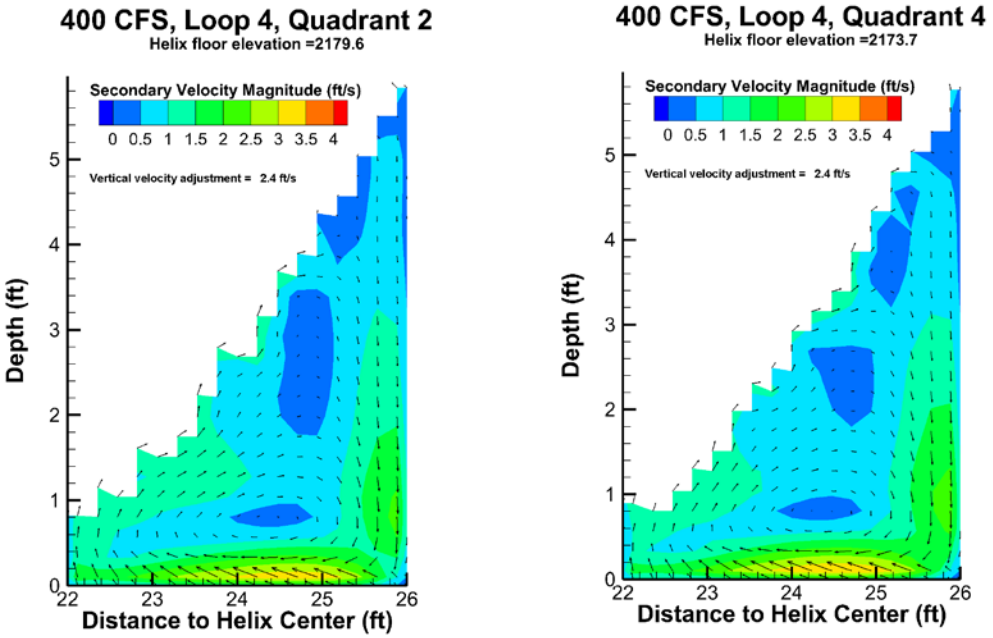

Figure 25. Helix flow cross section (fish's perspective) at 400 ft^3/s, Loop 4, quadrants 2&4

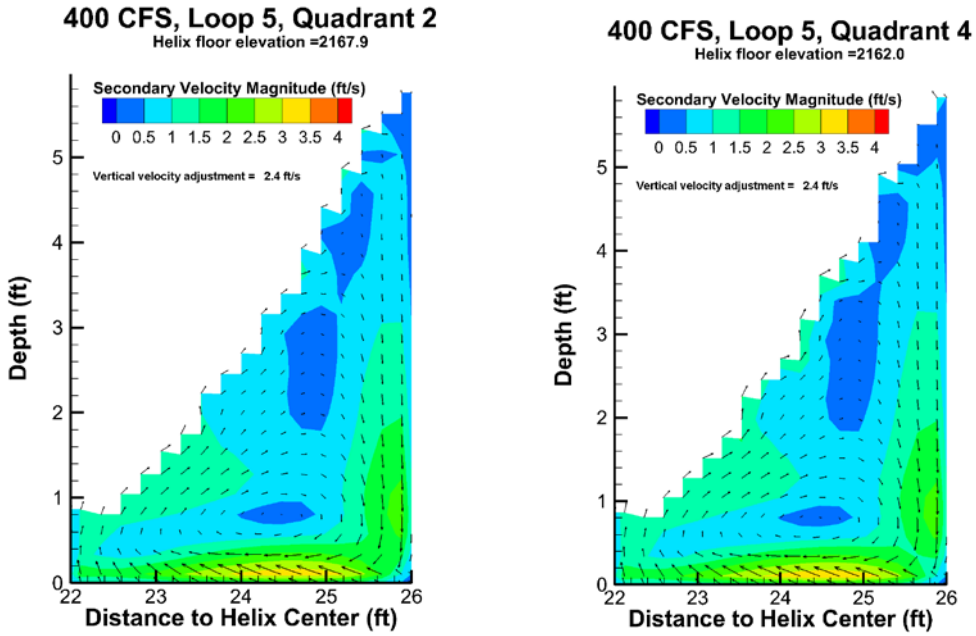

Figure 26. Helix flow cross section (fish's perspective) at 400 ft^3/s, Loop 5, quadrants 2&4

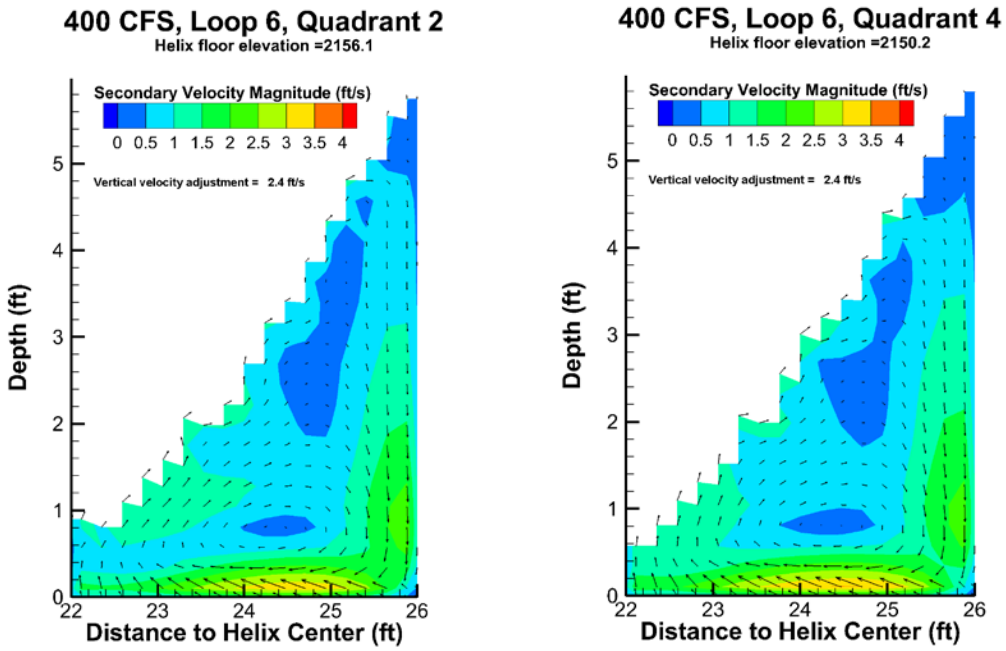

Figure 27. Helix flow cross section (fish's perspective) at 400 ft^3/s, Loop 6, quadrants 2&4

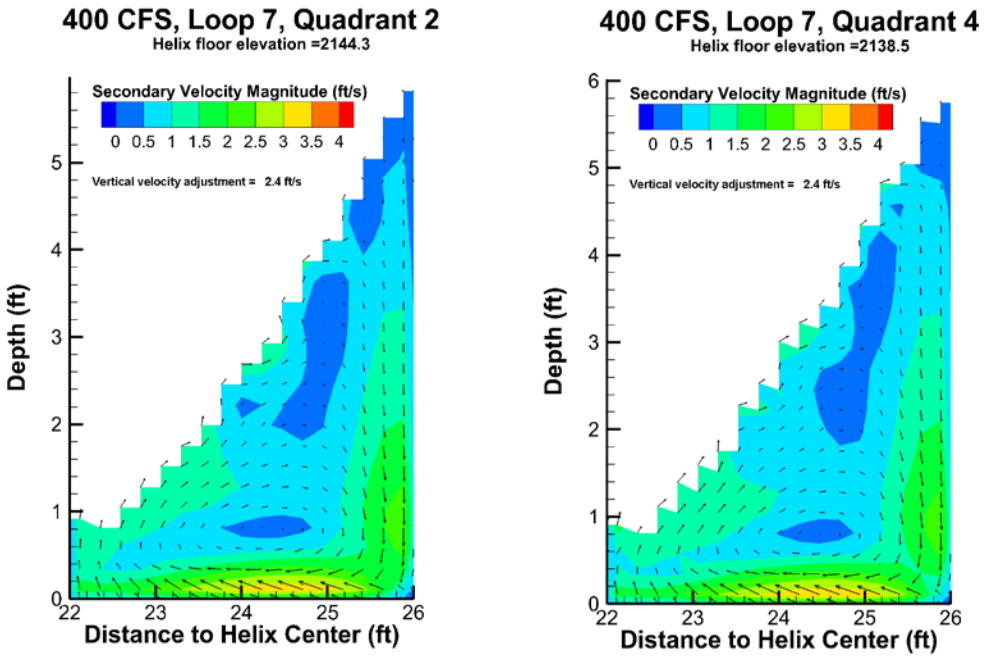

Figure 28. Helix flow cross section (fish's perspective) at 400 ft^3/s, Loop 7, quadrants 2&4

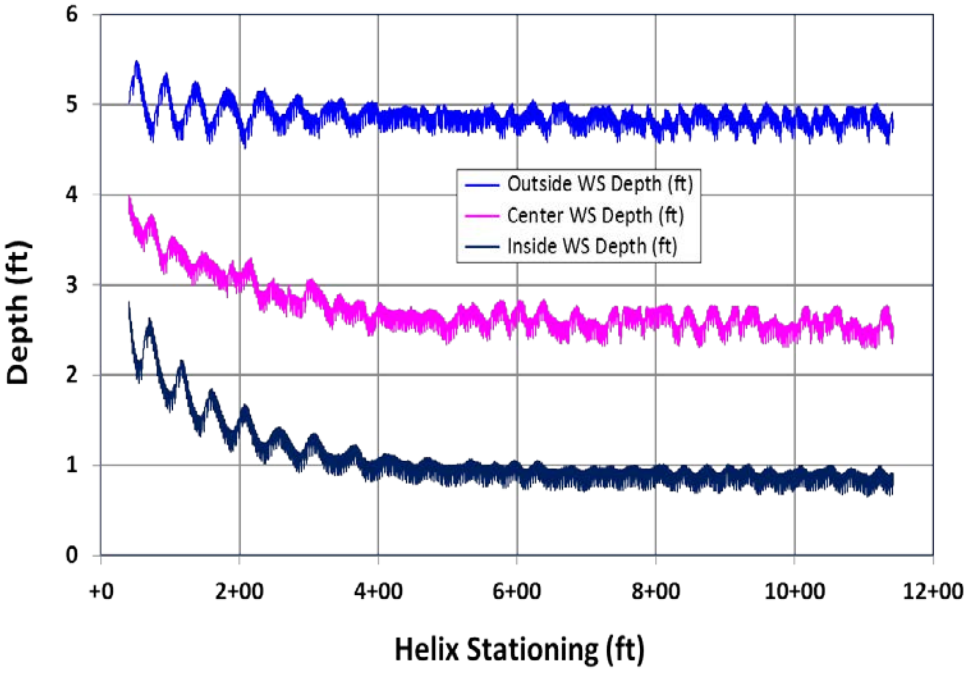

Figure 29. Helix chute flow depths at 400 ft^3/s.

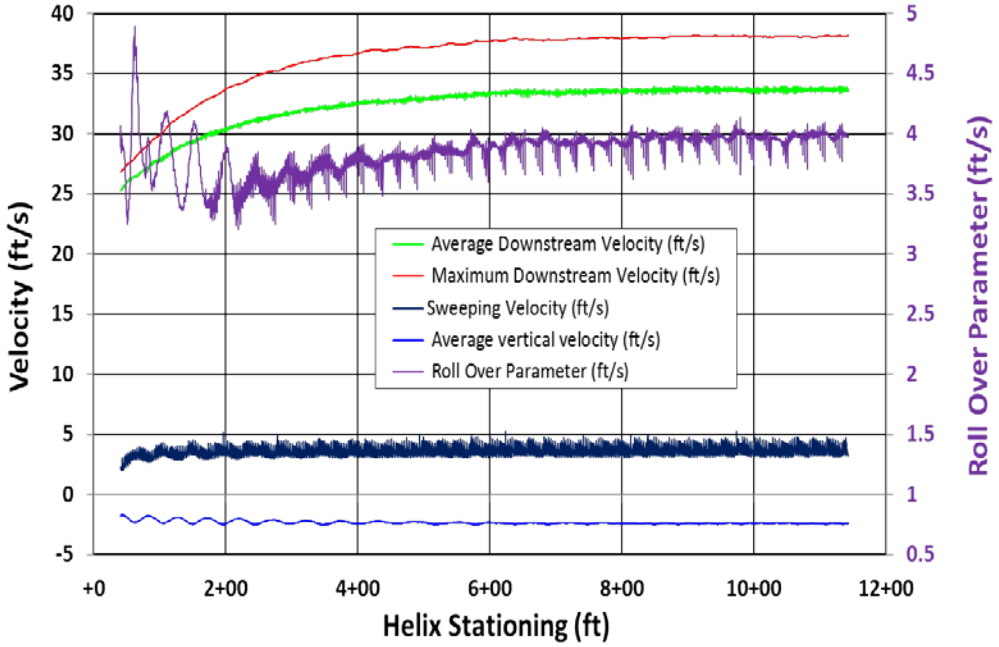

Figure 30. Helix chute flow velocities and roll over parameter (ROP) at 400 ft^3/s.

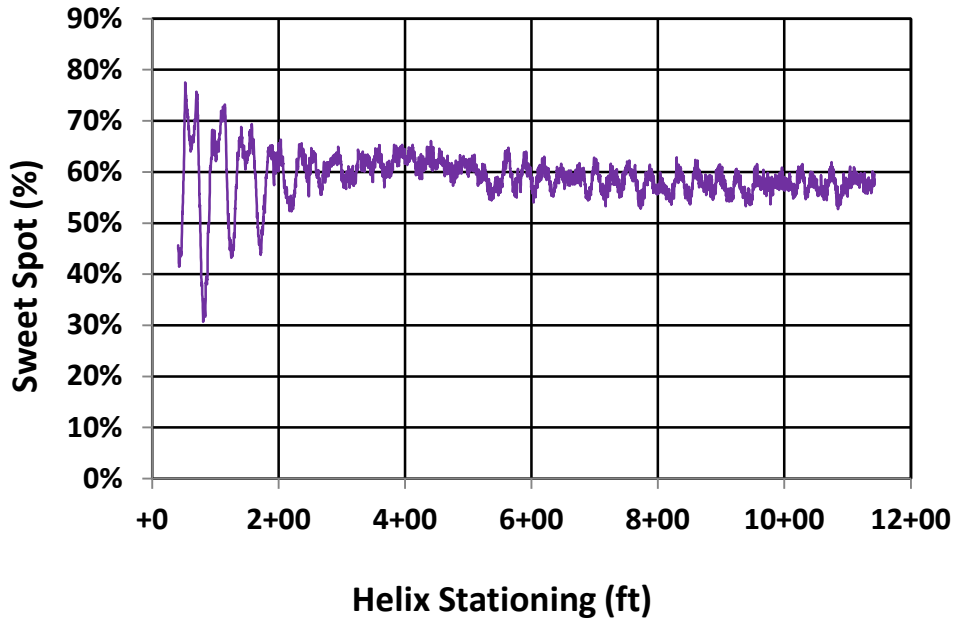

Figure 31. Helix chute sweet spot percentage at 400 ft^3/s.

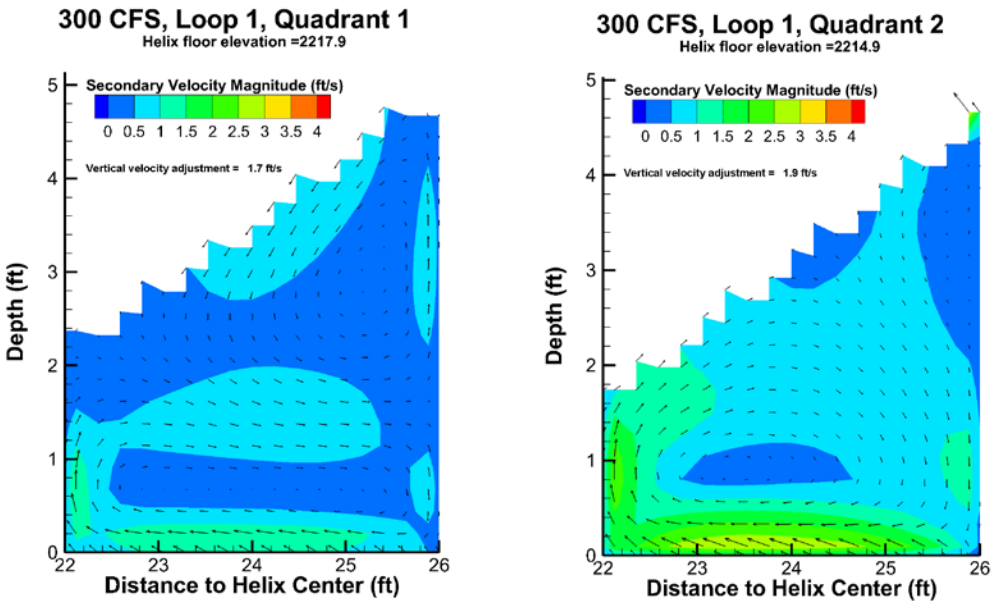

Figure 32. Helix flow cross section (fish's perspective) at 300 ft^3/s, Loop 1, quadrants 1&2

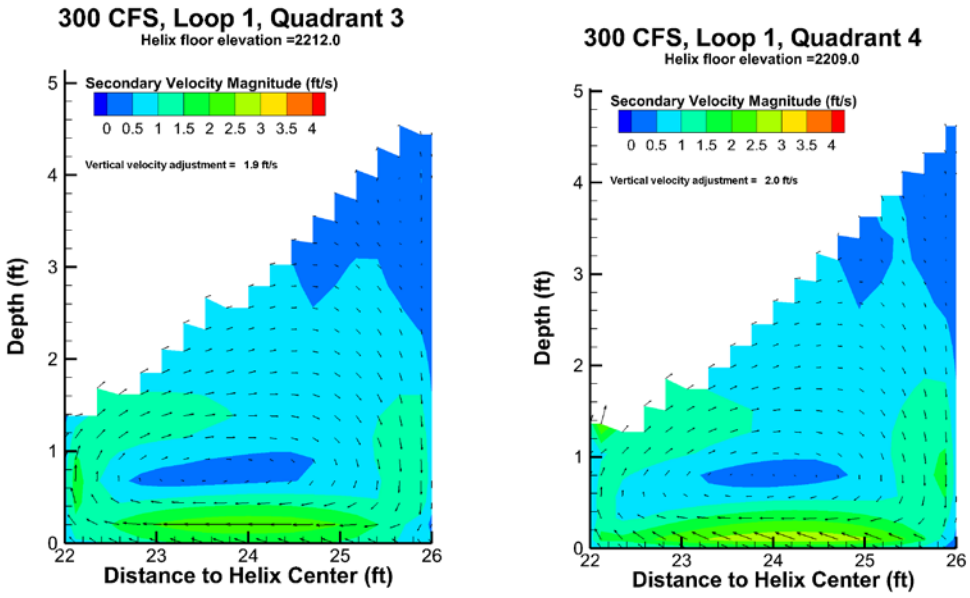

Figure 33. Helix flow cross section (fish's perspective) at 300 ft^3/s, Loop 1, quadrants 3&4

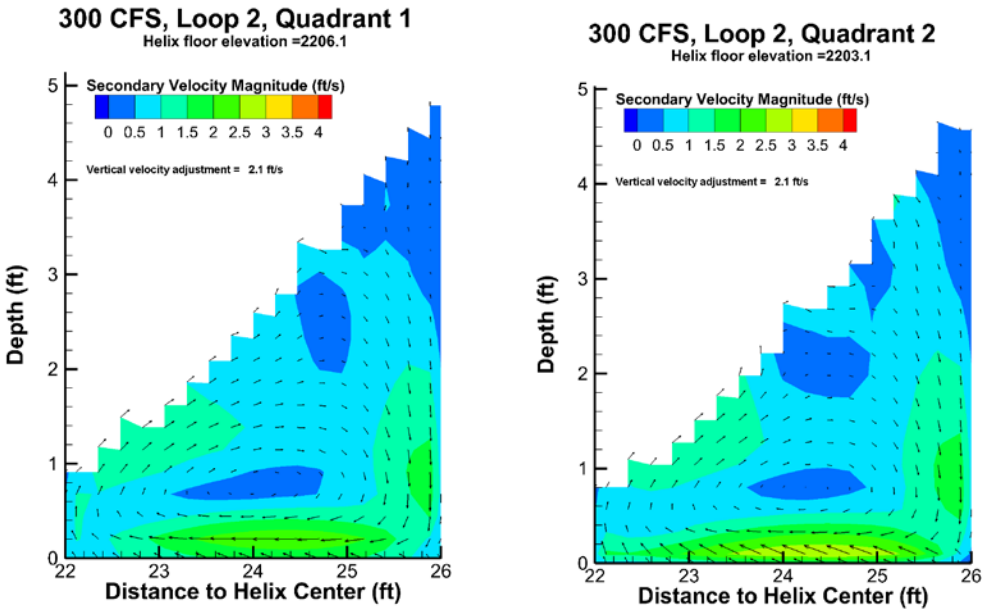

Figure 34. Helix flow cross section (fish's perspective) at 300 ft^3/s, Loop 2, quadrants 1&2

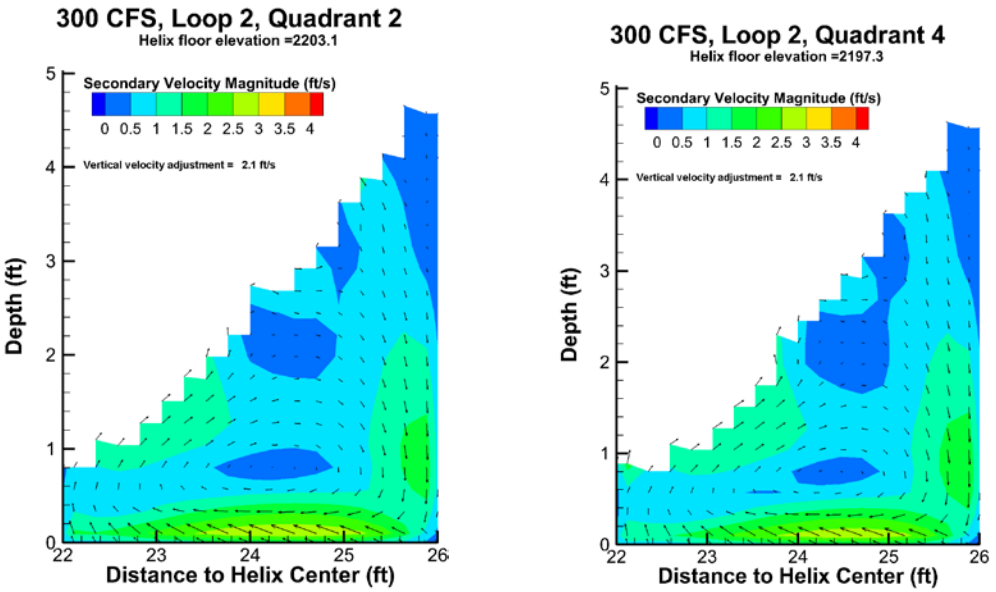

Figure 35. Helix flow cross section (fish's perspective) at 300 ft^3/s, Loop 2, quadrants 3&4

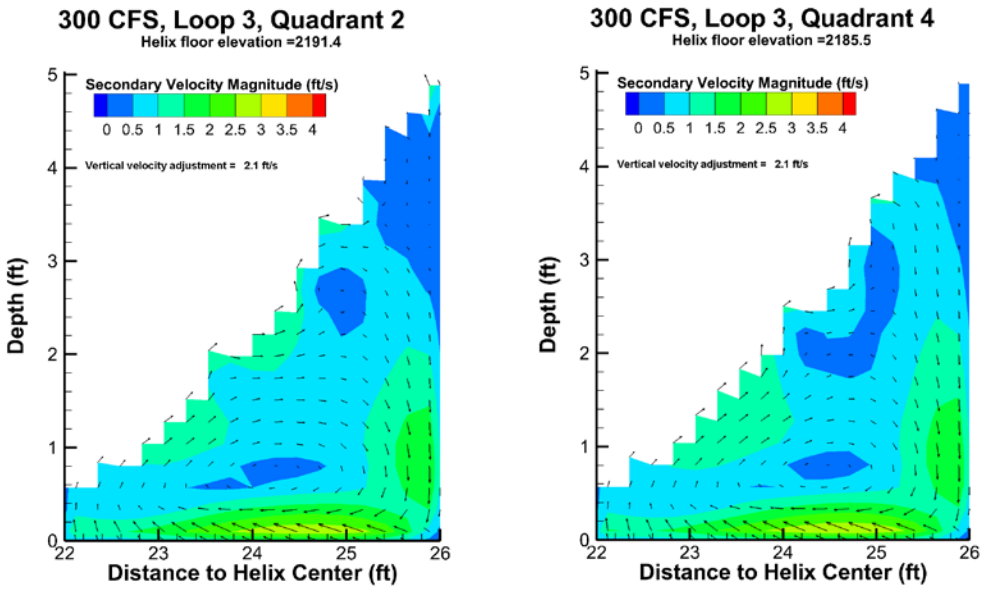

Figure 36. Helix flow cross section (fish's perspective) at 300 ft^3/s, Loop 3, quadrants 2&4

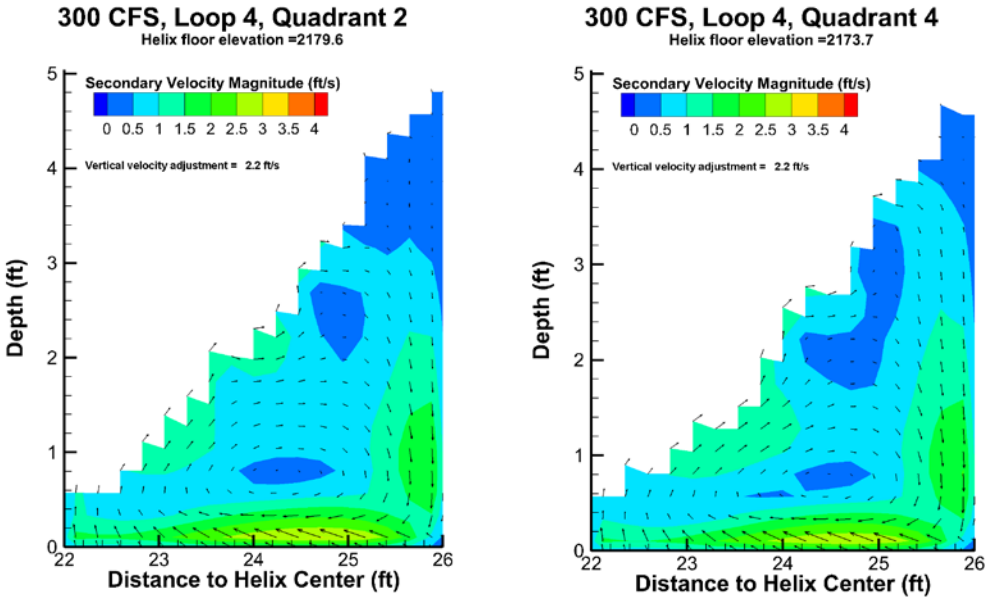

Figure 37. Helix flow cross section (fish's perspective) at 300 ft^3/s, Loop 4, quadrants 2&4

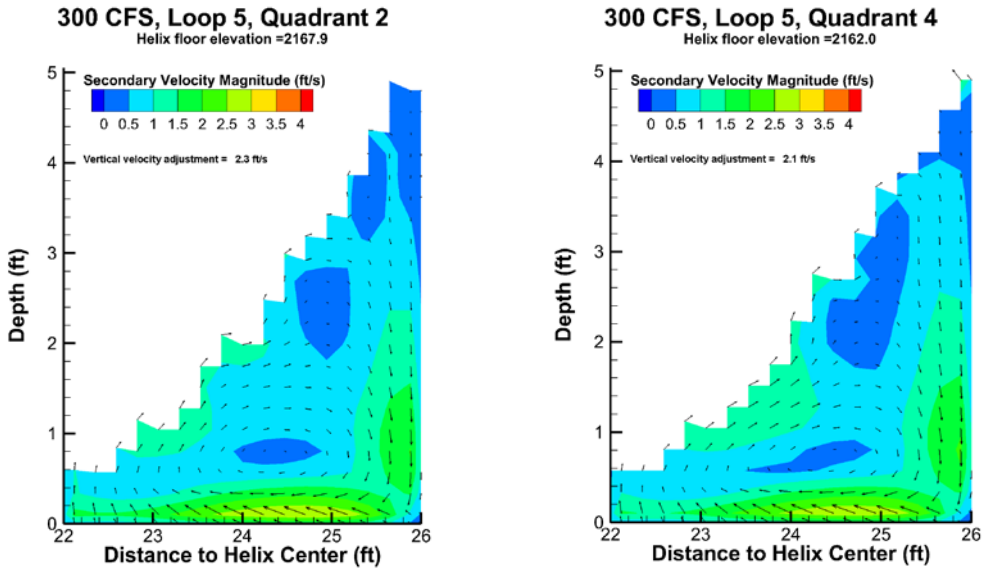

Figure 38. Helix flow cross section (fish's perspective) at 300 ft^3/s, Loop 5, quadrants 2&4

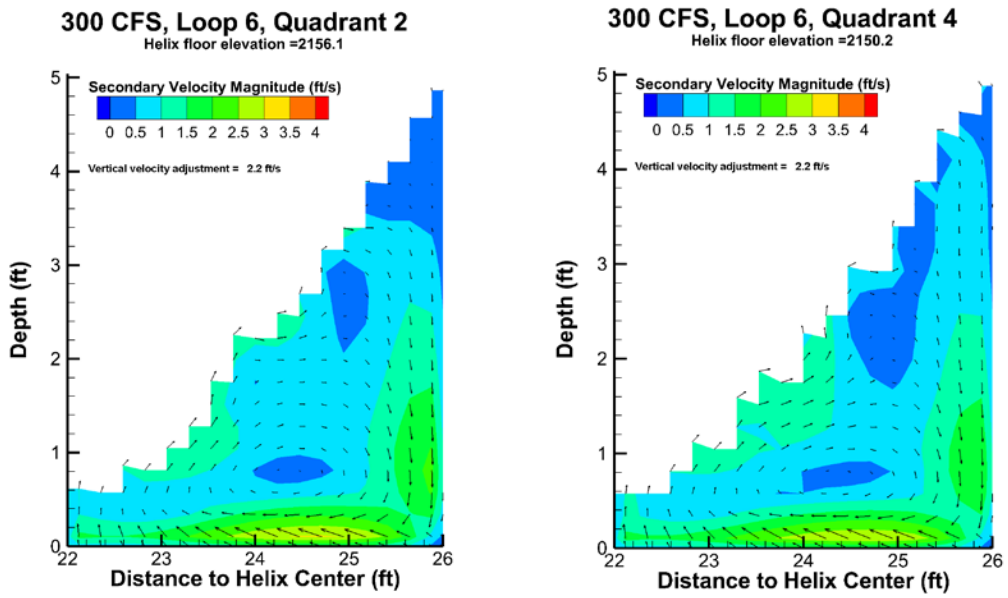

Figure 39. Helix flow cross section (fish's perspective) at 300 ft^3/s, Loop 6 quadrants 2&4

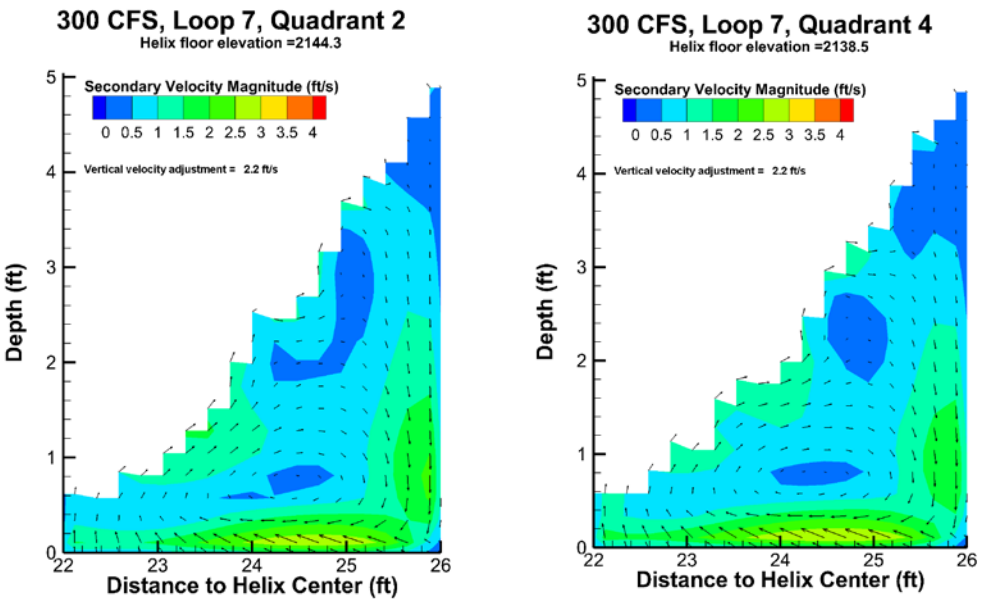

Figure 40. Helix flow cross section (fish's perspective) at 300 ft^3/s, Loop 7, quadrants 2&4

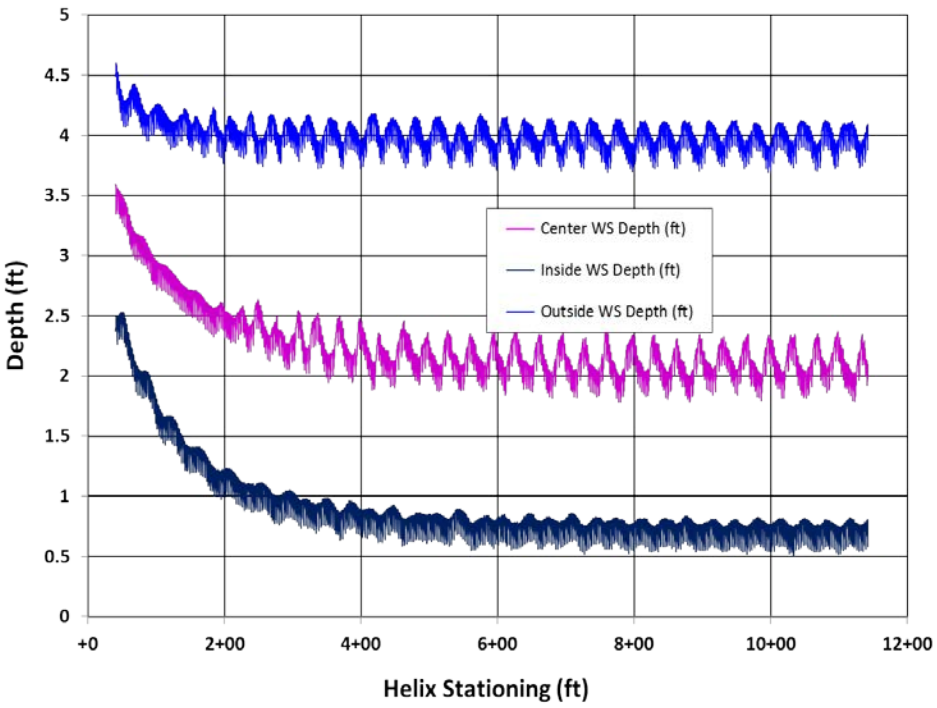

Figure 41. Helix chute flow depths at 300 ft^3/s.

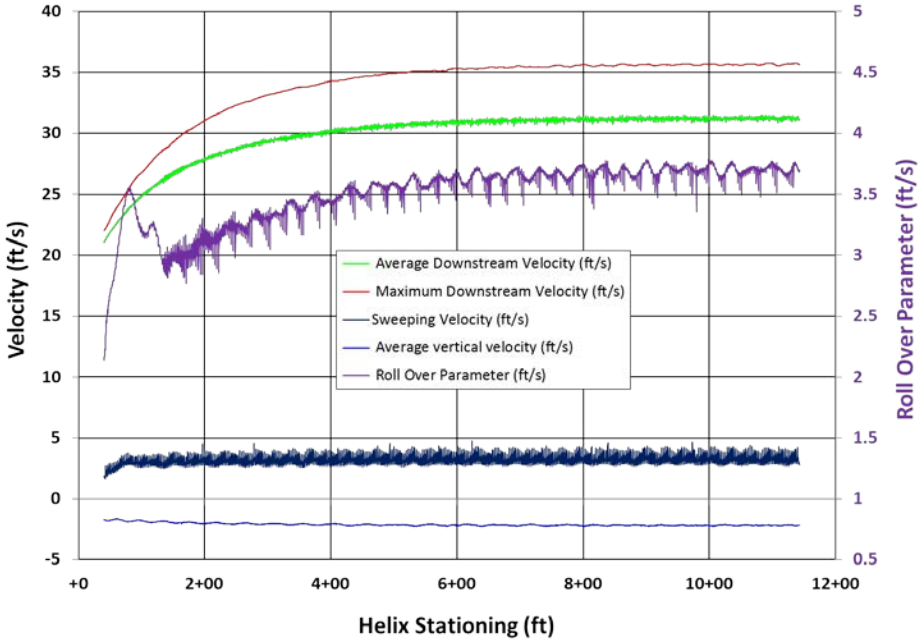

Figure 42. Helix chute flow velocities and roll over parameter (ROP) at 300 ft^3/s

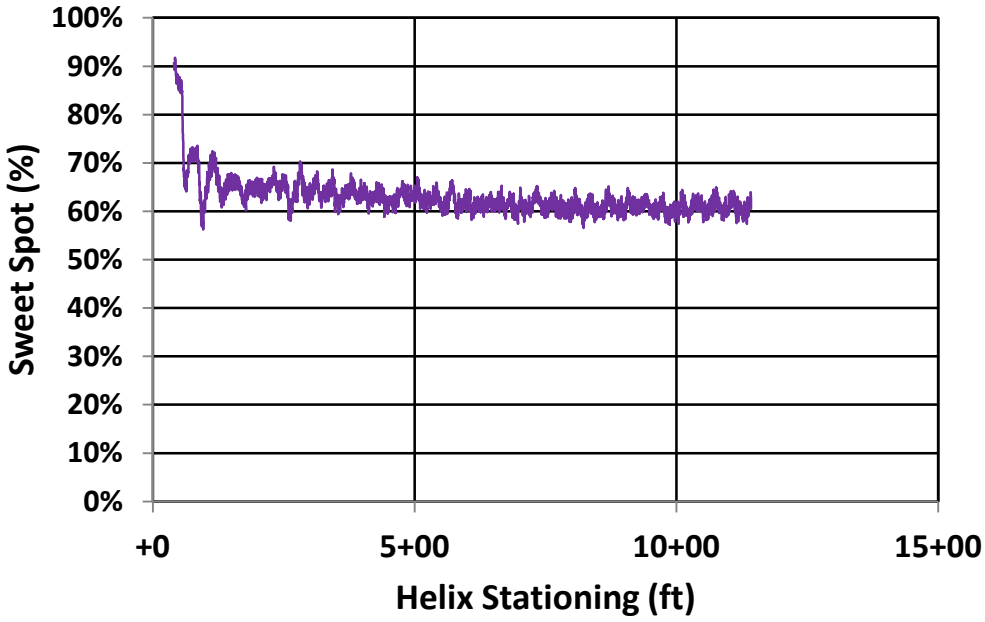

Figure 43. Helix chute sweet spot percentage at 300 ft^3/s.

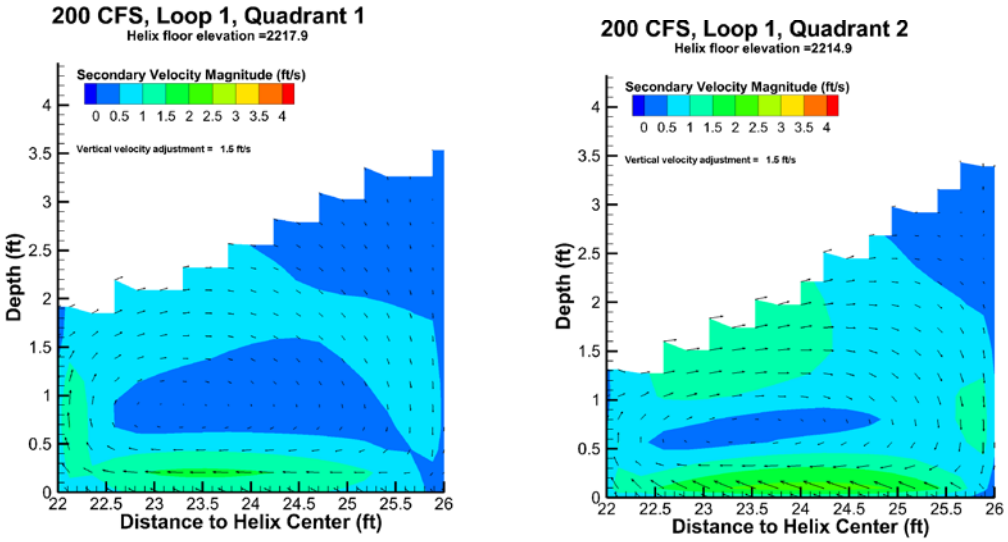

Figure 44. Helix flow cross section (fish's perspective) at 200 ft^3/s, Loop 1, quadrants 1&2

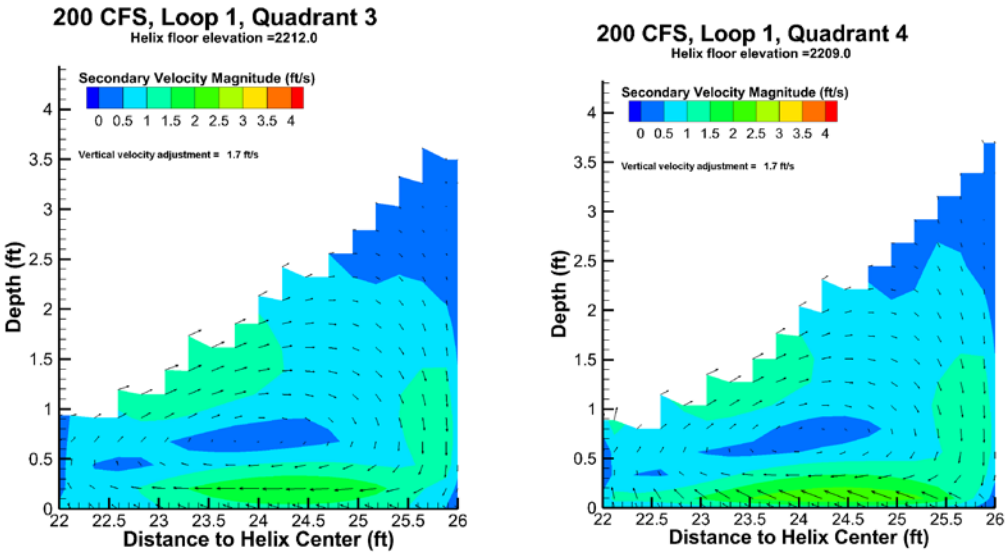

Figure 45. Helix flow cross section (fish's perspective) at 200 ft^3/s, Loop 1, quadrants 3&4

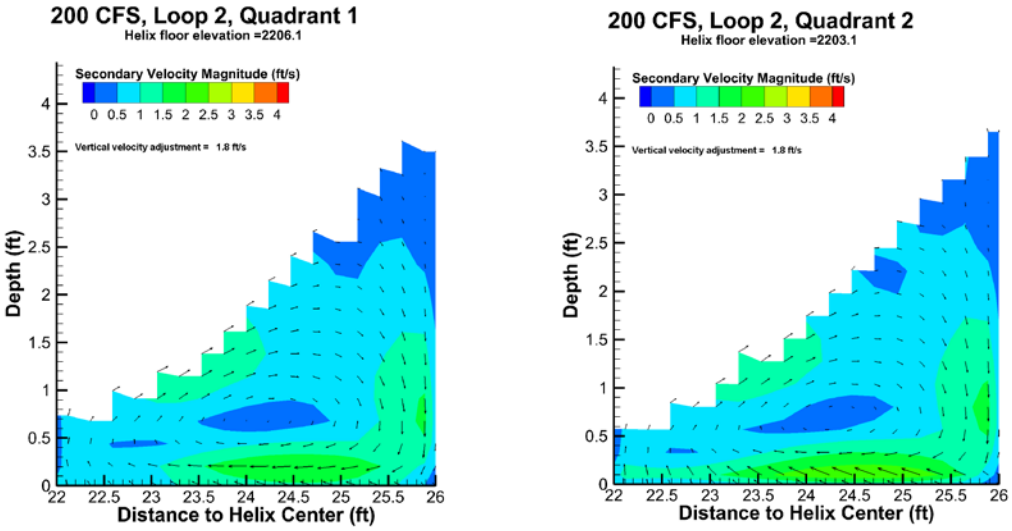

Figure 46. Helix flow cross section (fish's perspective) at 200 ft^3/s, Loop 2, quadrants 1&2

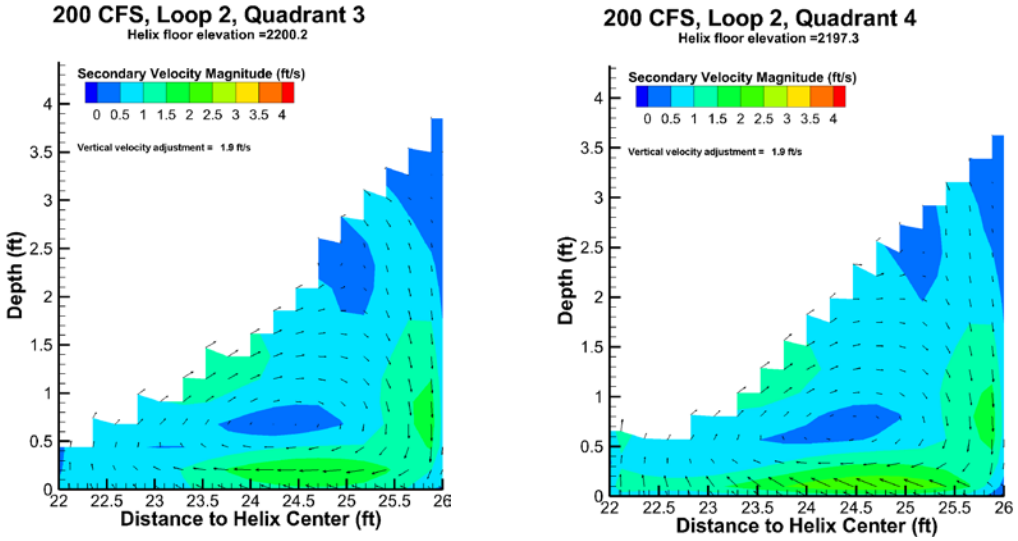

Figure 47. Helix flow cross section (fish's perspective) at 200 ft^3/s, Loop 2, quadrants 3&4

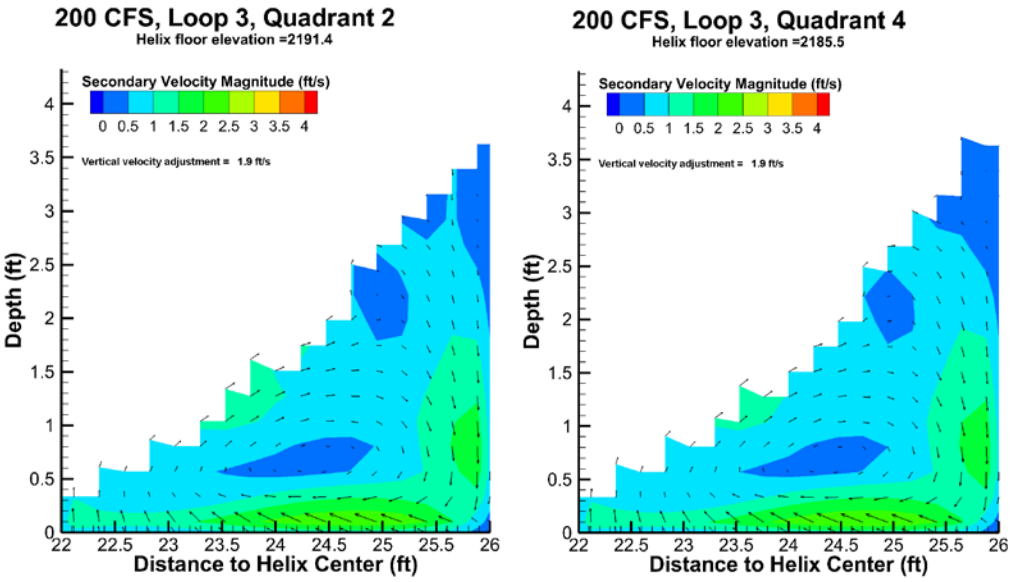

Figure 48. Helix flow cross section (fish's perspective) at 200 ft^3/s, Loop 3, quadrants 2&4

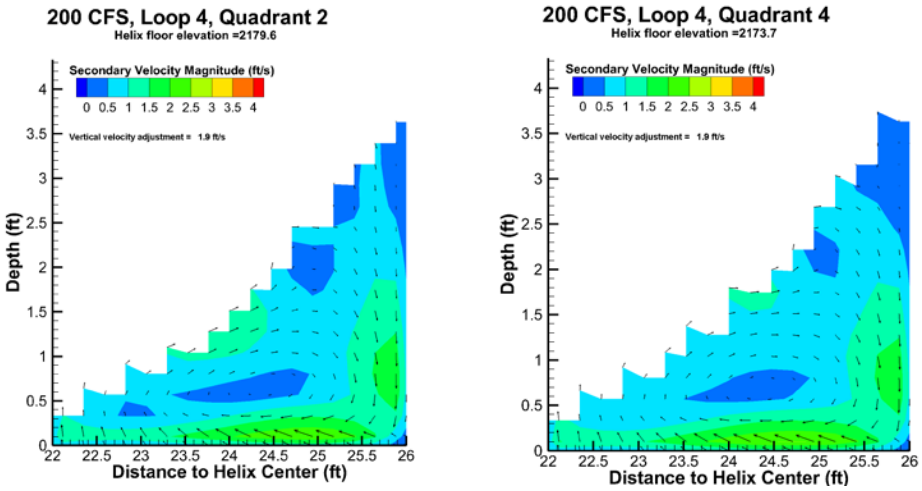

Figure 49. Helix flow cross section (fish's perspective) at 200 ft^3/s, Loop 4, quadrants 2&4

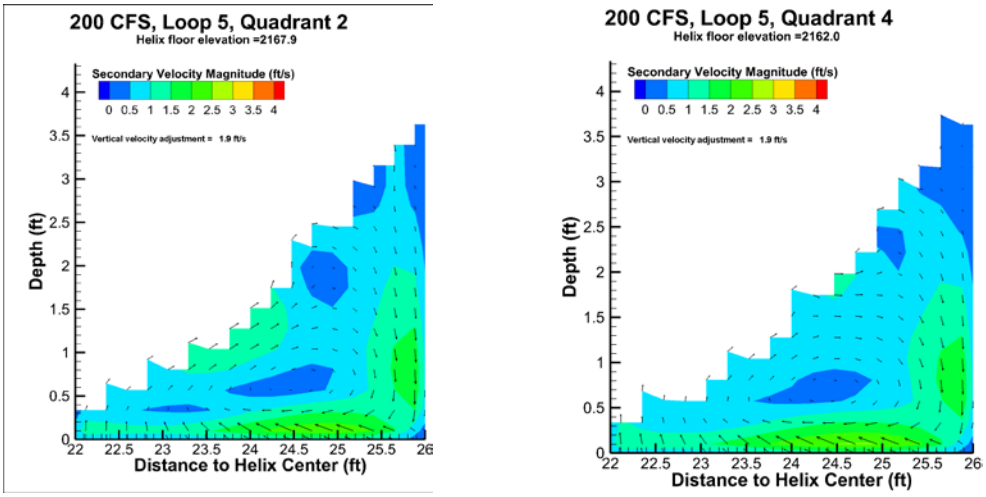

Figure 50. Helix flow cross section (fish's perspective) at 200 ft^3/s, Loop 5, quadrants 2&4

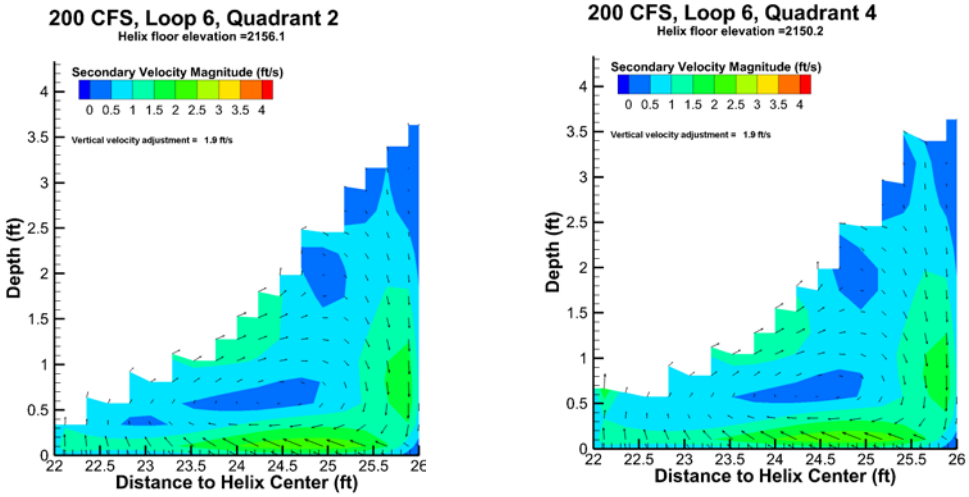

Figure 51. Helix flow cross section (fish's perspective) at 200 ft^3/s, Loop 6, quadrants 2&4

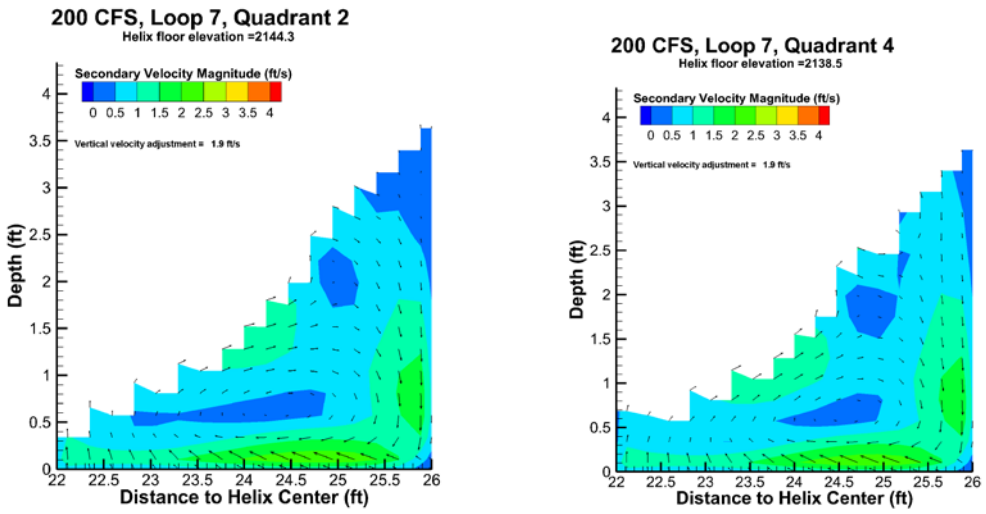

Figure 52. Helix flow cross section (fish's perspective) at 200 ft^3/s, Loop 7, quadrants 2&4

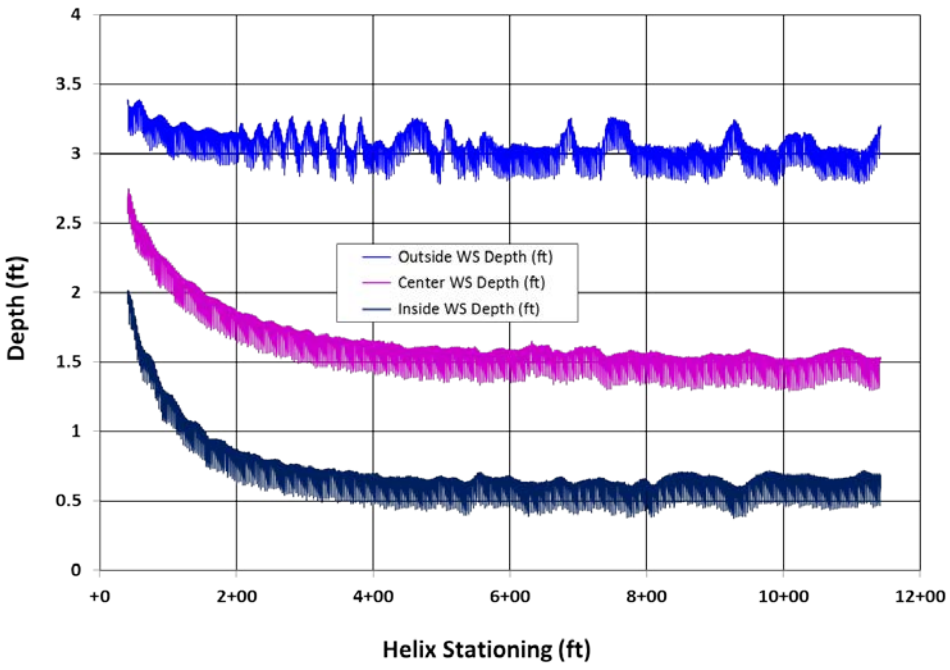

Figure 53. Helix chute flow depths at 200 ft^3

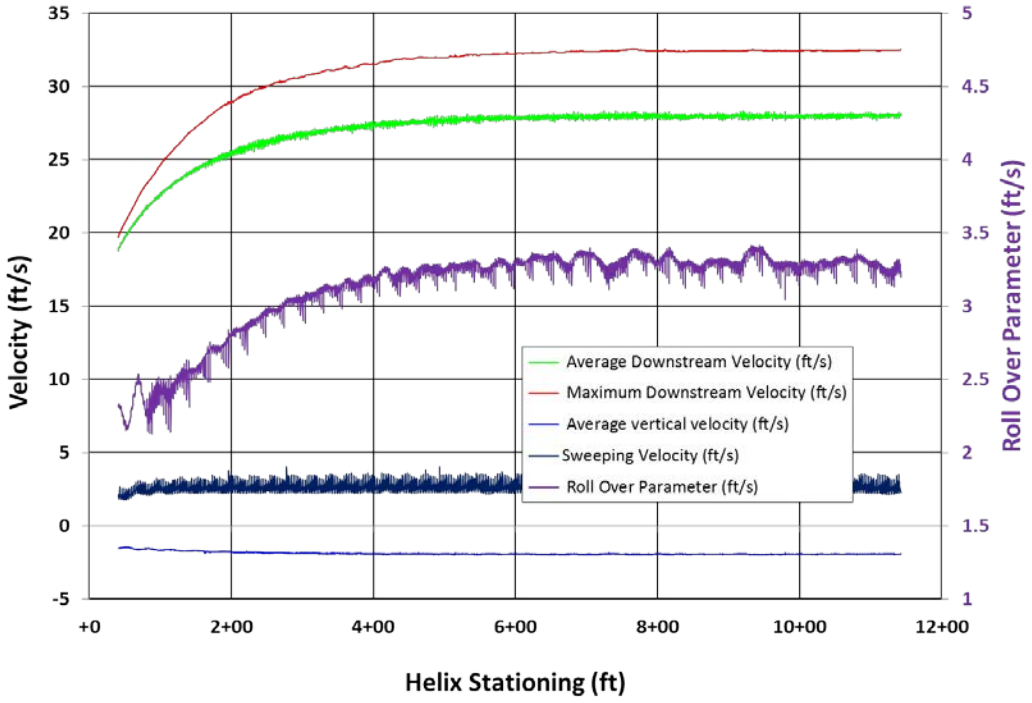

Figure 54. Helix chute flow velocities and roll over parameter (ROP) at 200 ft^3/s

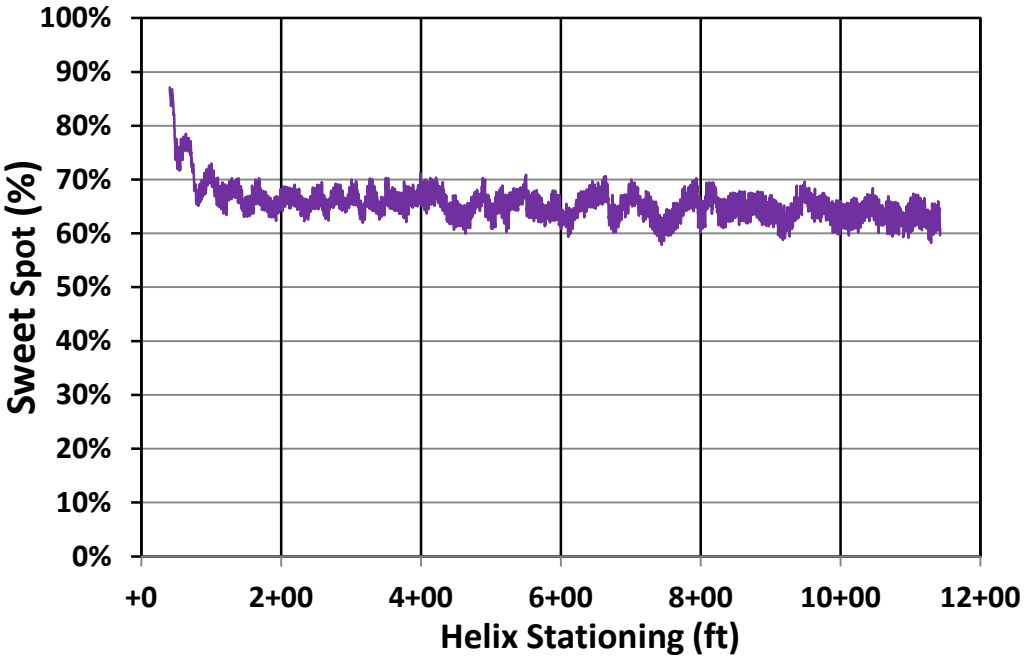

Figure 55. Helix chute sweet spot percentage at 200 ft^3/s.

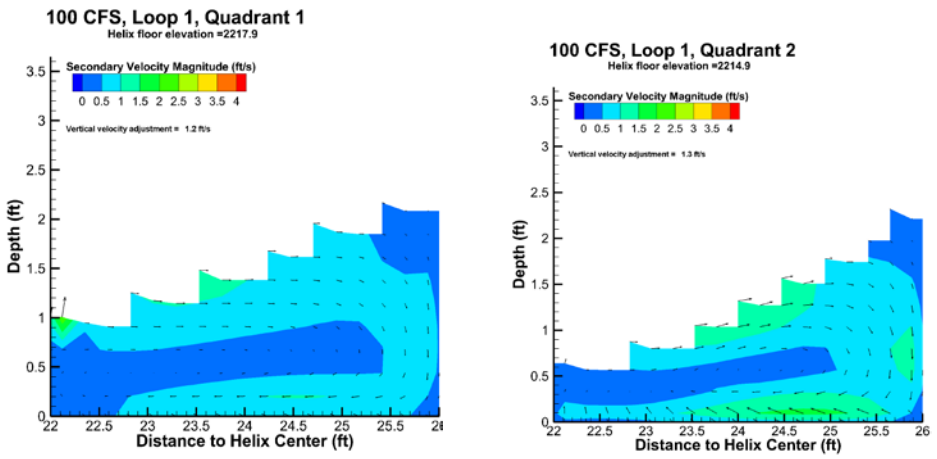

Figure 56. Helix flow cross section (fish's perspective) at 100 ft^3/s, Loop 1, quadrants 1&2

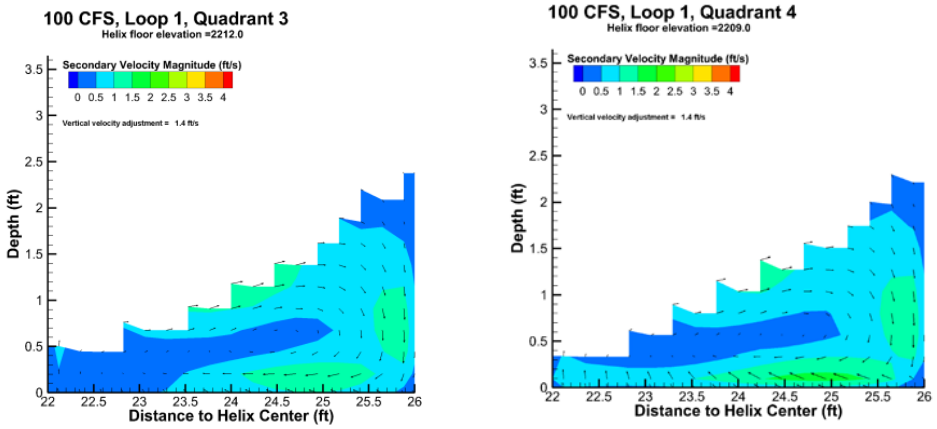

Figure 57. Helix flow cross section (fish's perspective) at 100 ft^3/s, Loop 1, quadrants 3&4

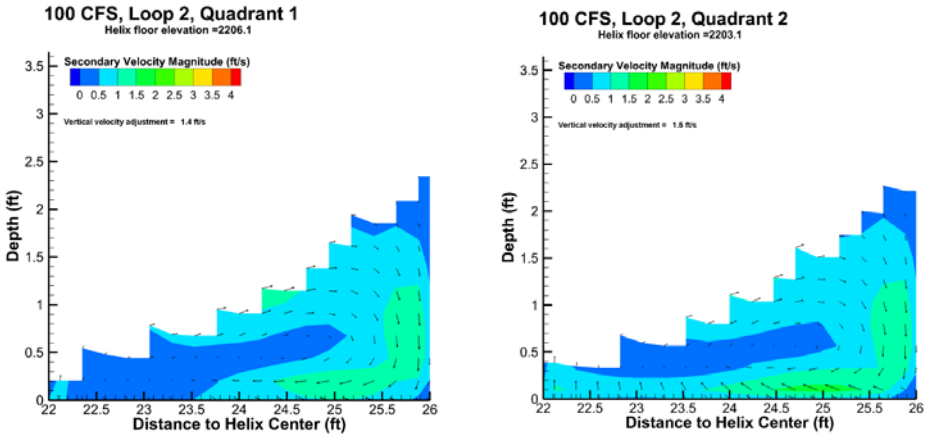

Figure 58. Helix flow cross section (fish's perspective) at 100 ft^3/s, Loop 2, quadrants 1&2

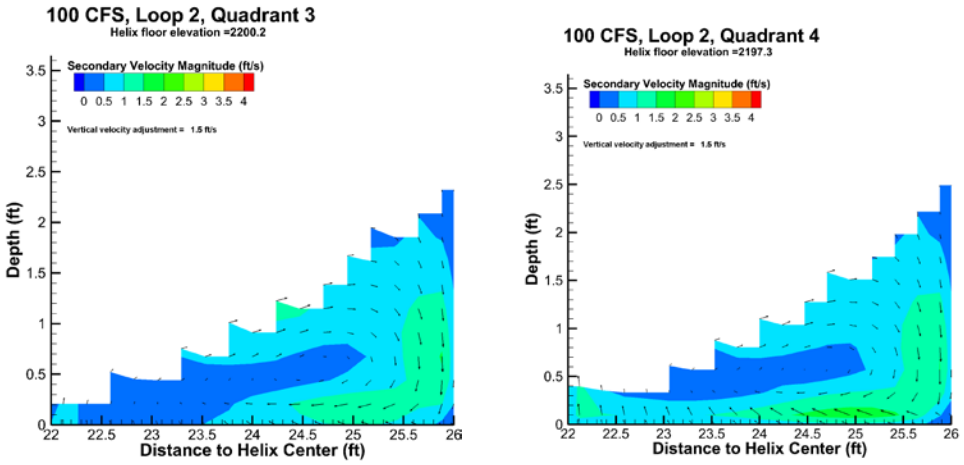

Figure 59. Helix flow cross section (fish's perspective) at 100 ft^3/s, Loop 2, quadrants 3&4

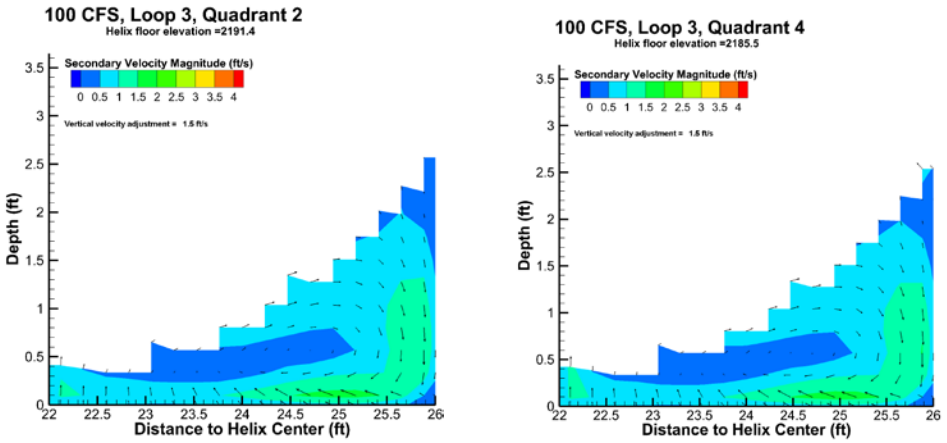

Figure 60. Helix flow cross section (fish's perspective) at 100 ft^3/s, Loop 3, quadrants 2&4

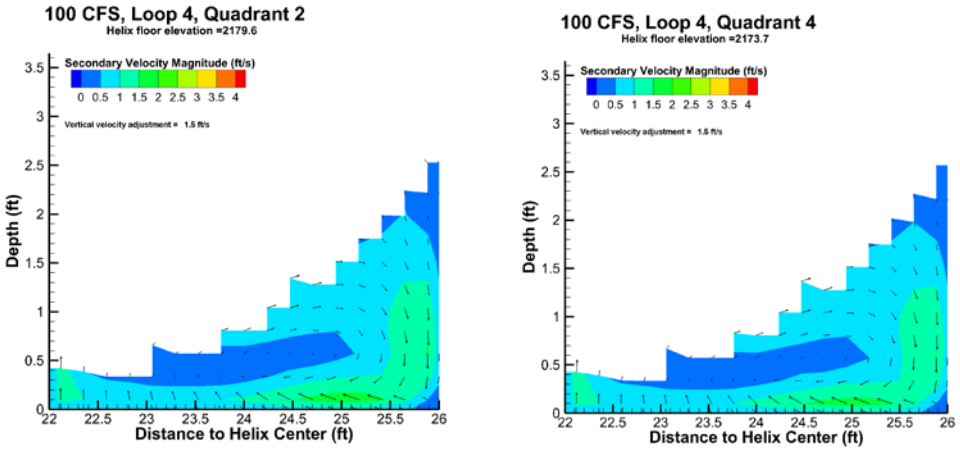

Figure 61. Helix flow cross section (fish's perspective) at 100 ft^3/s, Loop 4, quadrants 2&4

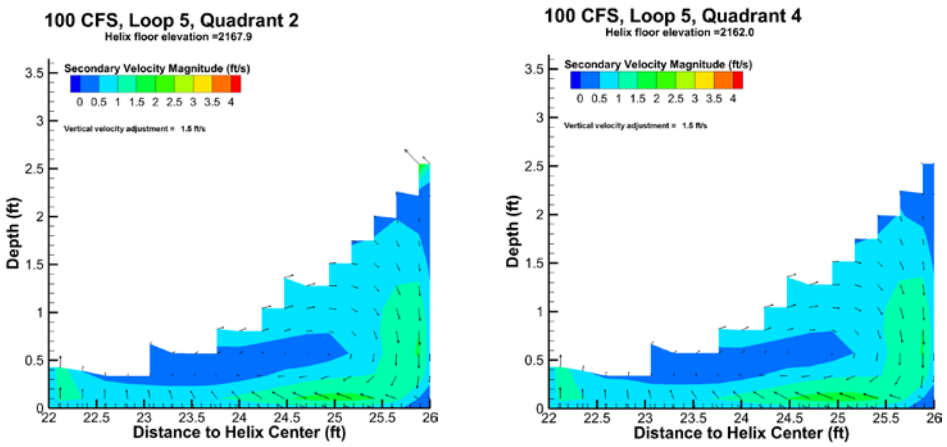

Figure 62. Helix flow cross section (fish's perspective) at 100 ft^3/s, Loop 5, quadrants 2&4

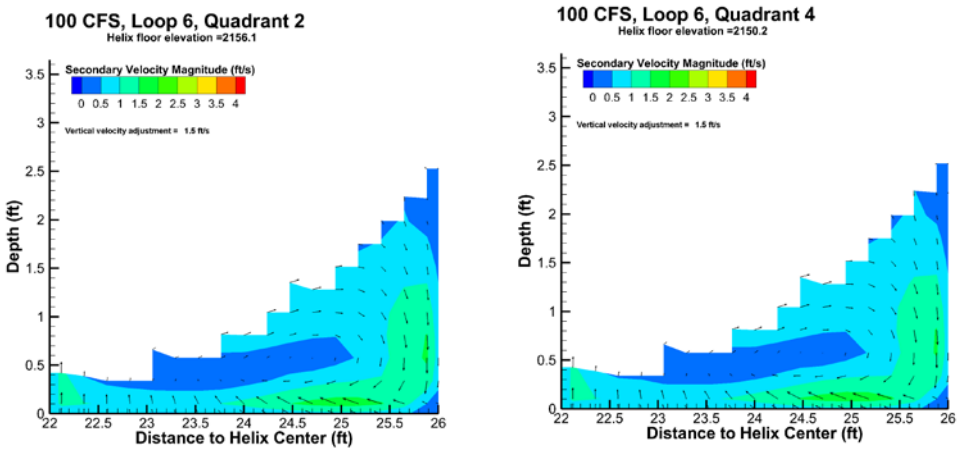

Figure 63. Helix flow cross section (fish's perspective) at 100 ft^3/s, Loop 6, quadrants 2&4

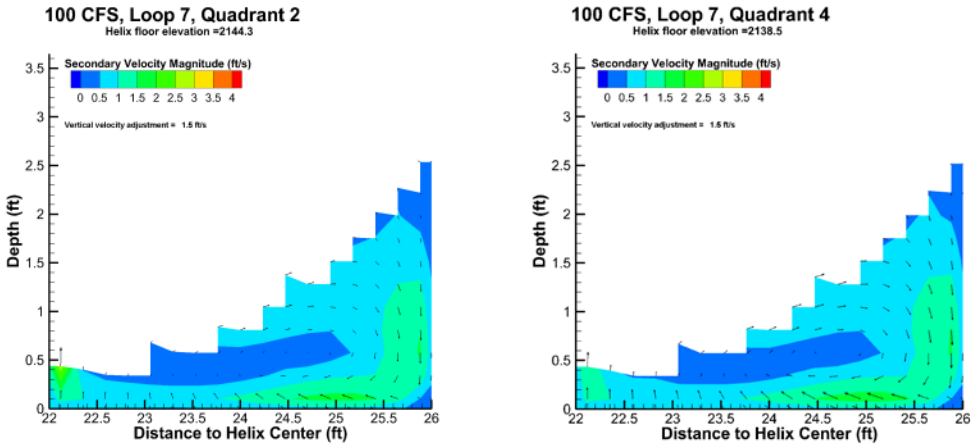

Figure 64. Helix flow cross section (fish's perspective) at 100 ft^3/s, Loop 7, quadrants 2 and 4.

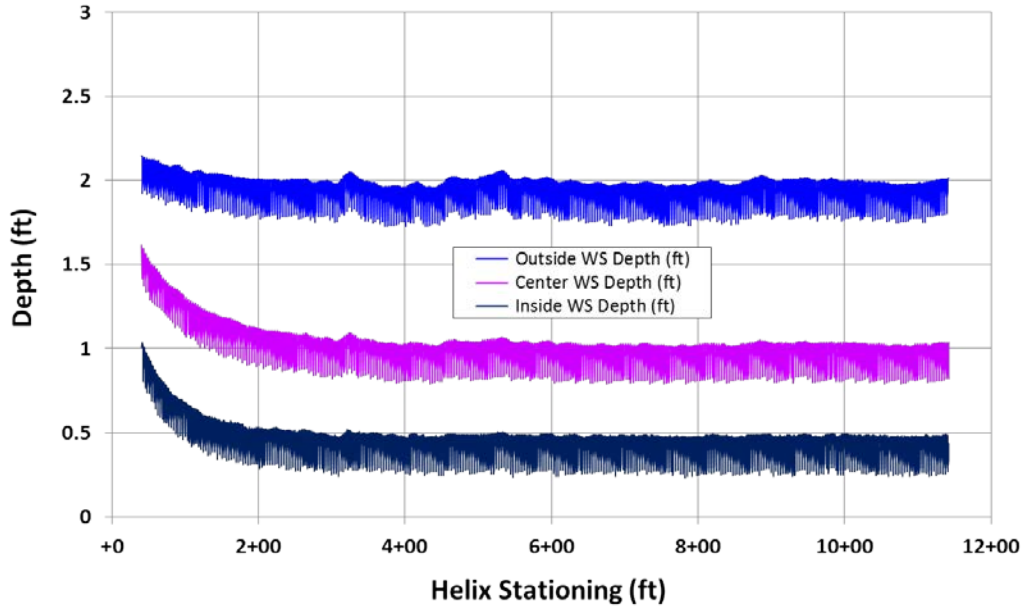

Figure 65. Helix chute flow depths at 100 ft^3/s.

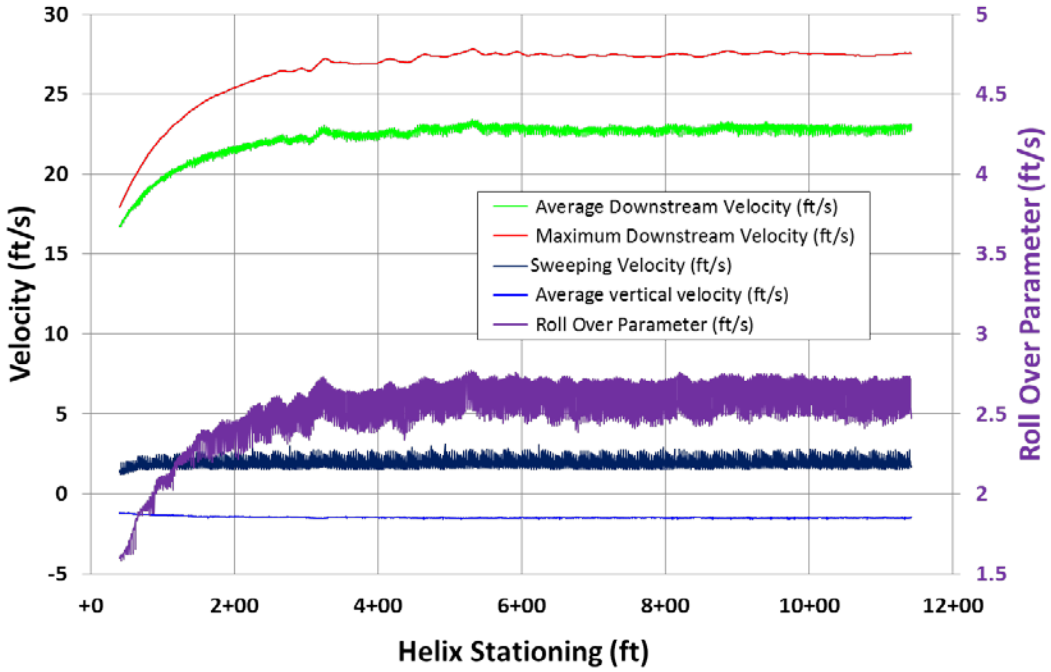

Figure 66. Helix chute flow velocities and roll over parameter (ROP) at 100 ft^3/s.

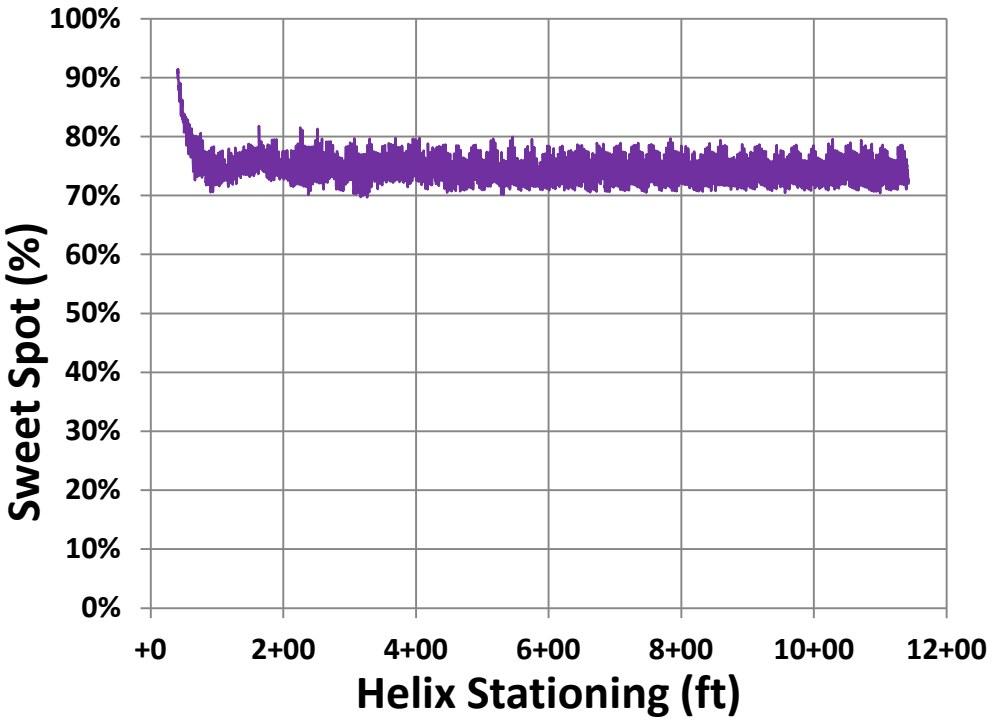

Figure 67. Helix sweet spot percentage at 100 ft^3/s.

Physical Model

The purposes of the physical model were to:

- Verify the performance of the numerical model and refine it if necessary. This step was important to ensure accurate representation of the prototype structure since various assumptions were made when developing the numerical model.

- Evaluate flow conditions in the helix flume to ensure no excessive sloshing or roll-over.

- Determine flow depths and velocities within the helix chute.

The physical hydraulic model was constructed at a 1:9.5 geometric scale. Similitude between the model and the prototype is achieved when the ratio of the major forces controlling the physical processes are the same. Since gravitational and inertial forces dominate open channel flow, Froude scale similitude was used to establish a kinematic relationship between the model and the prototype. The Froude number is expressed as

$$F_r = \frac{v}{\sqrt{gd}}$$

where v = velocity, g = gravitational acceleration, and d = flow depth. When equal Froude numbers are maintained between the model and the prototype, specific scaling relationships exist between model and prototype values of key flow parameters. In the equations that follow, the *r* subscript refers to the ratio of the prototype and model values:

Length ratio: $L_r = 9.5$

Velocity ratio: $V_r = L_r^{1/2} = (9.5)^{1/2} = 3.08$

Discharge ratio: $Q_r = L_r^{5/2} = (9.5)^{5/2} = 278.17$

The helix chute was constructed entirely out of Plexiglas so each floor and wall component was heated and molded into shape (figure 68). This was a complicated process since the floor of the helix chute is horizontal at any given cross section, meaning that the slope of the chute varies across its width with a centerline slope at 7.8%. The Plexiglas material is assumed to provide a reasonable and conservative representation of the scaled down roughness of concrete to be used for construction of the prototype. Once the components were set to shape, they were assembled and installed in the Denver laboratory (figure 69). Only 3½ loops of the helix chute were included in the physical model since

the numerical model had shown that flow within the flume stabilized after about 2½ loops.

Figure 68. Plexiglas components for helix model setting up to mold into shape.

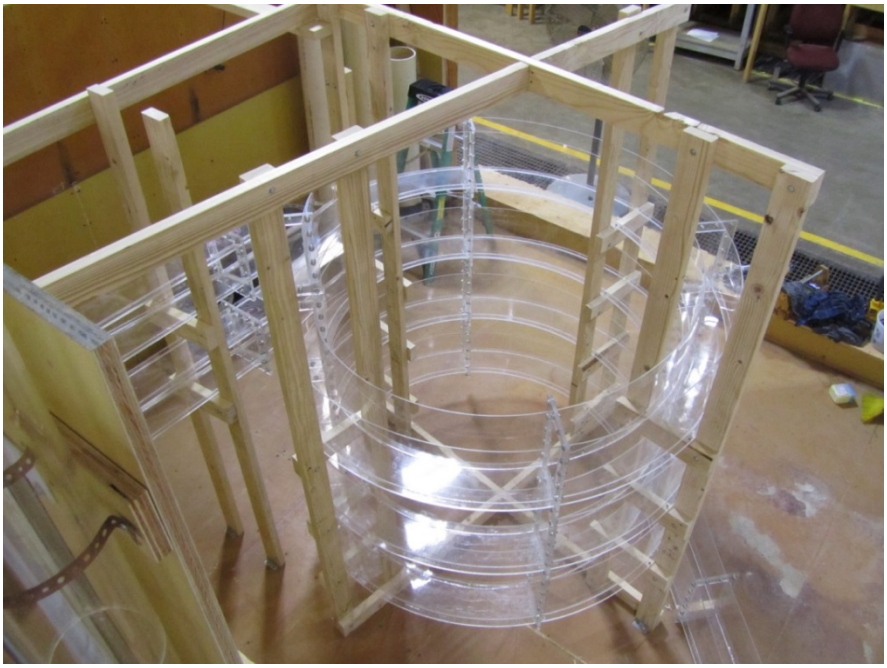

Figure 69. Helix Plexiglas components assembled and installed.

Initial evaluation of flow conditions in the helix chute were made with visual observations while operating at a flow rate of 400 ft^3/s (figures 70 and 71). There were no obvious indications of excessive sloshing or rollover throughout the length of the flume at all three flow rates. Beads injected into the flow appeared to maintain their relative position to the sidewall and floor as they moved down the flume. Strings inserted into the flow also stayed on a downstream track without excessive swirling. These observations appeared to indicate that there were no excessive rotational currents occurring within the body of flow.

Figure 70. Helix operating at 400 ft^3/s.

Figure 71. String in flow at 400 ft^3/s maintains downstream track.

Average velocity and flow depth were measured at cross sections at every half loop of the helix chute. Flow depths were measured next to the inside and outside chute wall through the Plexiglas panels for 300 ft^3/s and 400 ft^3/s (figure 72). Velocity was measured at each cross section, at quarter points across the width of the flume and at 1 ft increments (prototype dimensions) from the bottom of the flume with a Swoffer propeller meter, The average velocity at each quarter point and the overall average of the quarter-point velocities at each measurement location are presented in figures 73-74. Since it was difficult to position the meter, for each measurement location, the Swoffer propeller alignment was varied until a maximum velocity reading was obtained. The resulting velocities are considered to be a reasonable representation of the average velocity at each measurement location.

Figure 72 shows that the minimum flow depth near the inside wall of the helix ranges from about 0.57 ft to 0.81 ft for 300 ft^3/s and from about 0.57 ft to 1.14 ft for 400 ft^3/s. Maximum depth measured on the outside wall is 5.6 ft for 300 cfs and 6.3 ft for 400 cfs. Overall average velocity measured in the helix chute ranged from about 27 ft/s to 35 ft/s for 300 ft^3/s and from about 29 ft/s to 37 ft/s for 400 ft^3/s (figures 73 and 74). Maximum average velocity measured near the outside wall ranged from about 36 ft/s to 39 ft/s for 300 ft^3/s and from about 37 ft/s to 40 ft/s for 400 ft^3/s. Maximum velocities measured in the flume accelerate in the first half loop by about 22% and 16% for 300 ft^3/s and 400 ft^3/s respectively. In loop 3 the flow acceleration drops to 2.5% and 0.7% for 300 ft^3/s and 400 ft^3/s, respectively.

The velocities measured in the physical model were significantly higher than those measured in the initial numerical model. In addition, flow in the physical model continued to accelerate throughout the length of the chute whereas the numerical model showed that velocities stabilized after about 2½ loops. In this case the physical model was assumed to be more accurate than the numerical model since it directly represents the prototype on a scaled basis and fewer assumptions were made in the model setup. As a result of these findings, the numerical model was further analyzed and refined, as discussed in the previous section (Helix Chute Model Refinement), until velocities in the numerical model matched reasonably well with the physical model.

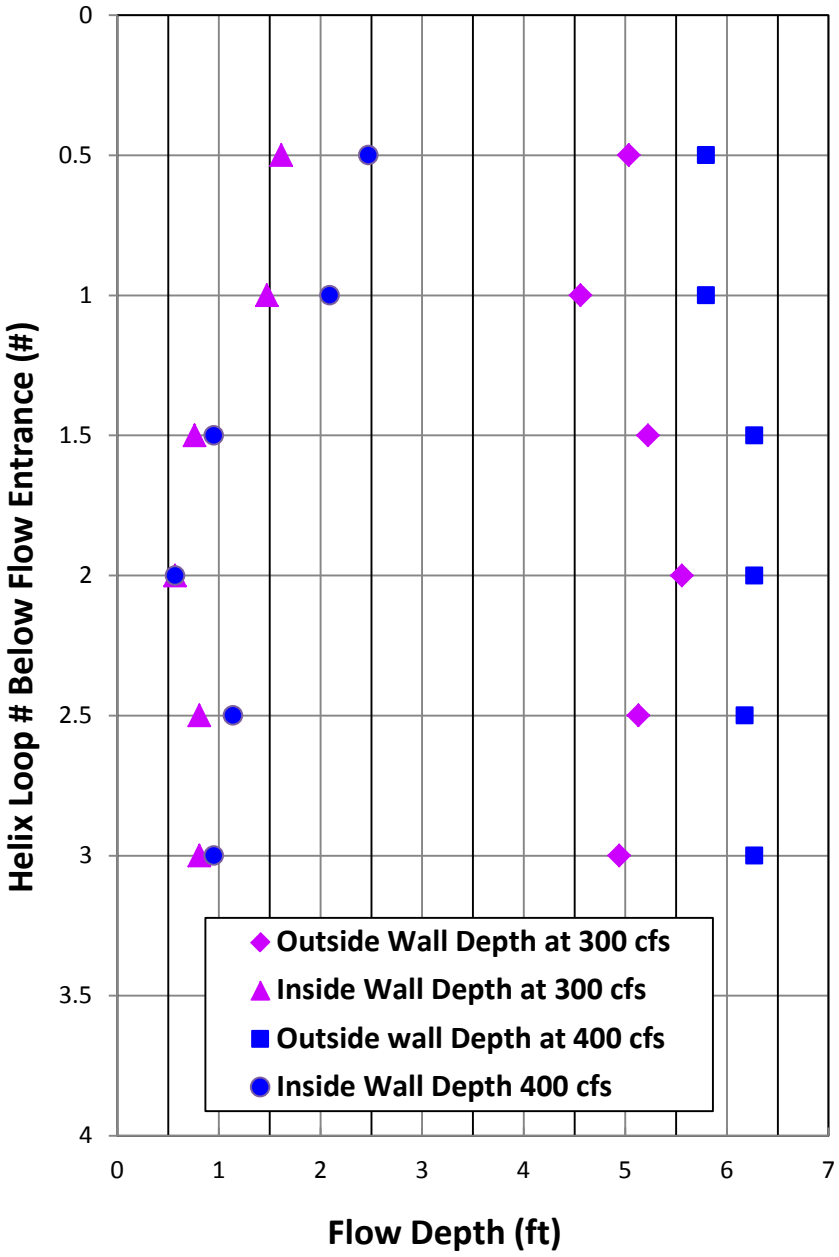

Figure 72. Flow depth measured along inside and outside walls at 300 ft^3/s and 400 ft^3/s.

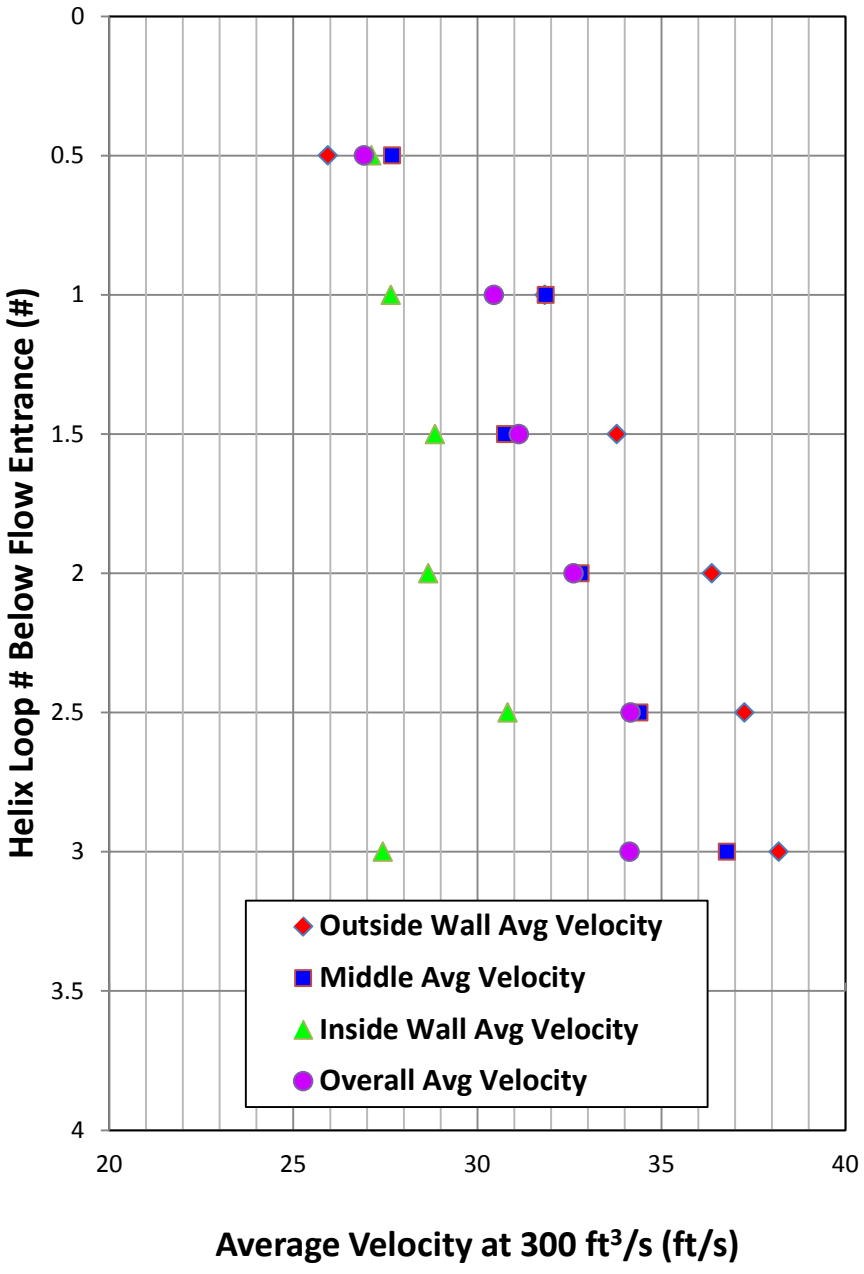

Figure 73. Velocities measured at quarter-points across flume width for 300 ft^3/s.

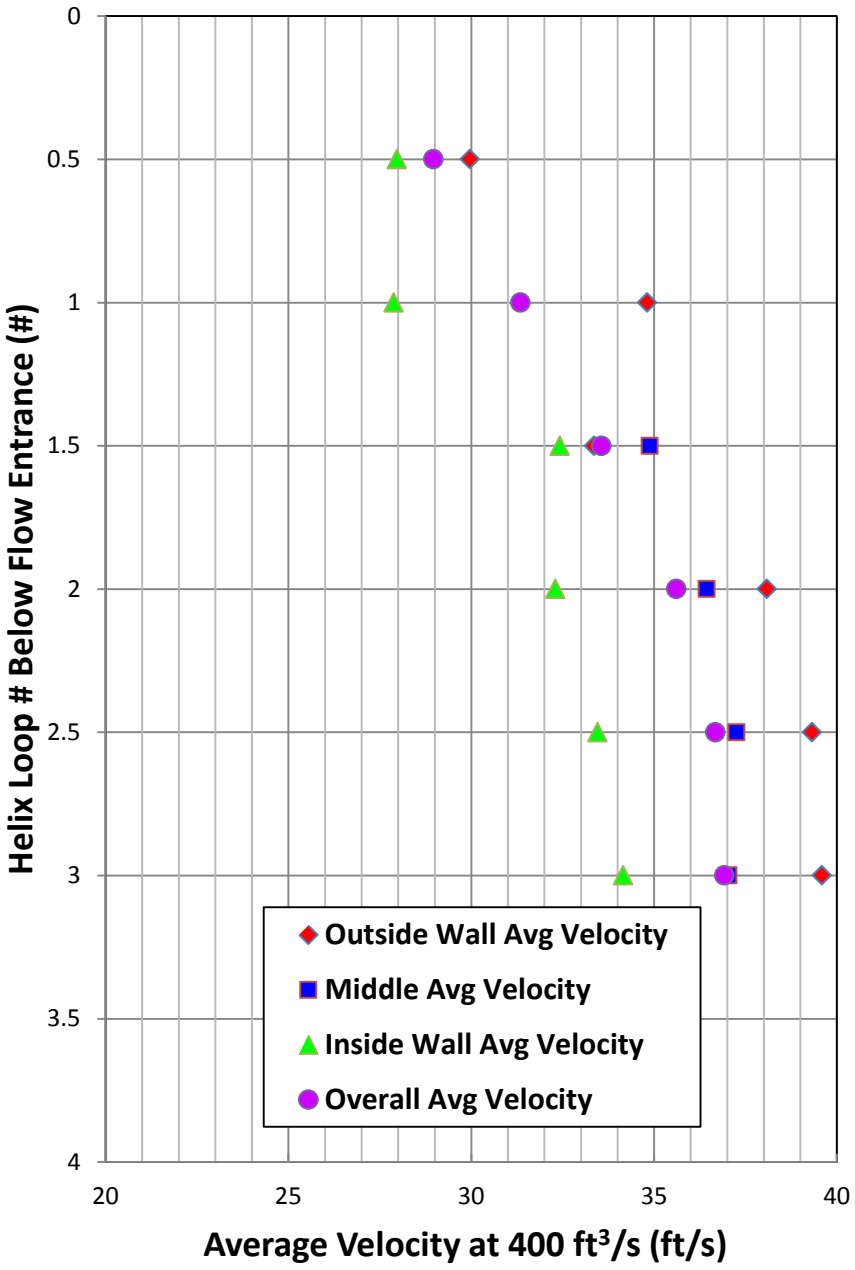

Figure 74. Velocities measured at quarter-points across flume width for 400 ft^3/s.

Helix Transitions

Helix Chute Entrance

Initial simulations in the numerical model investigated a dual-entrance design in which, for some operating conditions, flow could enter the helix at two adjacent loops from reservoir intakes at different elevations. This meant that the transition into the chute had to be smooth with minimal turbulence or shear, whether flow was entering from a single intake or from dual intakes. Determining the chute and gate geometry that performed well for both conditions was a very complicated and time consuming process. After a number of these concepts were tested in numerical simulations, a viable option was determined for final design. However, subsequently, operational criteria were changed so that only one helix inlet needed to be operated at a time. Since the development of a dual-entrance design could be pertinent to future fish passage sites, an abbreviated description of this development is provided in Appendix B.

This modification simplified the helix gate design so that it was fully open or fully closed at all times and needed to remain flush with the helix in only two positions to minimize disturbances in flow. This also simplified the design of the transition from the fish intake chute to the helix chute so that the conduit floor simply merged into the helix chute floor, matching the downstream edge of the chute transition with the outer edge of the helix chute, as shown in figure 75.

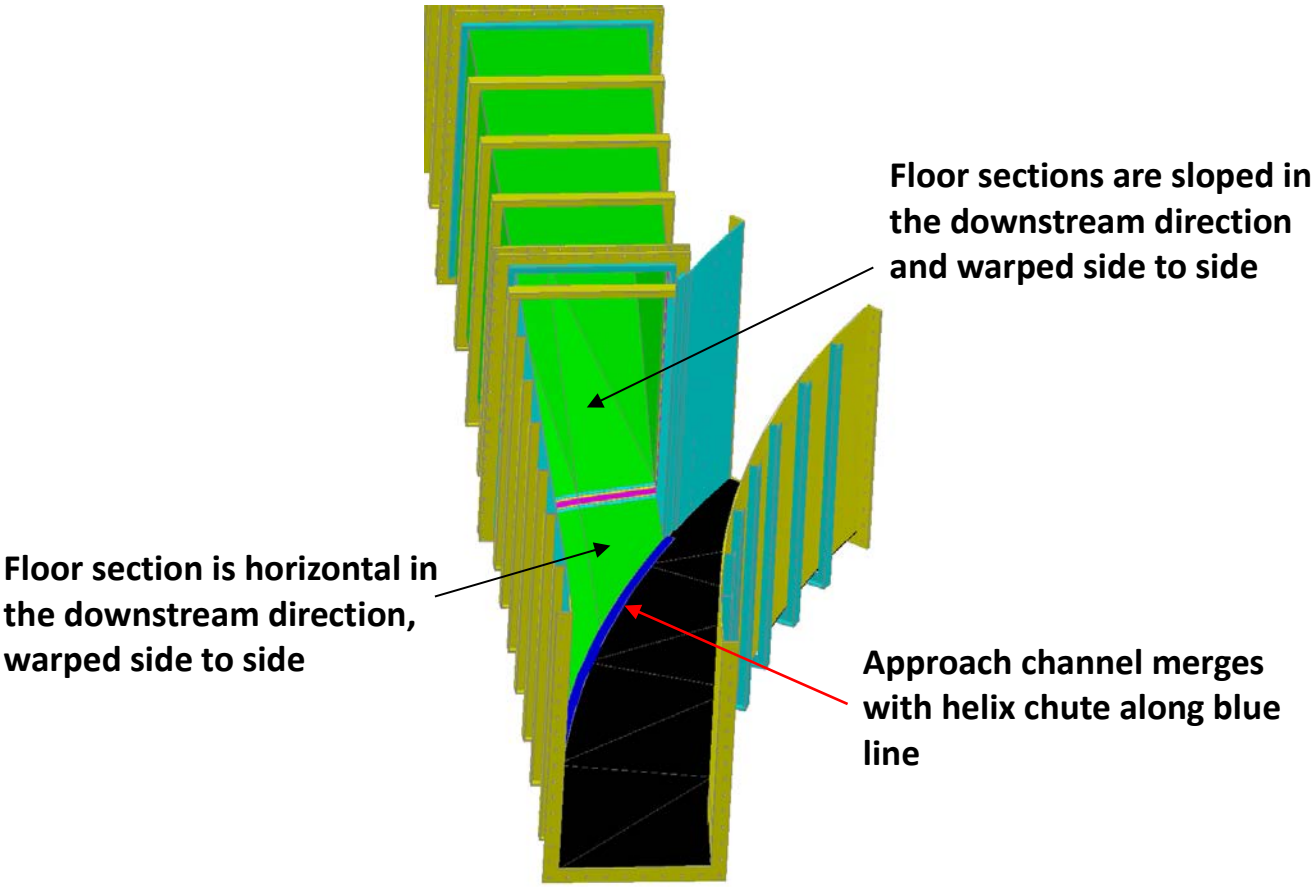

Figure 75. Transition into helix chute.

Helix to Tunnel Transition

The helix design provides relatively smooth and stable flow throughout the length of the helix. However, at the end of the helix the conduit must transition into the seven foot diameter conduit that will be tunneled through the right abutment of the spillway (figure 76). If the 4 foot wide helix channel, was merely straightened at the downstream end of the helix without changing the geometry, sweeping flows near the bottom of the chute that were stable within the helix chute would become unstable and would cause the body of flow to roll over itself in a reverse banking motion, causing potential injury to fish (figure 77). Thus, further investigations were necessary to determine a geometry for the flume that would allow the helix chute to be straightened and transitioned into the downstream conduit without causing excessive turbulence or roll-over.

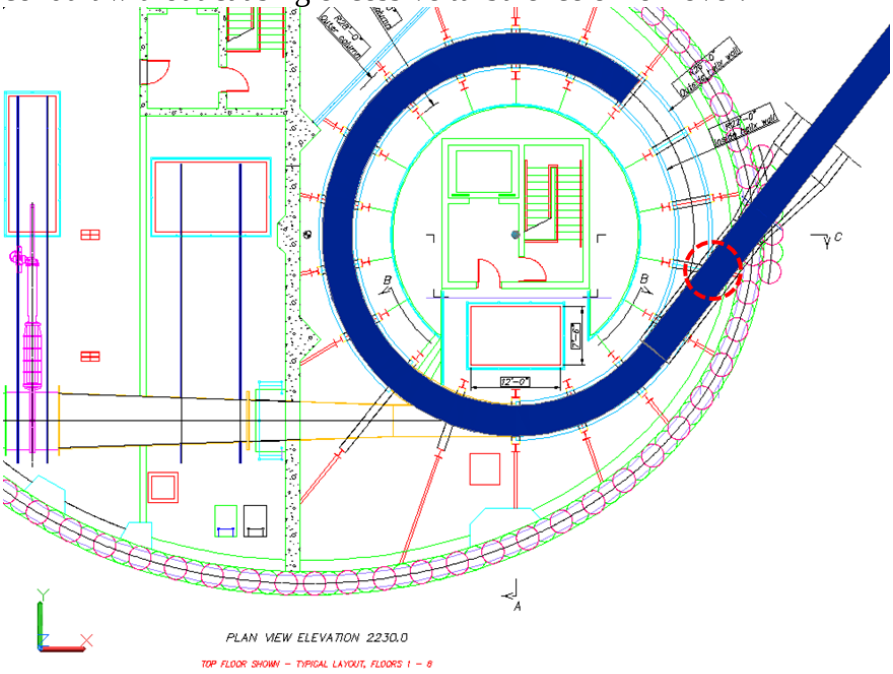

Figure 76. Layout for the initial physical model of the helix to tunnel transition. The flow path is displayed in solid blue. The red dashed circle is centered on one helix chute column support that would require structural bridging over the transition. Other "I"-shaped helix chute columns are shown in red.

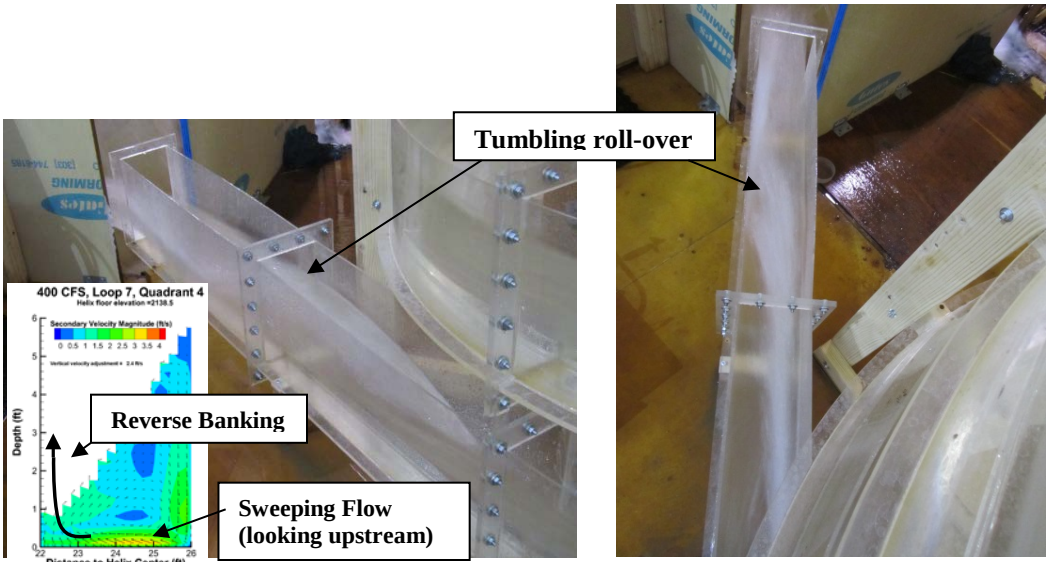

Figure 77 Tumbling roll-over occurs when helix chute is straightened without changing the chute geometry. Sweeping flow component near the bottom becomes unstable, causing reverse banking and rollover.

Helix to Tunnel CFD Modeling

The helix to tunnel transition study was initiated by observing the physical model's outlet. The initial physical model used a straight chute with the same 4-ft width as the helix chute (figure 77). While it was not intended to be a first attempt at modeling this transition, it demonstrated that the sweeping flow component near the bottom of the flume needed to be controlled to prevent sloshing and sharp run-up from secondary cross currents that produced tumbling roll over about 16-ft downstream from the end of the helix chute.

The hydraulic design goals included 1) maintain an air path along the top of the tunnel which has a minimum height of 5 feet, 2) minimize or eliminate tumbling roll over, 3) do not allow sudden into-the-flow offsets, and 4) minimize standing wave peaks.

The original layout concept for the helix to tunnel transition was to minimize water run-up and side to side sloshing by shaping the transition much like a French curve, using a series of curves to transition from the helix exit to the straight tunnel section. However, prior to the modeling of this layout, three constructability issues associated with this design were identified. 1) more than one column support would require structural bridging over the transition, 2) the tunneling machine would enter the helix chamber at an awkward angle (pointing more toward the wall) making machine removal from the helix chamber difficult or impossible, and 3) the tunneling machine would have difficulty matching the alignment of the varied curved sections.

As a result, the new layout goals were to obstruct only one column support, and to maintain or improve the entry angle to facilitate maintaining entrance alignment and removal of the tunneling machine. These parameters set the basis for the initial transition design set up in the CFD model using Flow-3D. Several transition section geometries that fell within this criteria were modeled and are described in Appendix C. The transition geometries initially tested with the numerical model produced a variety of issues including tumbling roll-over and surging flows that produced areas of turbulence and shallow flow depths.

The final configuration for the transition section is shown in figure 78. This configuration uses changes in flume width and geometry, along with an elliptical shaped guide wall to produce a channel geometry similar to an "S" shape. This geometry helps to control and dampen the sweeping component near the bottom of the flume to produce a reasonably smooth flow condition within the transition section. The size and shape of the guide wall was chosen by attempting to fill in a shallow depth zone observed from previous investigations. Flow conditions were improved further by adding a straight section tangent to the ellipse on the downstream side to stabilize flow depths along the right wall. Although the final design produced several standing waves near the beginning of the guide wall, flow conditions were significantly improved over previous geometries tested and this geometry produced the best flow conditions of all helix to tunnel configurations that were investigated.

As the flow exits the helix in the final design, the deepest flow that occurs within the transition section is 4.2 feet deep (minimum tunnel height is 5 feet), and the face of the initial standing wave is at a favorable slope which is a strong indication that tumbling roll over will not occur (figure 79). A three-dimensional view with the locations of the guide wall is shown in figure 80. Figure 81 is angled to show the best view of the initial standing wave, and figure 82 shows a slight amount of sloshing. Figure 83 shows velocity cross sections at two locations, 126 ft and 155 ft downstream from the entrance to the transition section. The left cross section shows a gradual transition in velocity from about 27 ft/s for the two standing waves near the surface to about 36 ft/s near the center of the main body of flow. The right cross section shows a similar transition in velocity from the surface to the main body, after the two standing waves have merged.

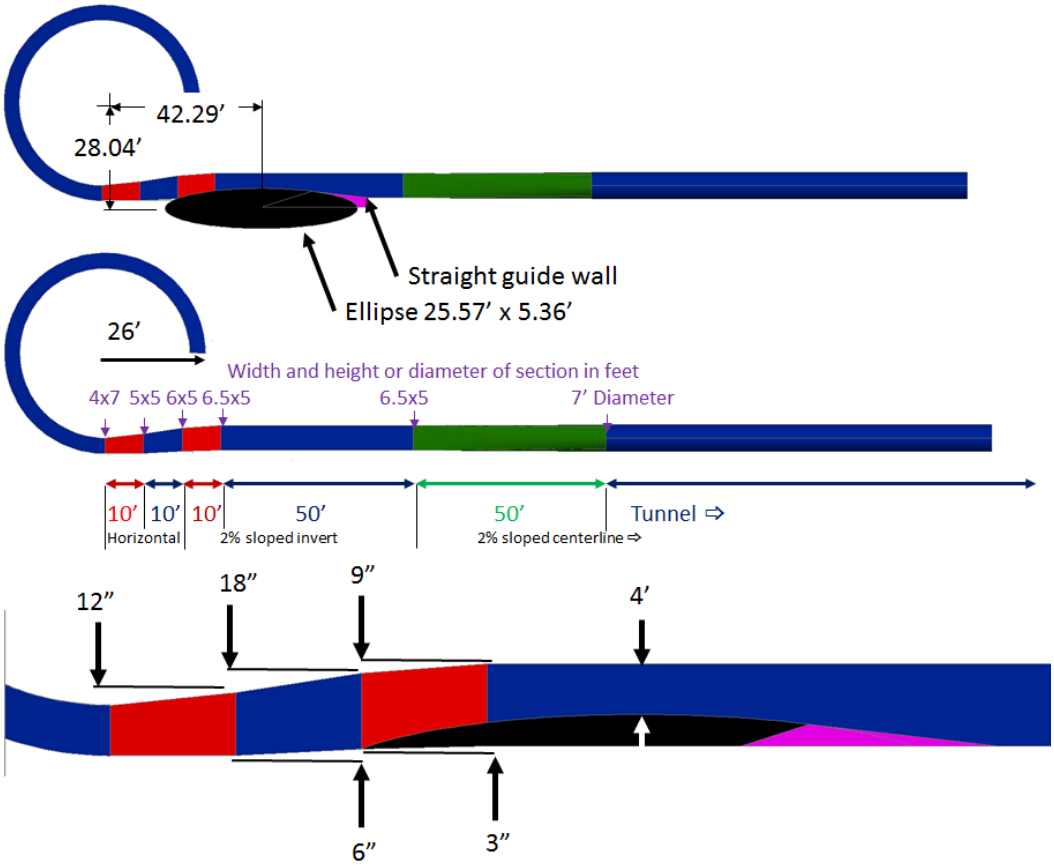

Figure 78. Plan view for final transition section design. This configuration includes changes in geometry and a guide wall to provide a piecewise channel shape similar to an "S".

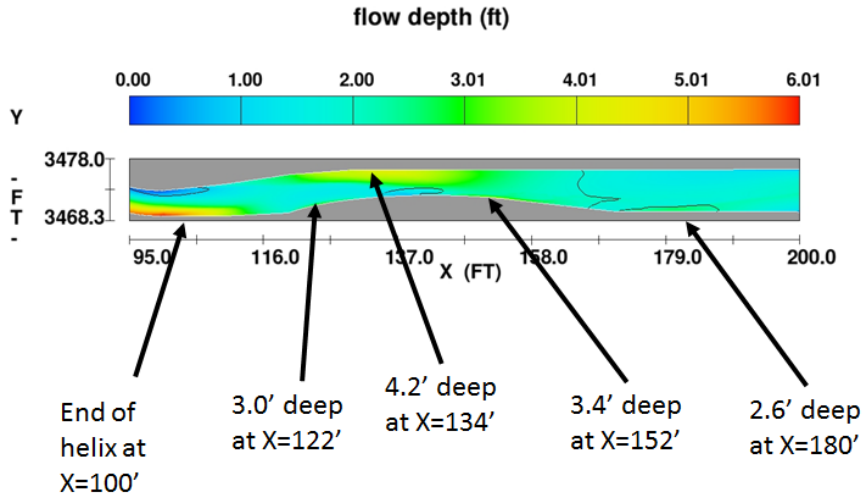

Figure 79. Maximum depths at key areas for final simulation of the helix to tunnel transition (400 ft^3/s). X=100 ft is the entrance to the transition section.

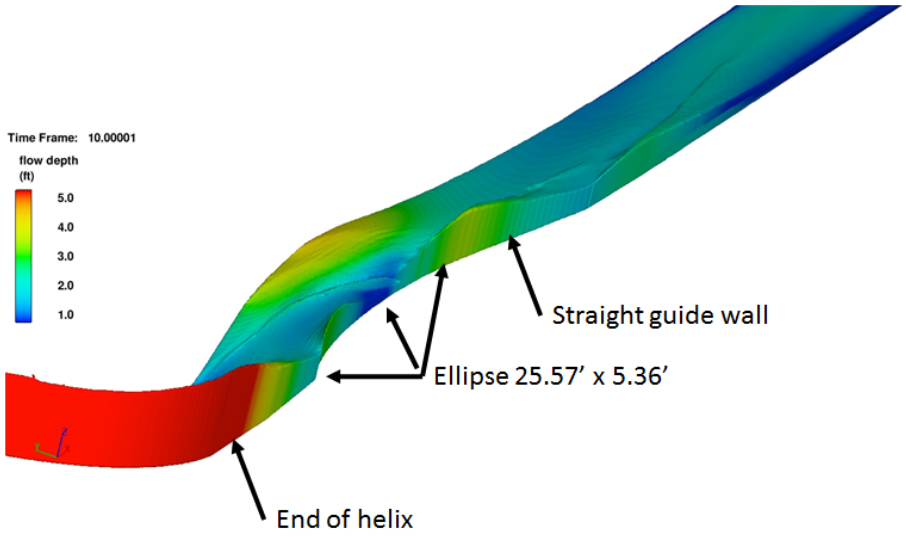

Figure 80. Looking downstream at flow depths for the final simulated helix to tunnel transition in 3D view (400 ft^3/s). Flow depths throughout and downstream from the transition are improved over previous designs investigated.

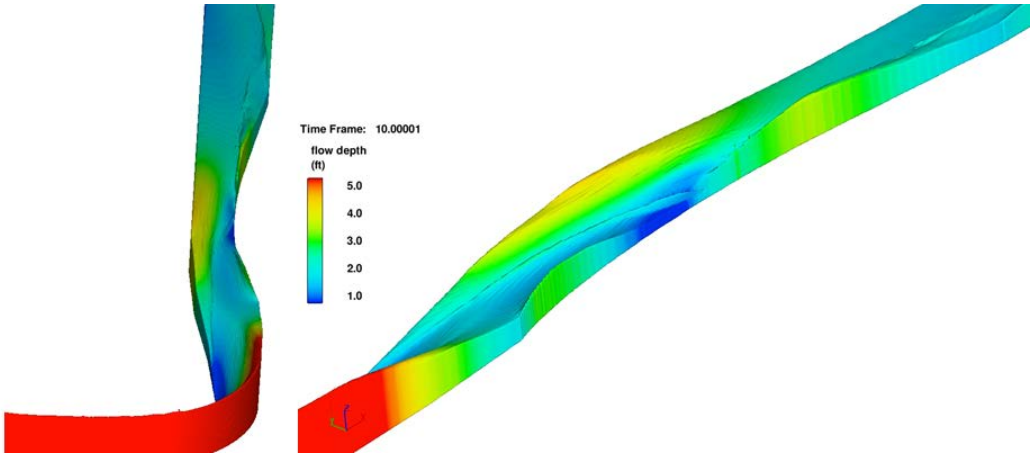

Figure 81. Looking downstream at flow depth color contours of Configuration Q with 400 ft^3/s. The flow is banked from the right wall when exiting the helix, sloshes to the left wall to a peak depth just over 4 ft with a favorable slope that would not induce tumbling roll over. The flow sloshes back to the right wall but it is not excessive.

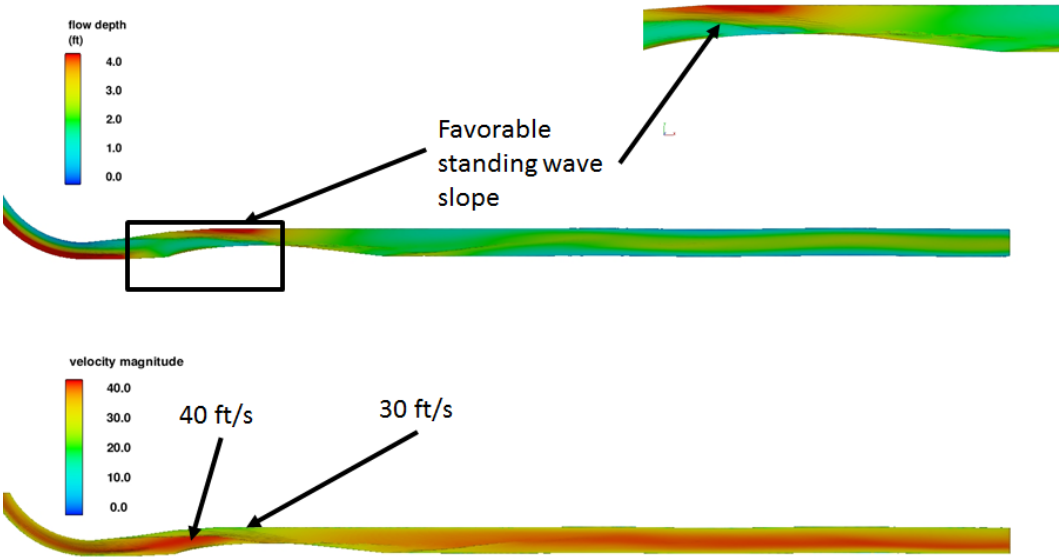

Figure 82. Flow depths (top) and surface velocities (bottom) for final configuration. The 10 ft/s shear zone caused by the direct helix flow (40 ft/s) shooting under the standing wave (30 ft/s) meets the shear zone criteria. The first standing wave surface is favorable (laid back) and no tumbling roll over was observed. The sloshing in the tunnel appears minimal.

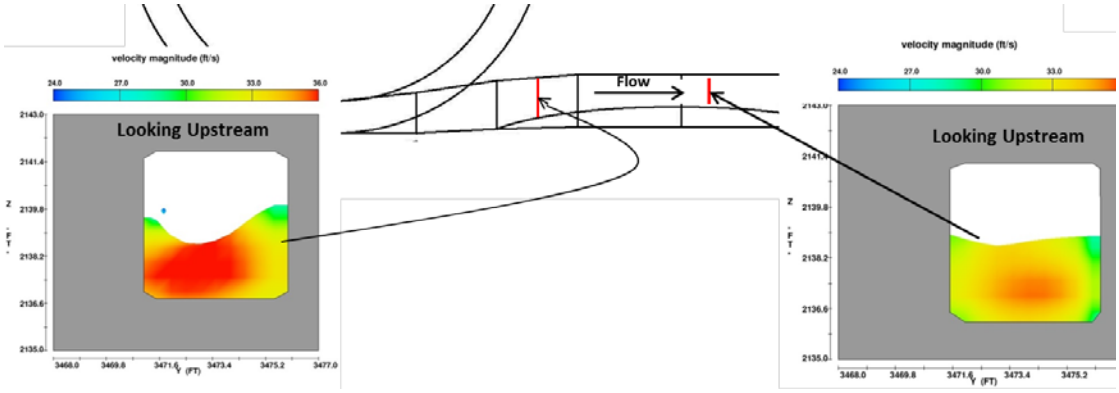

Figure 83. Velocity cross sections looking upstream shown 126 ft (left) and 155 ft (right) downstream from the transition entrance.

For this final transition configuration, a flow rate of 200 ft^3/s was tested to assure that smooth flow conditions would be provided throughout the full range of

operations expected in the prototype (figure 84). Downstream from the helix, the peak flow depth was around 3.0 ft (figure 85). The flow appeared smooth with very minor sloshing occurring in the tunnel.

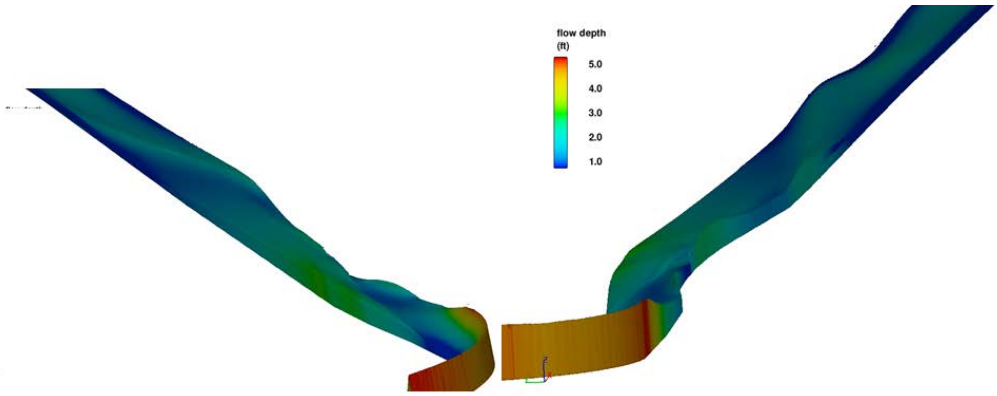

Figure 84. Flow depths with a flow rate of 200 ft^3/s through the final transition configuration, viewed from two different angles. Flow conditions appear good.

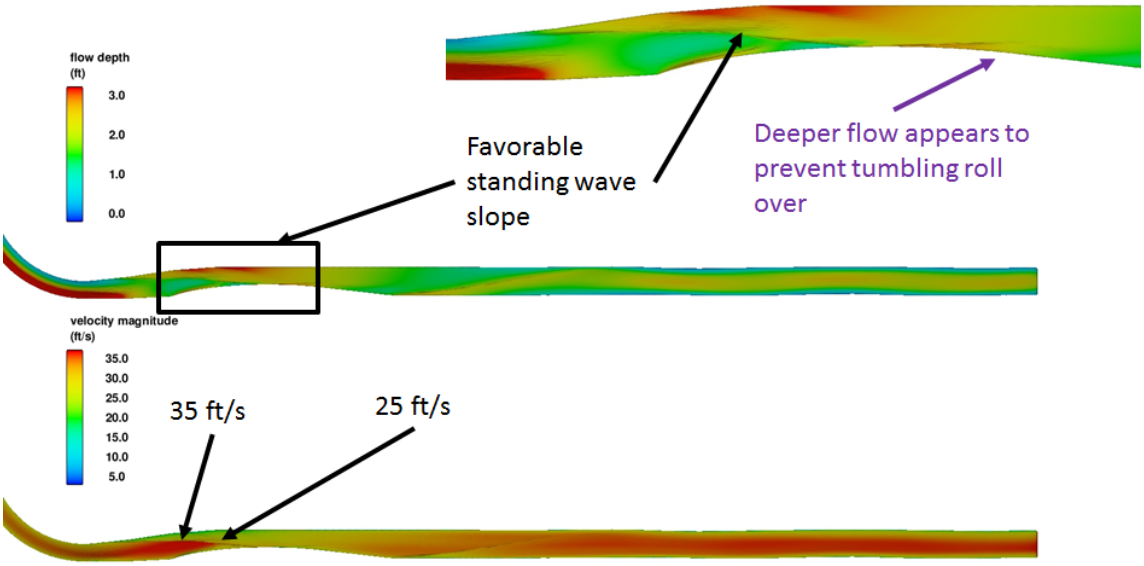

Figure 85. Flow depths (top) and surface velocities (bottom) for 200 ft^3/s discharge through the final transition configuration. The 10 ft/s shear zone caused by the direct helix flow (35 ft/s) shooting under the banked flow (25 ft/s) meets the established shear zone criteria. The first standing wave surface slope is favorable (laid back) and no tumbling roll over was observed. The sloshing in the tunnel appeared minimal.

Helix to Tunnel Transition - Physical Modeling

Once the transition geometry was determined using the numerical model, a physical model of the final configuration was constructed on a 1:9.5 geometric scale and attached to the downstream end of the existing helix model. The outer shell of the transition section was constructed from Plexiglas with the guide wall constructed of polyurethane (figure 86). Investigations were conducted for prototype-scale flow rates of 200 ft^3/s, 300 ft^3/s and 400 ft^3/s. Flow conditions through the transition section of the physical model were similar to what was observed in the numerical model.

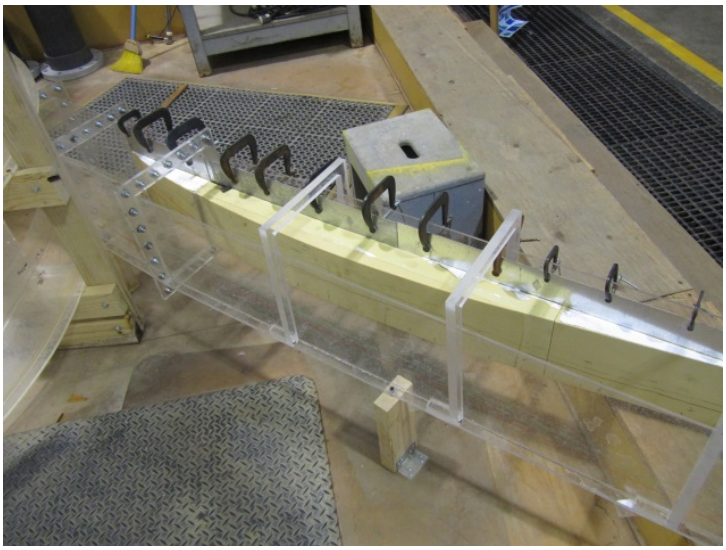

Figure 86. Transition section from helix is constructed out of Plexiglas with urethane guide wall.

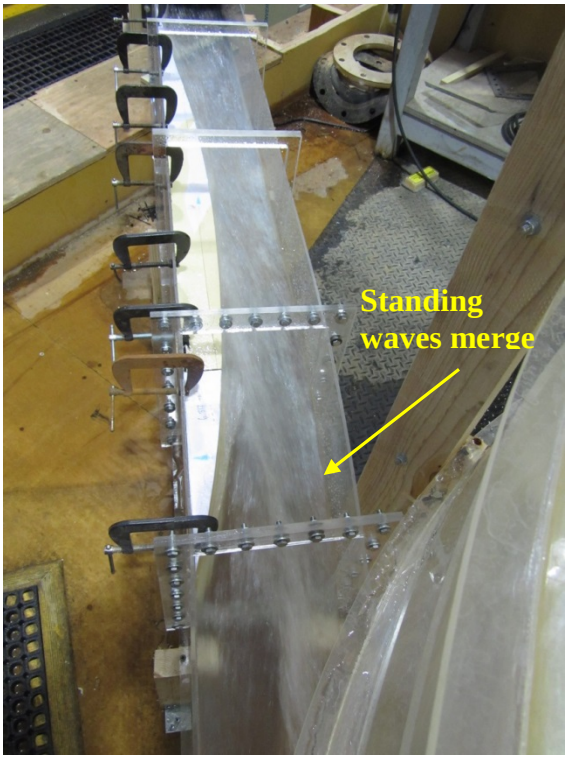

Figure 87. Looking downstream at transition section, standing waves form near upstream end of transition section and quickly merge into one.

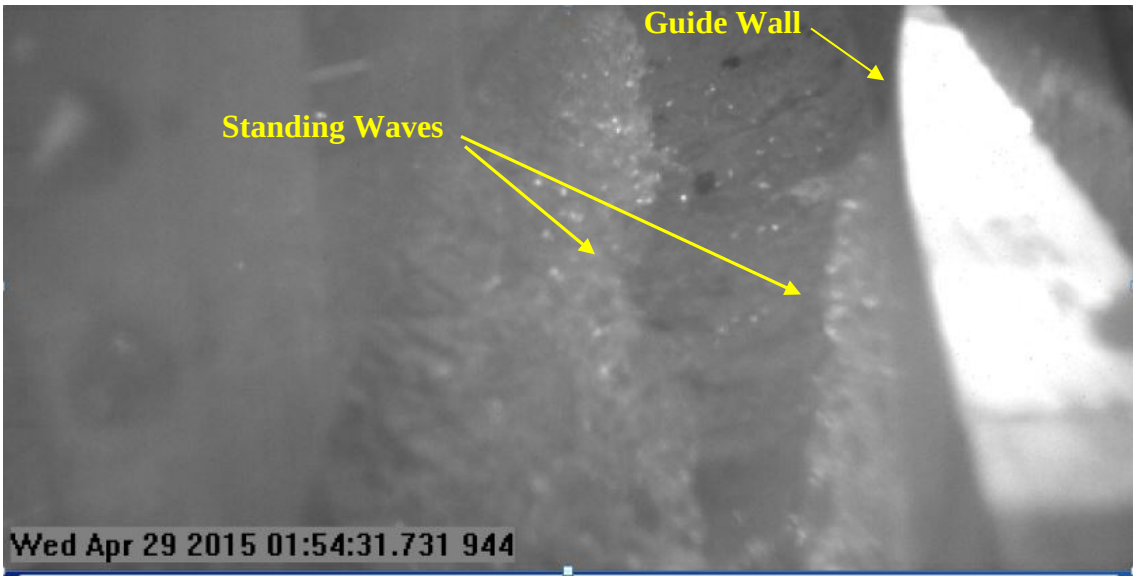

Figure 88 Close up view of standing wave, looking upstream, near upstream end of guide wall.

Figure 89. Small surface standing wave occurs downstream from guide wall.

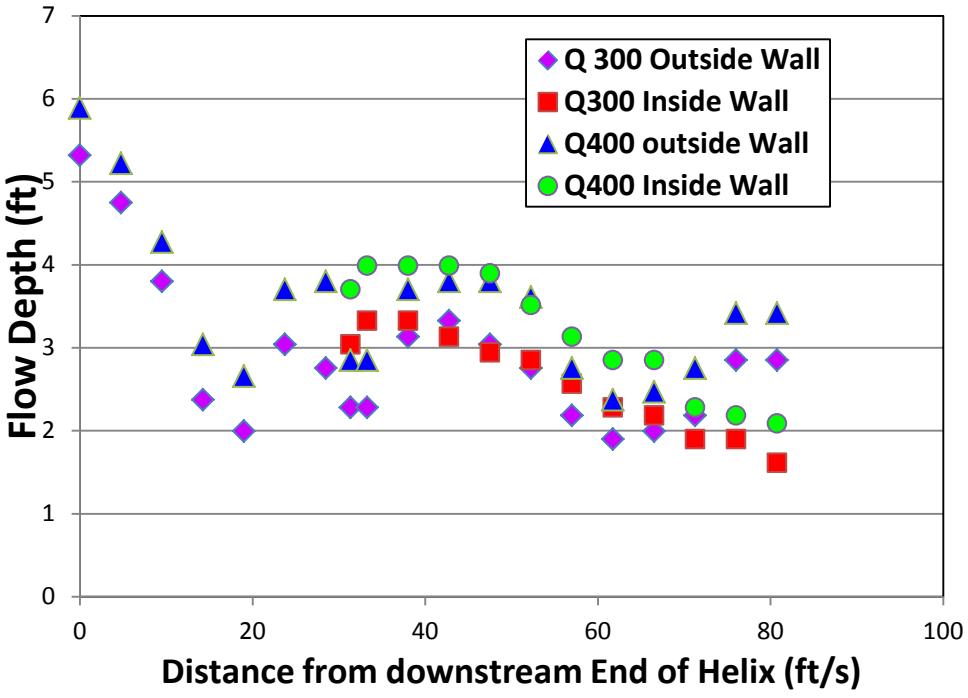

Figure 90 . Flow depth measured along the inside and outside walls of the helix-to-tunnel transition section.

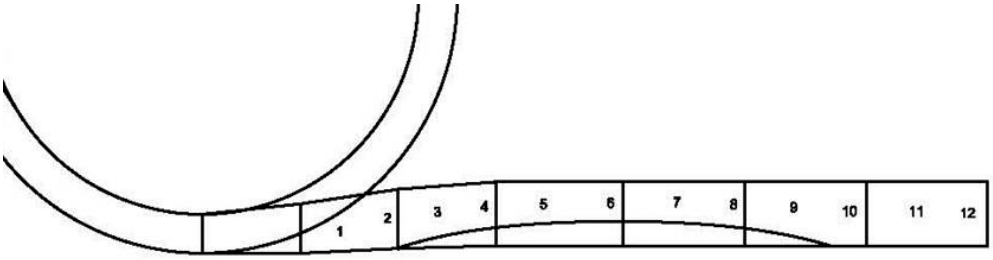

Figure 91. Locations of velocity cross sections.

Although flow conditions within the transition were not perfectly smooth, no tumbling roll-over was observed. Two standing waves that quickly merged into one were produced on the water surface along a portion of the transition section near the upstream end of the guide wall. In addition, a small fin or surface standing wave occurred immediately downstream from the guide wall, (figures 87 - 89). However, the standing waves appeared to be stable and no rollover was observed.

Flow depths measured along the inside and outside walls of the transition section at 300 ft^3/s (Q300) and 400 ft^3/s (Q400) are shown in figure 90. The maximum flow depth was about 4 ft which provides sufficient space below the top of the tunnel. Velocities were measured at quarter points across the width of the flume at cross sections along the length of the transition, for each flow rate tested (locations labeled 1 through 12, figure 89). At each quarter point location, average velocity was measured near the vertical center of the upper standing-wave portion of the flow and also within the lower body of flow (tables 3-5). Comparison of velocities between flow layers showed that a maximum velocity differential between parallel layers of 6.6 ft/s, 8.6 ft/s and 9.7 ft/s occurs at 200 ft^3/s, 300 ft^3/s and 400 ft^3/s (tables 6-8). These values are much less than NOAA's criteria for maximum outfall velocity of 25 ft/s, which represents a more abrupt shear zone, (i.e a jet entering nearly perpendicular to the body of flow) [7]. In addition, observations of injected beads moving between the upper and lower flow layers indicated that the shear zone between layers is relatively mild, with a gradual transition in velocities between the two layers (figure 91).

As a result of these investigations this transition geometry was accepted for final design.

Table 3. Velocities measured in transition section at 200 ft^3/s.

Flow rate Marker Number	Distance from end of Helix (ft)	Average Velocity Outside (ft/s)	Average Velocity Outside-Top (ft/s)	Average Velocity Center (ft/s)	Average Velocity Center-Top (ft/s)	Average Velocity Inside (ft/s)	Average Velocity Inside - Top (ft/s)
1.0	9.8	34.0	27.4				
2.0	15.6	31.5	25.3	31.2	28.1	32.4	25.6
3.0	20.0	31.0	28.0	32.1	31.5	28.2	24.7
4.0	25.7	31.4	29.7	32.6	29.0	29.8	25.3
5.0	33.1	31.2	25.3	30.9	28.4	29.9	26.4
6.0	38.7	29.5	23.9	30.6	24.7	30.9	27.3
7.0	45.7	28.6	23.6	29.9	26.1	28.0	27.6
8.0	51.5	29.2	23.4	30.0	23.8	29.6	24.4
9.0	57.6	28.5	23.5	29.5	23.4	31.0	25.3
10.0	63.1	26.9	22.1	29.1	22.8	30.8	24.4
11.0	70.2	24.4	22.7	26.0	23.7	28.7	26.6
12.0	75.6	24.5	22.8	25.9	24.4	26.0	26.9

Table 4 Velocities measured in transition section at 300 ft^3/s.

Flow rate Marker Number	Distance from end of Helix (ft)	Average Velocity Outside (ft/s)	Average Velocity Outside-Top (ft/s)	Average Velocity Center (ft/s)	Average Velocity Center-Top (ft/s)	Average Velocity Inside (ft/s)	Average Velocity Inside - Top (ft/s)
1.0	9.8	37.7	29.8				
2.0	15.6	37.6	33.0	37.8	30.5	31.7	27.2
3.0	20.0	38.6	30.0	34.7	31.2	30.8	24.9
4.0	25.7	36.1	35.5	33.2	28.1	30.4	27.0
5.0	33.1	29.6	23.2	30.1	28.5	31.5	26.3
6.0	38.7	29.7	24.8	31.7	28.9	32.6	27.7
7.0	45.7	30.5	29.7	32.1	29.3	33.4	30.5
8.0	51.5	30.1	28.7	32.6	30.2	34.0	31.4
9.0	57.6	30.5	28.4	32.9	29.8	35.3	29.5
10.0	63.1	30.6	24.6	31.9	25.9	35.4	26.9
11.0	70.2	30.5	26.0	32.3	26.2	34.9	27.0
12.0	75.6	25.1	25.6	31.6	26.1	34.9	26.8

Table 5 Velocities measured in transition section at 400 ft^3/s.

Flow rate Marker Number	Distance from end of Helix (ft)	Average Velocity Outside (ft/s)	Average Velocity Outside-Top (ft/s)	Average Velocity Center (ft/s)	Average Velocity Center-Top (ft/s)	Average Velocity Inside (ft/s)	Average Velocity Inside - Top (ft/s)
1.0	9.8	39.6	31.5				
2.0	15.6	39.9	37.2	40.3	38.9	31.6	26.7
3.0	20.0	39.2	37.2	39.8	39.3	30.9	28.7
4.0	25.7	38.4	28.7	36.0	31.2	30.8	27.7
5.0	33.1	32.2	28.9	32.7	31.1	37.3	30.7
6.0	38.7	34.6	26.4	36.6	30.6	34.3	29.9
7.0	45.7	36.0	29.6	34.9	30.4	36.1	32.3
8.0	51.5	32.0	27.7	35.1	30.5	37.1	34.8
9.0	57.6	31.4	30.4	34.9	32.1	38.1	36.2
10.0	63.1	31.9	31.6	35.1	35.4	38.5	37.6
11.0	70.2	32.2	32.1	35.5	35.0	38.6	39.0
12.0	75.6	32.3	32.0	36.2	35.6	38.0	38.9

Table 6 Velocity differential between parallel layers at 200 ft^3/s

Flow rate Marker Number	Prototype Distance from End of Helix (ft)	Outside Velocity Differential (ft/s)	Center Velocity Differential (ft/s)	Inside Velocity Differential (ft/s)
1.0	9.8	6.6		
2.0	15.6	6.3	3.1	6.8
3.0	20.0	3.0	0.6	3.5
4.0	25.7	1.8	3.6	4.5
5.0	33.1	5.9	2.4	3.5
6.0	38.7	5.6	5.9	3.6
7.0	45.7	5.1	3.8	0.4
8.0	51.5	5.8	6.2	5.2
9.0	57.6	4.9	6.2	5.7
10.0	63.1	4.8	6.3	6.3
11.0	70.2	1.7	2.3	2.2
12.0	75.6	1.8	1.5	-0.9

Table 7 Velocity differential between parallel layers at 300 ft^3/s.

Flow rate Marker Number	Prototype Distance from End of Helix (ft)	Outside Velocity Differential (ft/s)	Center Velocity Differential (ft/s)	Inside Velocity Differential (ft/s)
1.0	9.8	7.9		
2.0	15.6	4.6	7.3	4.5
3.0	20.0	8.6	3.5	5.9
4.0	25.7	0.6	5.1	3.5
5.0	33.1	6.4	1.7	5.2
6.0	38.7	4.9	2.8	4.9
7.0	45.7	0.8	2.8	2.9
8.0	51.5	1.4	2.4	2.6
9.0	57.6	2.1	3.1	5.8
10.0	63.1	5.9	6.0	8.5
11.0	70.2	4.5	6.1	7.9
12.0		-0.5	5.5	8.1

Table 8 Velocity differential between parallel layers at 400 ft^3/s.

Flow rate Marker Number	Prototype Distance from End of Helix (ft)	Outside Velocity Differential (ft/s)	Center Velocity Differential (ft/s)	Inside Velocity Differential (ft/s)
1.0	9.8	8.1		
2.0	15.6	2.7	1.4	4.8
3.0	20.0	2.0	0.5	2.2
4.0	25.7	9.7	4.8	3.1
5.0	33.1	3.4	1.7	6.6
6.0	38.7	8.2	6.0	4.4
7.0	45.7	6.3	4.5	3.8
8.0	51.5	4.3	4.6	2.4
9.0	57.6	1.0	2.8	1.9
10.0	63.1	0.3	-0.3	0.9
11.0	70.2	0.1	0.5	-0.3
12.0	75.6	0.3	0.7	-0.9

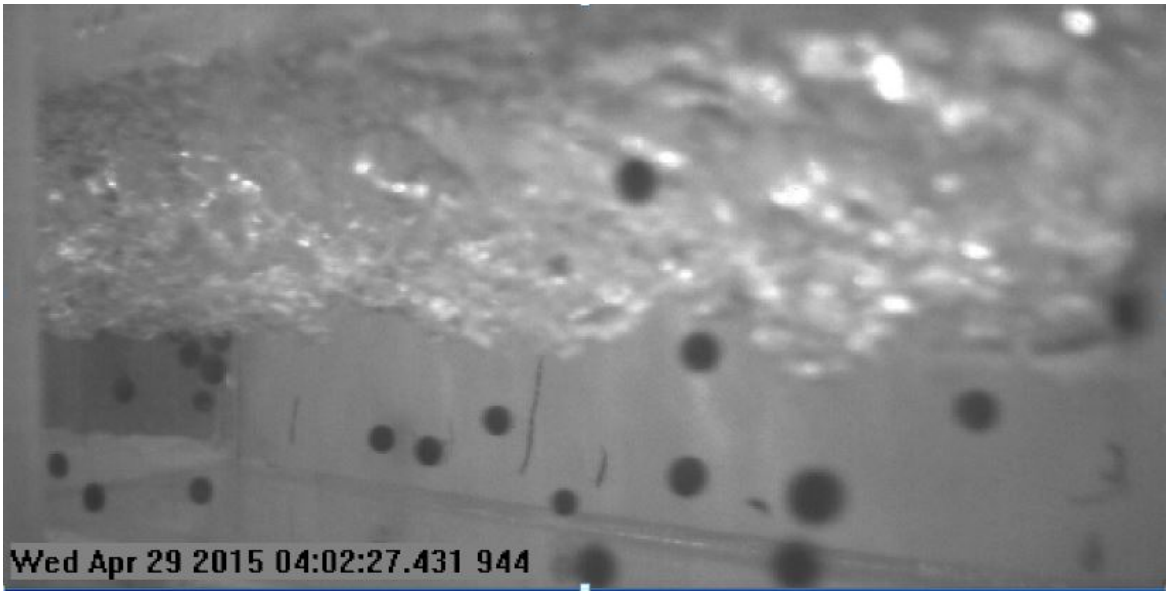

Figure 92 Beads injected into the flow travel downstream within the upper and lower flow layers.

Conclusions

Numerical and physical models were used in conjunction to determine the final design of the helix chute and transitions into and out of the helix. This study began with a sensitivity analysis using numerical modeling to determine a geometry that would produce acceptable hydraulic flow conditions to provide a stable environment for downstream fish passage. This analysis determined that by using a rectangular geometry to minimize secondary flow current rotation and sweeping flow currents, a large sweet spot could be produced within the body of flow to provide a relatively smooth and stable environment for fish as they traveled downstream within the helix flume. Once an acceptable design was determined from the numerical modeling, the physical model was used to refine and verify the final design.

Final results from the model investigations demonstrated that the helix can be used to provide stable and continuous downstream fish passage while dropping fish more than 80 feet in elevation through a sloping rectangular channel at Cle Elum Dam.

A similar process was used to determine the geometry of the transition section from the helix to the 7-foot diameter downstream conduit. Analyses were conducted, first using a numerical model to determine an adequate design to provide acceptable flow conditions throughout the transition section. Once an

adequate geometry was determined, a physical model was used to verify the final design.

Using this study as a starting point, future studies will be conducted to determine the limits and guidelines for applying this technology to other high head dams where juvenile downstream fish passage is desired.

References

1. Hanna, Leslie J. and Higgs, Jim,, "Intake Structure Design for Downstream Fish Passage at Cle Elum Dam", U.S. Bureau of Reclamation, Hydraulic Laboratory Report HL-2015-03.

2. Hanna, Leslie J., " Hydraulic Model Study of Fish Passage Features Below Cle Elum Dam" ,U.S. Bureau of Reclamation, HL-2015-02, November 2015.

3. Bureau of Reclamation." Final Planning Report Cle Elum Dam Fish Passage Facilities", United States Department of the Interior, , Pacific Northwest Region Columbia-Cascades Area Office Yakima, Washington, April 2011.

4. Bureau of Reclamation. "Phase I Assessment Report Storage dam Fish Passage Study", Yakima Project, Washington, Technical Series No. PN-YDFP-001, 2003, rev. 2005.

5. Bureau of Reclamation ,"Cle Elum Dam Interim Fish Passage Operations '2006-2009'Annual Reports", Technical Series No. PN-YDFP-'011-015', 2006 through 2009.

6. Hanna, Leslie J., " Physical Modeling of Drop-Pool and Upwelling Intake Structures for Downstream Fish Passage at Cle Elum Dam" ,U.S. Bureau of Reclamation, PAP-1123, December 2015.

7. National Marine Fisheries Service Northwest Region, "Anadromous Salmonid Passage Facility Design, July2011.

Appendix A – CFD Modeling

FLOW-3D

This part of the study used the commercially available Computational Fluid Dynamics program FLOW-3D Version 10.1.1.05 by Flow Science Inc. [1], which is a finite difference, free surface, transient flow modeling system that was developed from the Navier-Stokes equations, using up to three spatial dimensions.

The finite difference equations are based on a fixed Eulerian mesh of non-uniform rectangular control volumes using the Fractional Area Volume Obstacle Representation (FAVOR) method[2]. Free surfaces and material interfaces are defined by a fractional volume-of-fluid (VOF) function. FLOW-3D® uses an orthogonal coordinate system as opposed to a body-fitted system.

When using the Cartesian coordinate system in FLOW-3D, sides of the control volumes are parallel to the Cartesian coordinate system. Part way through the study, shortcomings of the Cartesian coordinate system were identified including lower average channel velocities compared to the physical model caused by high turbulent dissipation rates along the helix outside wall. The cause is discussed in this report. It was found that using a cylindrical coordinate system and mesh greatly improved agreement with the physical model, so cylindrical coordinates were used during the final helix simulations. Cylindrical meshes were advantageous because the flow path matched the radial cell sides, whether the flow was axial (e.g. down a pipe) or rotational (e.g. around a helix).

The results from FLOW-3D simulations were analyzed to identify, quantify, and qualify the key hydraulic characteristics.

Simulation Assumptions

The following assumptions were made and options selected for each simulation:

- One fluid (air simulated with void space)
- Free surface

---

[1] Flow Science Inc., Introduction to FLOW-3D, 1996.
[2] J.M. Sicilian, "A FAVOR Based Moving Obstacle Treatment for FLOW-3D," Flow Science, Inc. Technical Note #24, April 1990 (FSI-90-TN24).

- For Cartesian meshes, cubed cell volumes (length, width, and height of each cell were equal) to reduce numerical errors.
- For Cylindrical meshes, cells were approximately cubic.
- Turbulence model: Renormalized Group (RNG) model with dynamically computed maximum turbulent mixing length
- Pressure solver: Generalized Minimal Residual (GMRES)
- Water at 20° Celsius (68° degree Fahrenheit)
    - Water density = 1.9403 slugs/ft^3
    - Dynamic viscosity = 2.08855×10^{-5} lb-s/ft^2
    - Incompressible fluid
    - Water from the withdrawal zone (top 10 feet) has been described as warm
- Volume of Fluid Advection: Automatic fluid convection
- Momentum Advection: first order
- Convergence controls: Default values were used
- Gravity: -32.2 ft/s^2 in the vertical (Z) direction

Solids model development

Structural objects were defined in stereolithography files that were generated using commercially available AutoCAD 2014 and imported into FLOW-3D.

Tecplot 360

Various Tecplot 360 2013 Beta versions and commercially available Tecplot 360 EX 2014 R1 were used for the analysis of the three dimensional CFD results. This software allows flexible analysis and presentation of results. For the Cle Elum helix chute, Tecplot 360 was used to adjust flow field velocities so that they could be presented relative to (as perceived by) fish traveling down the chute at the average channel velocity. This analysis procedure is presented below.

Analysis of a Fish's Point of View in the chute

One cross sectional velocity plot from FLOW-3D results is presented in Figure A-1. Since the average downward velocity is greater than the flow circulation velocities within the channel cross section, plotting absolute velocity vectors makes it very difficult to visualize flow features that fish would experience as they pass downstream with the flow. Key features like rotational flow were very difficult to visualize without adjustment.

For visualization, each sensitivity analysis simulation result was imported into Tecplot 360, as shown in Figure A-2. Then using Tecplot 360, the vertical velocity was adjusted to remove the average downward velocity of the section, as shown in Figure A-3. For example, when the average vertical velocity W was -2.3 ft/s, the average fish would also have an average vertical velocity of -2.3 ft/s. To

view the flow field as the average fish experiences it, 2.3 was added to W. This provided a better understanding of the strength of secondary rotational flows that juvenile fish would need to endure. For each cross section presented, the average vertical velocity was calculated and adjusted in a similar fashion. To simplify the analysis, sections were only analyzed at quadrants where the x- and y-velocity components recorded in FLOW-3D coincided with the plane of the cross section. Thus, the x- and y-velocity components matched the downstream or sideways components (depending on the quadrant) used in the secondary velocity magnitude plots. This process was time consuming and tedious, so only one cross section was extracted from each Sensitivity Analysis simulation.

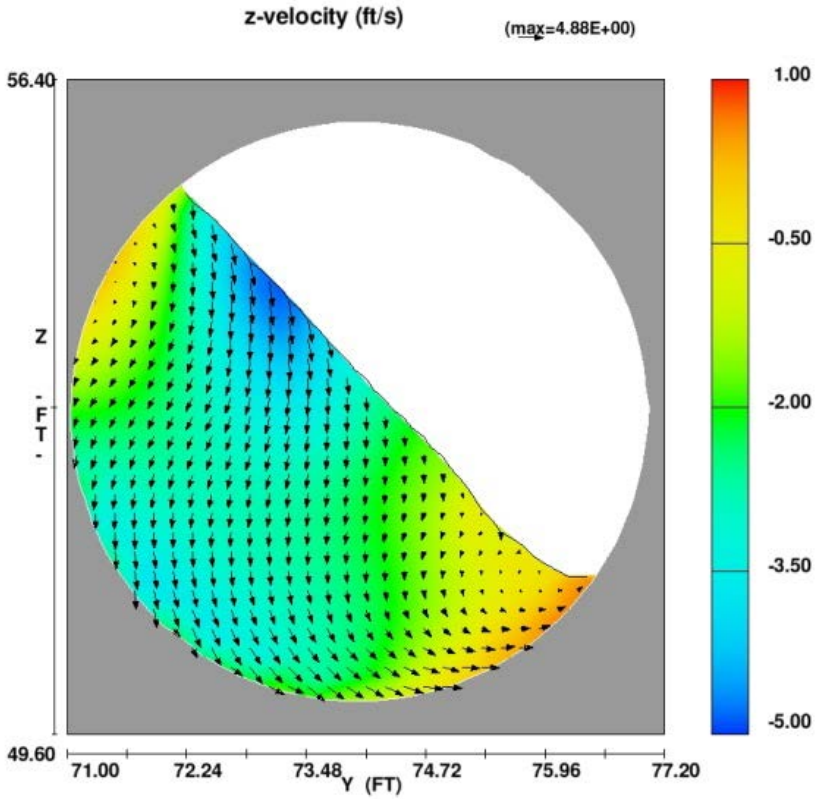

Figure A- 1. Cross section of flow from a FLOW-3D simulation. The average vertical velocity (z-velocity) in this cross section is -2.3 ft/s (downward). The color shading indicates the simulated vertical velocity. Due to the average vertical velocity being -2.3 ft/s, it is difficult to visualize the rotational flow the fish would experience.

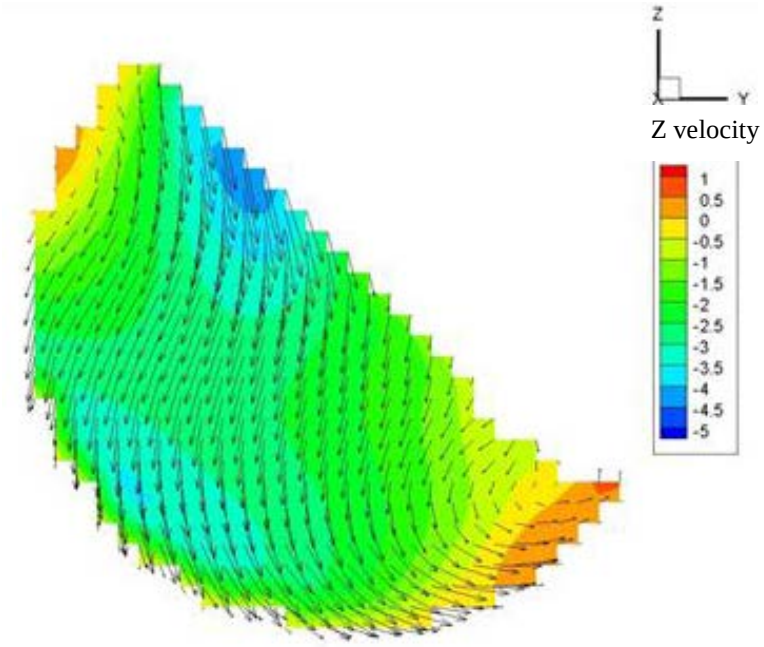

Figure A- 2. Cross section of the flow is displayed in figure A-1 using Tecplot. Tecplot shows the flow edges to be choppy, but the FLOW-3D simulations smooth these edges.

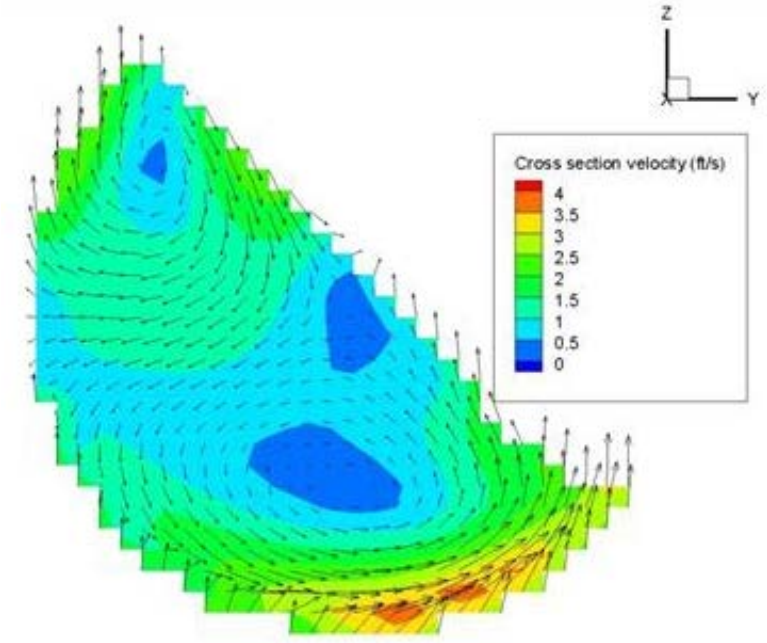

Figure A- 3. Cross section of the flow displayed in figure A-2 adjusted by adding 2.3 ft/s to W. The velocity vectors shown are the vector sums of the Y and adjusted Z velocities. Color shading indicates the magnitude of these velocity vectors.

Data extraction

For cylindrical mesh studies, a FORTRAN program was written using the flsgrf reader[3] library provided by Flow Science. The flsgrf reader library "libflsrdr.lib" (for Windows) provides an interface for applications that need to read data directly from the FLOW-3D binary results file ("flsgrf" data file). Key results were extracted such as velocities in each direction, cell size, and the amount of fluid in each cell, and these were then used to compute key flow parameters used in the study. Results were output to a Comma Separated Value (.csv) format that was directly imported into Microsoft Excel. This process created flow parameter plots (i.e. Figure 29) which extracted the value for every cross section in the simulation, that is to say, continuous.

The same FORTRAN program wrote Lagrangian (fish's perspective) data to Tecplot data format files for direct loading into Tecplot. A Tecplot macro was written to help provide similar presentation of all plots.

Rotational flow analysis

For this study, an assumption of the dominant forces affecting rotational fluid flow was developed for these helix chute analyses, and is similar to spiral flow describe by Chow[4]. Centrifugal and pressure forces appear to dominate secondary flow movements causing rotational flow in the helix chute (figure A-4).

Uncertainty Analysis of Helix Chute Simulations

Cartesian mesh studies

Simulations using Cartesian meshes runs produced lower average velocities in the fishway channel than those measured in the physical model.

Sensitivity Analysis 5, which is comparable to the physical model, had a maximum velocity of 30.0 ft/s and appeared to reach normal flow within 3 loops, whereas the physical model reached 39.1 ft/s at the third loop with indications that mild acceleration (estimated to be around 3 percent for the fourth loop) would continue. Several modeling options were tested that resulted in only minor improvements. These included decreasing the surface roughness, decreasing cell size, and using various turbulence models, with only minor improvements to results. It was noted that the turbulent dissipation was very uneven, most notably along the outside wall (Figure A-5). At this point it was suspected that non-alignment of the channel walls and cell boundaries was the source of the uneven turbulent dissipation and the decision was made to redevelop the model using a cylindrical mesh.

---

[3] Flow Science Inc., FLSGRF READER LIBRARY, May 2001.
[4] Chow, Ven Te, *Open-Channel Hydraulics*, 1959, Chapter 16

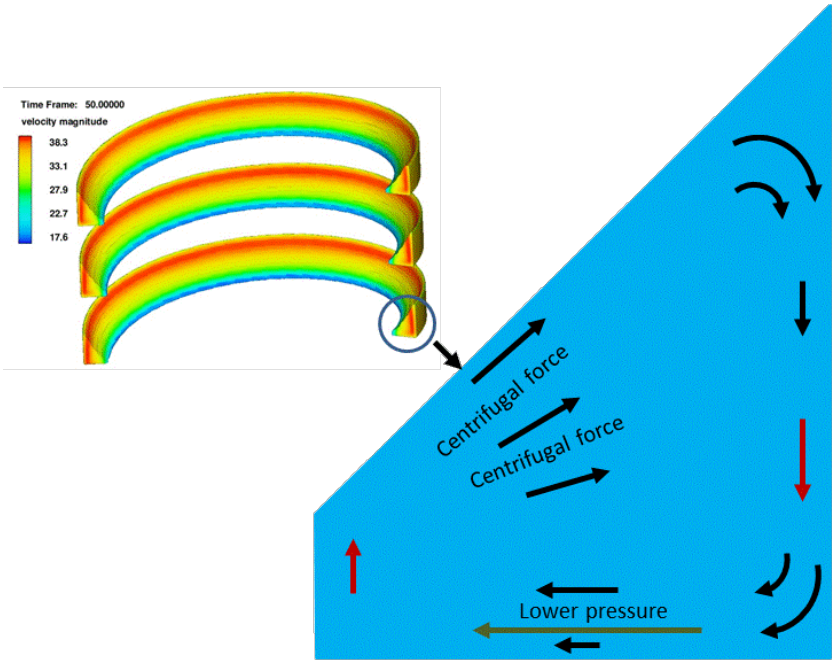

Figure A- 4. Assumption of the dominant forces affecting fluid flow after making the Lagrangian adjustment (average fish's perspective). The maximum velocity toward the center is defined as the Sweeping Velocity, shown in green, which was always observed to be toward the center and located near the bottom. The Roll-Over Parameter (ROP) is the velocity difference of the maximum and minimum vertical velocities, shown as red vectors

Cylindrical mesh studies

A cylindrical mesh is created using a cylindrical coordinate system (figure A-6) as opposed to the Cartesian mesh and coordinate system discussed above. For helix chute simulations, the cylindrical mesh can be set up such that the curved cell edges will match with the curved inner and outer walls of the helix chute. This avoids the non-physical turbulent energy dissipation discussed above. A significant disadvantage for this method is that the approach flow in the helix inlet transition is not aligned with the cylindrical mesh and is thus unstable and difficult to simulate. As such, simulating the approach flow was quickly abandoned and the flow at the helix entrance point was approximated. Any inadequacy of this flow-entrance approximation should be insignificant after the first quarter turn of the flow through the helix.

A simulation of the physical helix model was performed for comparison so that concerns with physical scaling effects (like Reynolds number and surface roughness) could be discounted. The inflow condition used for the first cylindrical mesh studies used a "source object" that was tilted so the water entered the simulation parallel to the chute floor. For the initial simulation the entrance velocities were both too low and very non-uniform. The low entrance velocity caused the velocities in the CFD model to lag behind those measured in the physical model. So, for comparisons at 300 ft^3/s (lead investigators recommended

this discharge) between the physical model and CFD model, locations of data extracted from the CFD model were rotated by 0.140 loops (50.5°) so that the maximum velocities of the physical model at loop 0.5 and CFD models matched. Later simulations used more appropriate entrance conditions so this rotation was not necessary.

Mesh comparisons of cylindrical mesh studies

Grid independence is found by refining a mesh until the output variables of consideration no longer change. That is, the solution is independent of the grid. Comparison simulations with 300 ft^3/s discharge were designated R00, R01, and R02 (Table A-1). Grid dependence comparisons of results are displayed in Table A-2. Maximum and average velocity data were directly extracted from simulation results. Comparison of physical and cylindrical CFD modeling results with 300 ft^3/s prototype discharges are shown in table A-3 of physical model results. It should be emphasized that to avoid scale effects, CFD simulations were carried out using model dimensions, although results are given at prototype scale. For the comparison in Table A-2, the largest percent change of maximum velocity and average velocity was 2.8 percent, indicating the 0.025 ft cell simulations were adequate.

Table A- 1. Mesh designations, comparisons, and details.

Designation	Cell size (ft)	Number of cells that simulated chute width	Total number of Cells	Run time (Seconds)	Simulation duration (hours)
R00	0.0500	8	500,864	20	4.5
R01	0.0250	17	4,257,344	20	149
R02	0.0125	34	34,058,752	2	258

Table A- 2. Cylindrical grid independence analysis.

	3rd Loop			Percent change	
Simulation designation	R00	R01	R02	R01-R00	R02-R01
Maximum velocity - model units (ft/s)	12.43	12.14	12.21	-2.38	0.63
Average velocity - model units (ft/s)	11.52	11.20	10.88	-2.81	-2.82

	6th loop			Percent change	
Simulation designation	R00	R01	R02	R01-R00	R02-R01
Maximum velocity - model units (ft/s)	13.32	12.85	12.96	-3.52	0.85
Average velocity - model units (ft/s)	10.80	11.59	11.47	7.25	-1.03

Table A- 3. Comparison of physical and cylindrical CFD modeling results with 300 ft^3/s discharges.

	Physical model data expressed as prototype values		CFD model of physical model at T=2.0 seconds, R01 run		
Loop	Maximum velocity (ft/s)	Percent Increase	Velocity at 230.5° or 129.5° - model units (ft/s)	Velocity adjusted to prototype scale (ft/s)	Percent difference from physical model
0.5	27.74		9	27.74	0.00
1	32.84	18.39	10.75	33.13	-0.89
1.5	35.14	6.99	11.25	34.67	1.32
2	37.29	6.14	12.09	37.26	0.08
2.5	38.22	2.48	12.35	38.07	0.40
3	39.07	2.22	12.7	39.14	-0.20

Turbulent dissipation comparisons

The intention of the cylindrical mesh studies was to improve inconsistent turbulent dissipation observed at the outer wall of the Cartesian mesh studies. Cartesian meshes showed turbulent dissipation that ranged between 100 to 400 ft-lbf/slug/s in one quadrant and appeared to be dependent on the FAVOR function used by FLOW-3D (Figure A-5). That is to say, the simulated face of the helix outer wall was too rough and caused excessive turbulence where the interpolated flow surfaces were not aligned with the principal directions of the Cartesian coordinate system. The same section using a cylindrical mesh which perfectly matched the outer helix wall had consistent turbulent dissipation at around 50 ft-lbf/slug/s (Figure A-6), providing greater confidence in the cylindrical mesh studies.

Cartesian mesh	Cylindrical mesh
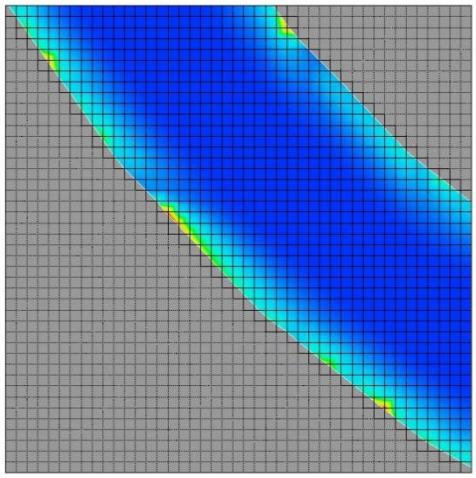	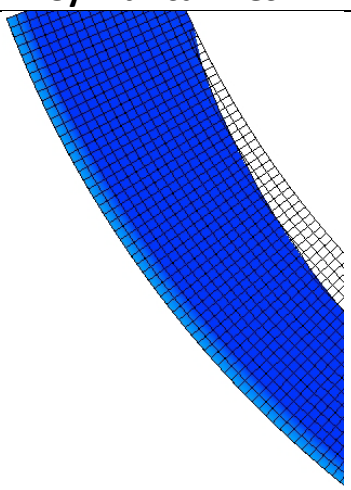
Figure A- 5. Cartesian coordinates at 400 ft3/s	Figure A- 6. Cylindrical coordinates.

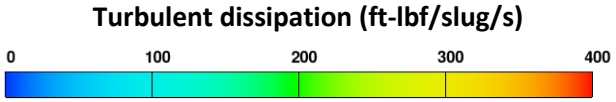

Recognition of other uncertainties

Other causes of uncertainties in the CFD results were determined to be insignificant, including:

- Instantaneous values were used as opposed to long term averages
- Total simulation time
- Temperature of water
- Salinity of water
- Density of water
- Surface roughness

Appendix B – Helix Design for Dual Entrances

Introduction

This appendix provides information concerning the flow characteristics of the proposed helix structure for downstream passage of fish at Cle Elum Reservoir. The original plan for helix operations allowed for two adjacent inlets at different elevations to operate simultaneously. This meant that the merging of these flows needed to be accomplished in a manner that was smooth and free of extreme turbulence or shear that could cause injury to fish. Various shapes and sizes of the helix chute and methods to transition water into the helix were investigated. A Computational Fluid Dynamics (CFD) study was used for this effort.

Methods

Investigation Approach

This study began by simulating the full helix structure including the inlets into the helix, helix chute, and outlet. Once the helix chute shape was optimized, the full helix study resumed with investigations of various methods to transition the flow into the helix structure at six different elevations. Specific objectives of the study included:

- Minimize impingement of flow and fish;
- Produce smooth flow conditions;
- Reduce secondary flow rotation that can cause fish roll-over;
- Minimize splashing, sloshing, and turbulence;
- Minimize pressure gradients; and
- Minimize shear zone and turbulence when merging flows from adjacent inlets.

Configurations and Results

To show the investigation discovery and development process, simulations are presented in the order in which they were investigated. Deciding the next configuration to investigate was a team effort and was generally an attempt to improve flow conditions observed in the previous case.

For each case the investigated helix had 11.76 ft elevation difference between each loop to match conduits from the reservoir inlet structure. Subsequent to the

study, the elevation difference between each loop was modified to 11.75 ft, and the team determined that the hydraulic difference would be insignificant.

Model Configurations

The initial intent of this part of the study was to confirm the adequacy of the designer's initial concept prior to the constructing the physical model of the helix structure.

Case 1 Helix – Initial drop chute design with asymmetric helix chute cross-section

Case 1 Configuration

Geometry for Case 1 was developed by the Water Conveyance Group. To prevent interference with flows entering above each helix inlet, Case 1 used a drop chute (Figure B-1), where water "dropped" from the helix inlet transition chute into the helix chute. The helix transition included the approximate opening diameter of a pinch valve (included in initial design for controlling flow into helix) for 400 ft^3/s with the maximum reservoir head for this case. A U-shaped 6 ft wide chute, which curved downward 5 feet over 28 feet length, dropped the water into the asymmetrical U-shaped, 7 foot wide, 52-foot diameter helix chute. The asymmetrical U-shaped helix chute was 7 ft wide with a 1 foot horizontal bottom and two different radii for the inner and outer wall.

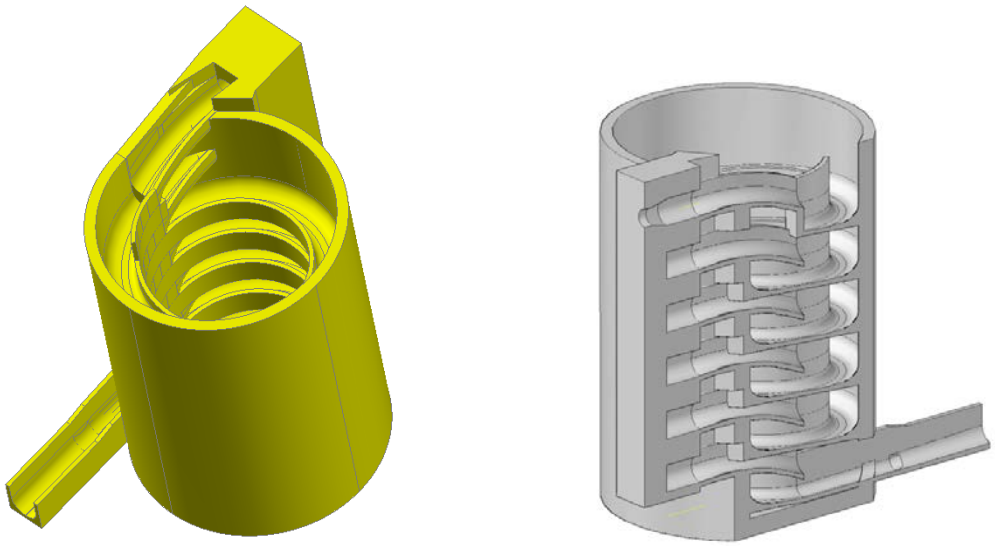

Figure B- 1. Solids view (left) of Case 1 helix configuration (top), and cut away view (right). Only the top inlet was completely modeled for Case 1. This configuration included the approximate opening diameter of a pinch valve for 400 ft^3/s with the maximum reservoir head for this case. The 6 foot diameter conduit was joined to a U-shaped chute, which curved downward 5 feet over 28 feet length, then dropped the water into the asymmetrical U-shaped, 7 foot wide, 52-foot diameter helix chute.

Case 1 Results

The simulation of Case 1 demonstrated flow run up inside of the drop chute, downstream from the pinch valve. Additional concerns included splashing due to the 5-foot drop into the helix chute, and excessive banking in the chute which caused concern of roll-over. The flow in subsequent loops impacted with the chute above (figure B-2).

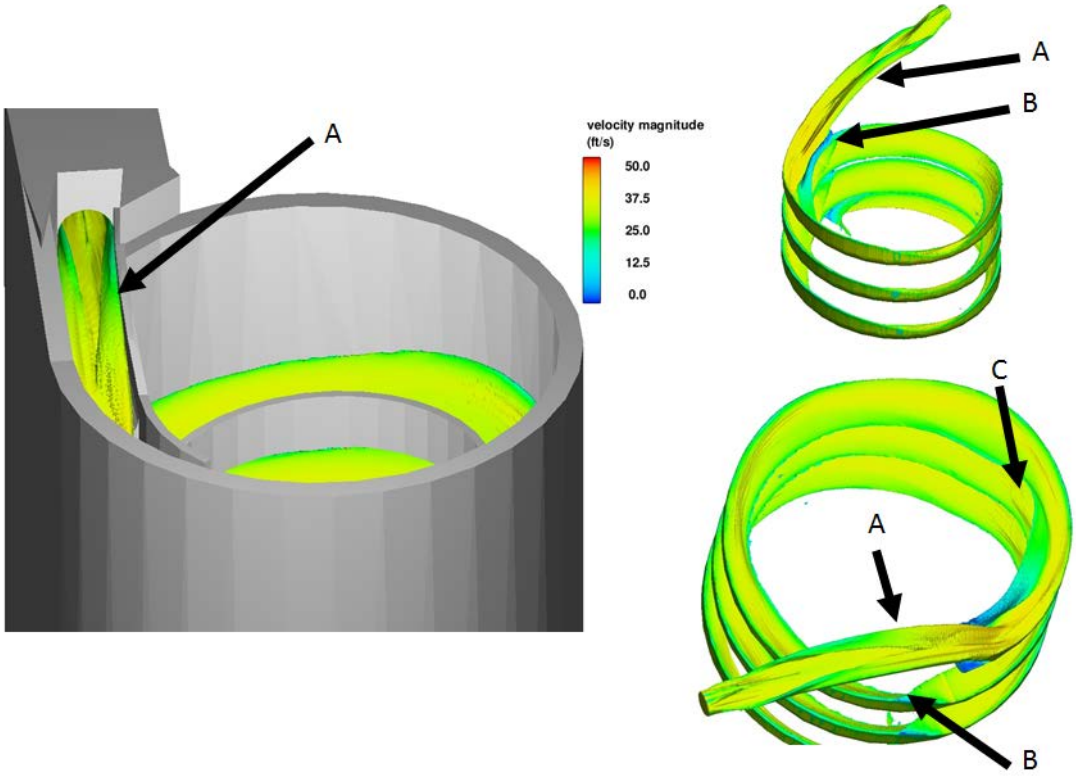

Figure B- 2. Case 1 velocity magnitude color contours. The simulation of Case 1 demonstrated A) high run up in the drop chute, B) flow from the second loop and each loop downward impacting with the drop chute above, and C) significant banking and run up.

Case 2 Helix – Realigned drop chute with 7 foot wide rectangular helix chute

Case 2 Configuration

To provide a smoother inflow condition into the helix, the section of the drop chute between the proposed pinch valve and the open section was sloped upward by 1 foot (figure B-3) to reduce run up and splashing. The drop chute was also realigned to enter at the centerline of the helix chute. The helix chute was modified to be a 7 foot wide rectangular shape. The thickness of the concrete at the end of the drop chute was reduced to allow more room for flow underneath.

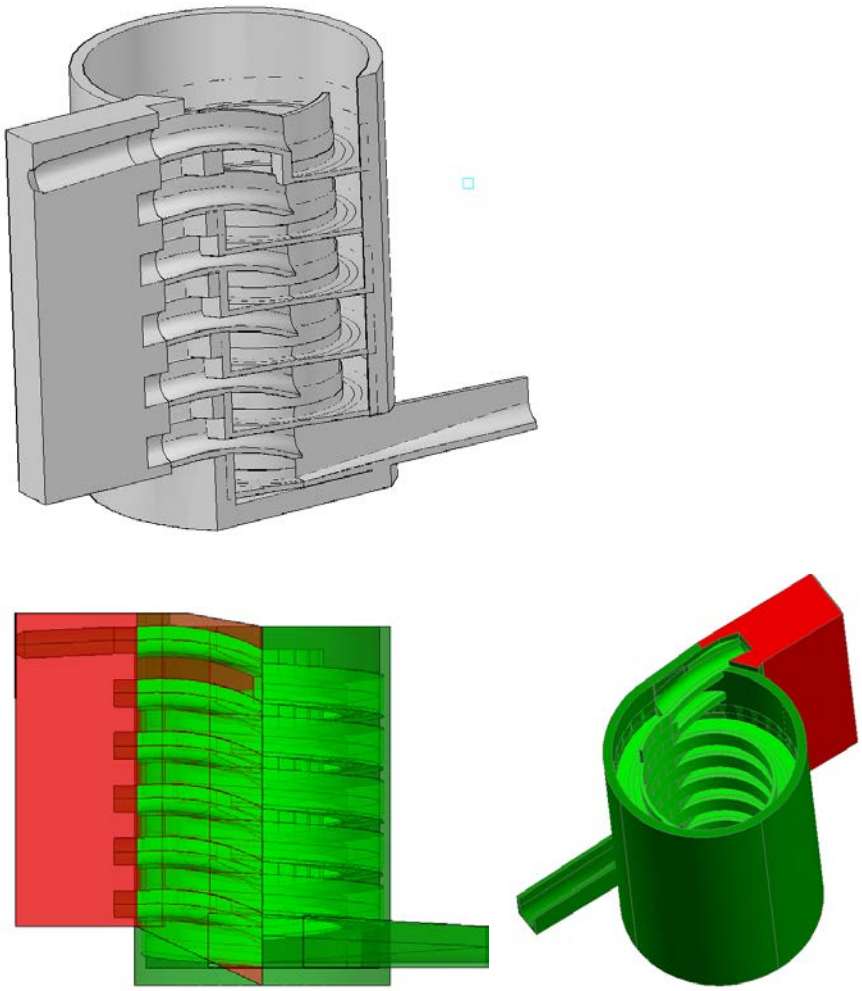

Figure B- 3. Cut away of Case 2 helix configuration (top), x-ray view (bottom left), and solids view (bottom right).

Case 2 Results

Flow run up inside the drop chute was reduced and less splashing was observed as the water entered the helix chute. There was still steady banking within the helix chute, and the flow in subsequent loops had a minor impact with the chute above (figure B-4).

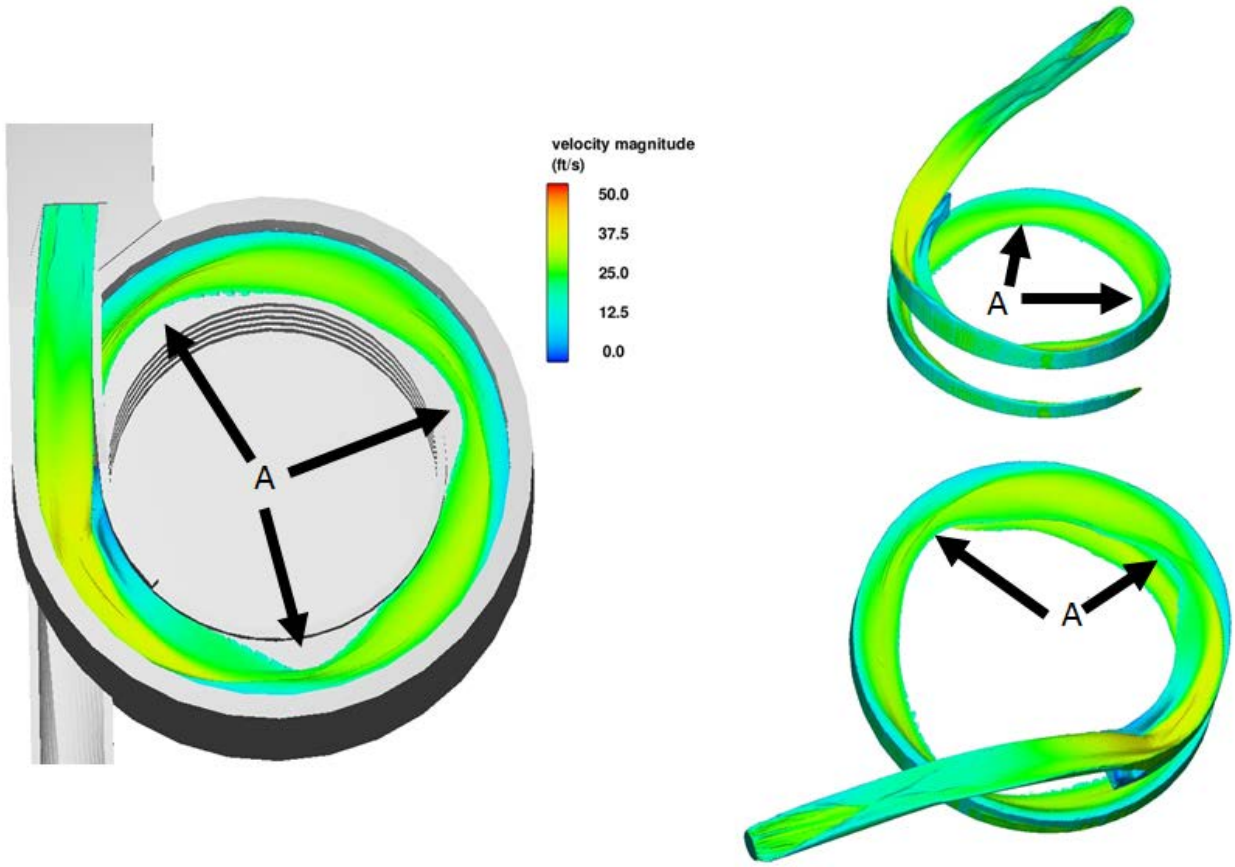

Figure B- 4. Case 2 velocity magnitude color contours. The simulation of Case 2 demonstrated A) significant banking and run up.

Case 3 Helix – Straightened Drop chute with 7 foot wide rectangular helix chute

Case 3 Configuration

To address banking concerns, Case 3 increased the helix diameter to 60 ft, as measured from the inside of the outside helix chute wall. The drop chute was straightened to enter perpendicular to the helix. The helix chute geometry was not modified from case 2 (figure B-5).

Case 3 Results

The simulation of Case 3 demonstrated that flow at the second loop would impact the drop chute above, and flow roll over may occur leading to potential injury or disorientation of fish (figure B-6).

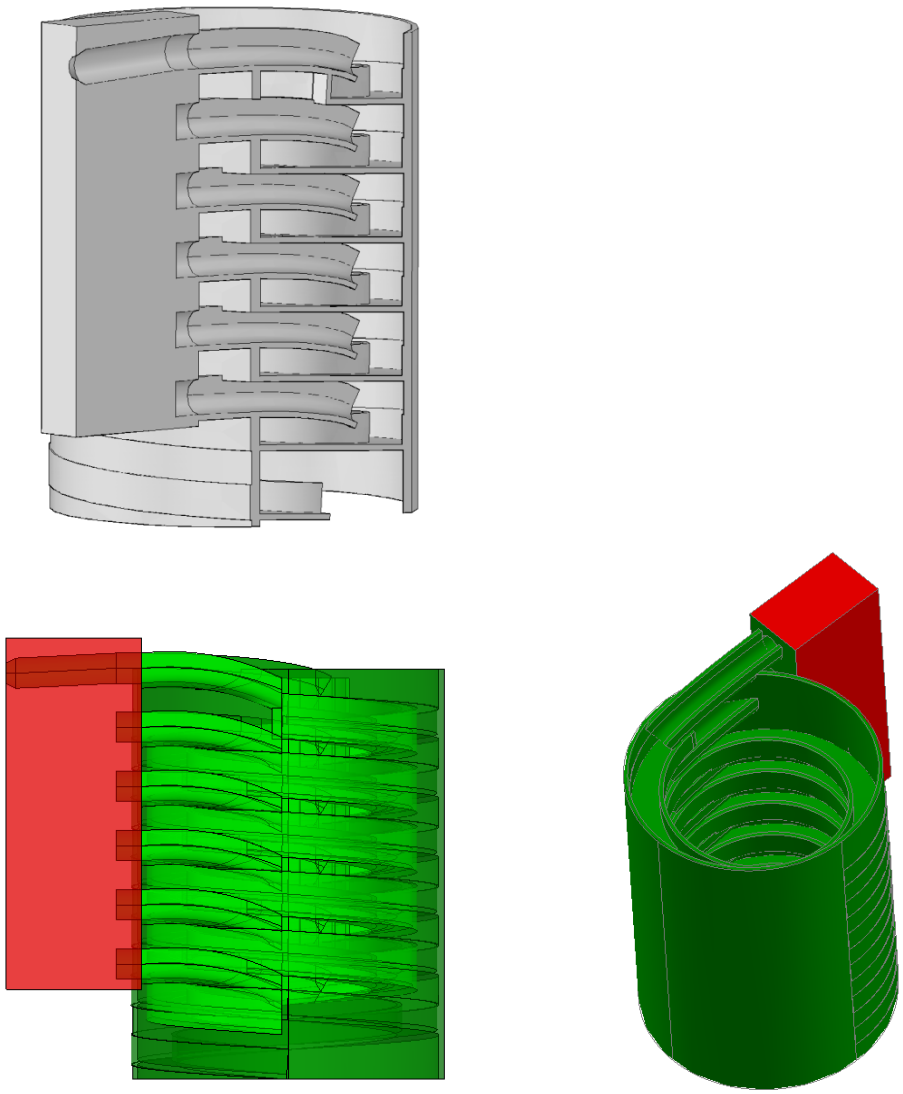

Figure B- 5. Cut away of Case 3 helix configuration (top), x-ray view (bottom left), and solids view (bottom right).

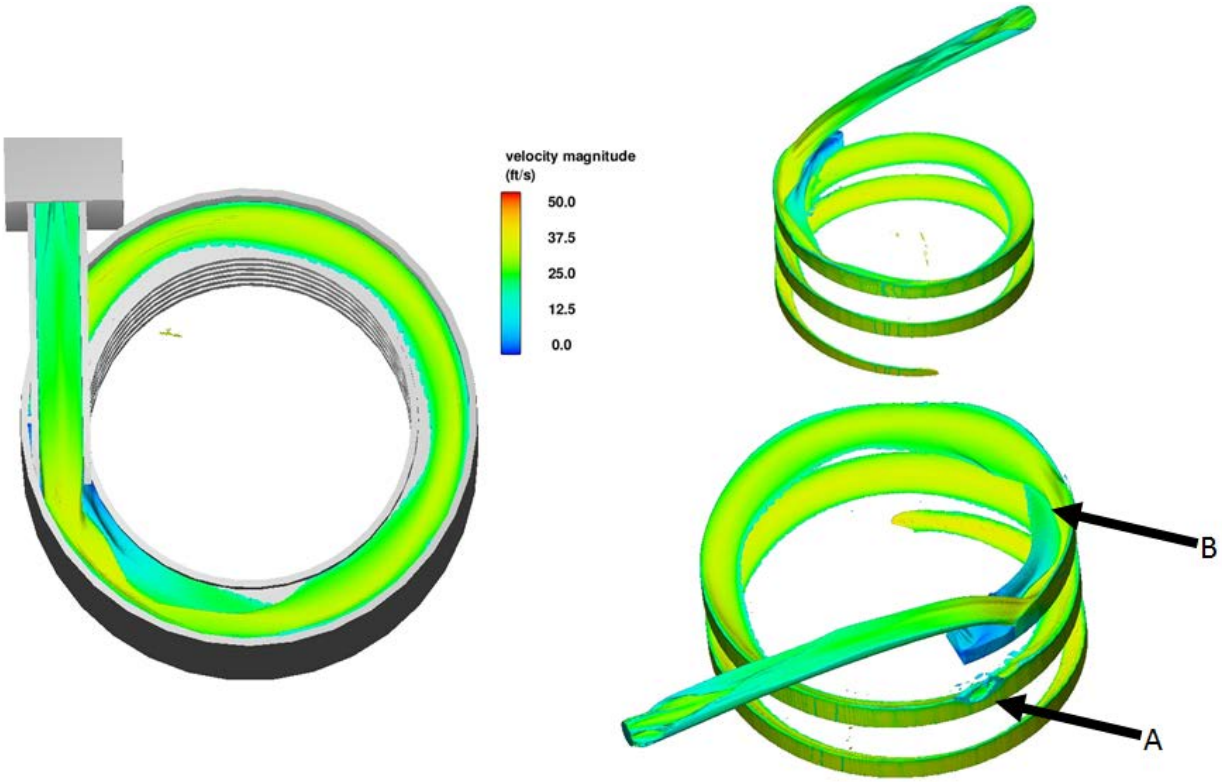

Figure B- 6. Case 3 velocity magnitude color contours. The simulation of Case 3 demonstrated A) flow at the second loop impacting with the drop chute above, and b) roll over of water that may roll over juvenile fish leading to disorientation.

Case 4 – Banked flow drop chute

Case 4 Configuration

This is the first case that used the ideal section from the Sensitivity Analysis (Sensitivity Analysis 5, 4 foot wide rectangular chute). The inlet channel curved along the first quarter of the helix structure so that the drop chute was at the second quarter point (figure B-7). In this design, flow control moved to the reservoir fish intake, and the channel upstream of the helix-inlet was opened up.

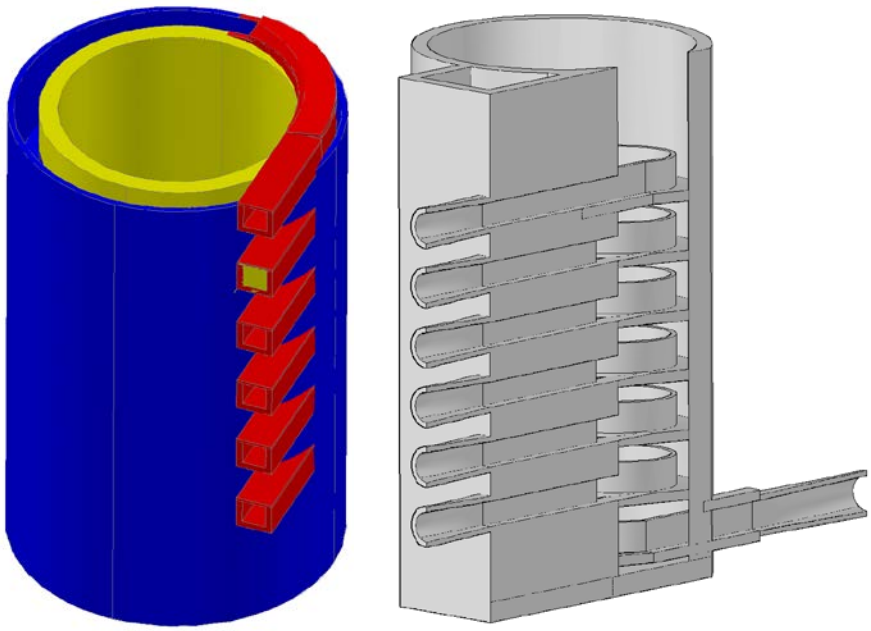

Figure B- 7. Case 4 helix configuration.

Case 4 Results

The simulation of Case 4 demonstrated that flow roll over may cause injury or disorientation of fish. Through the quarter turn to the drop, water was highly banked onto the outside wall as hoped. However, when the highly banked flow reached the chute floor, it shot across to the inside wall fairly quickly, initially causing a high banked flow on the inside wall. Also, shortly downstream from the drop there were indications of tumbling roll over. The flow also impacted the drop chute above at the second loop (figure B-8).

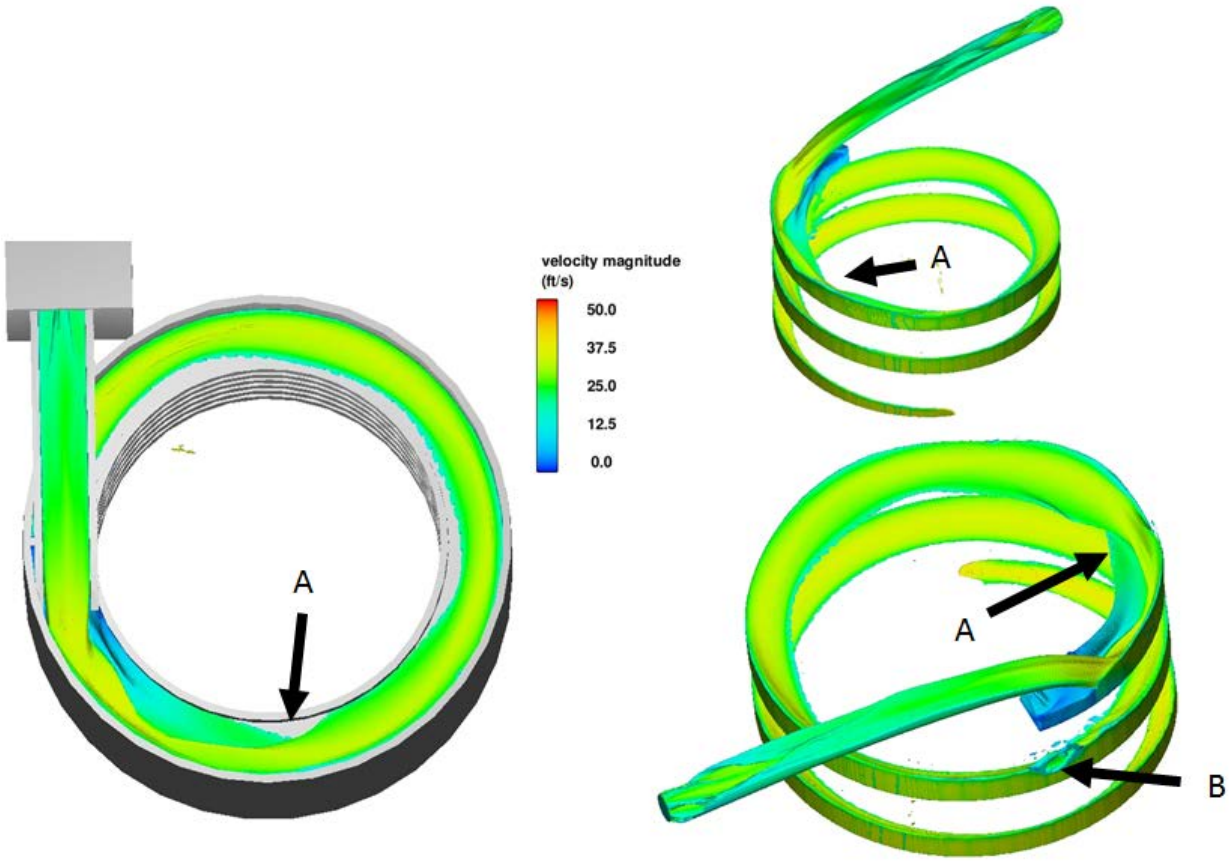

Figure B- 8. Case 4 velocity magnitude color contours. The simulation of Case 4 demonstrated A) tumbling roll-over of water that may roll over juvenile fish leading to disorientation and b) flow at the second loop impacting with the drop chute above.

Case 5

Case 5 Configuration

The helix chute slope was modified for Case 5 so that the helix inlet transition entrance was horizontal from side to side. This was achieved by steepening the helix slope approaching the inlet opening and maintaining a horizontal chute floor at and around the entrance. A straight gate was simulated at unused entrance locations (figure B-9).

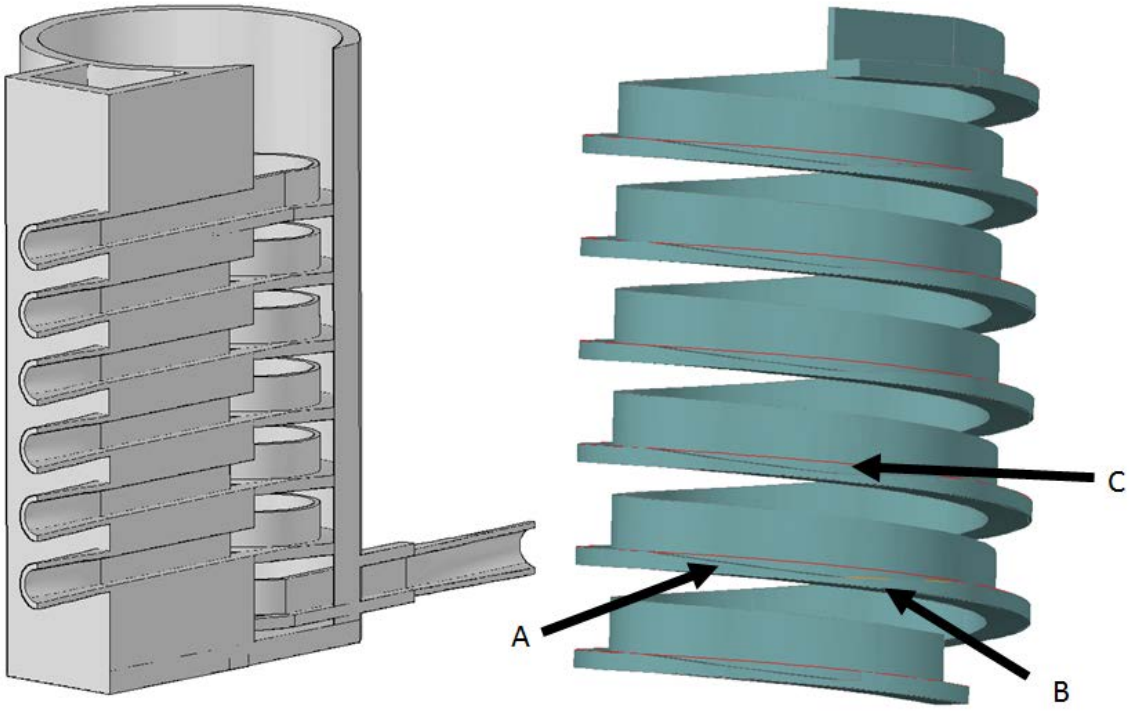

Figure B- 9. Case 5 Configuration. This configuration A) steepened the chute floor approaching the inlet, and B) maintained a horizontal chute floor near and around the entrance. The red line denoted by C) is the slope of the unmodified helix chute floor.

Case 5 Results

One significant issue was found with this configuration. The amount of run up at the downstream end of the closed straight gates was significant. This was due to both the steeper chute slope approaching this area and the abrupt change of direction of flow where the straight gate meets the curved helix wall.

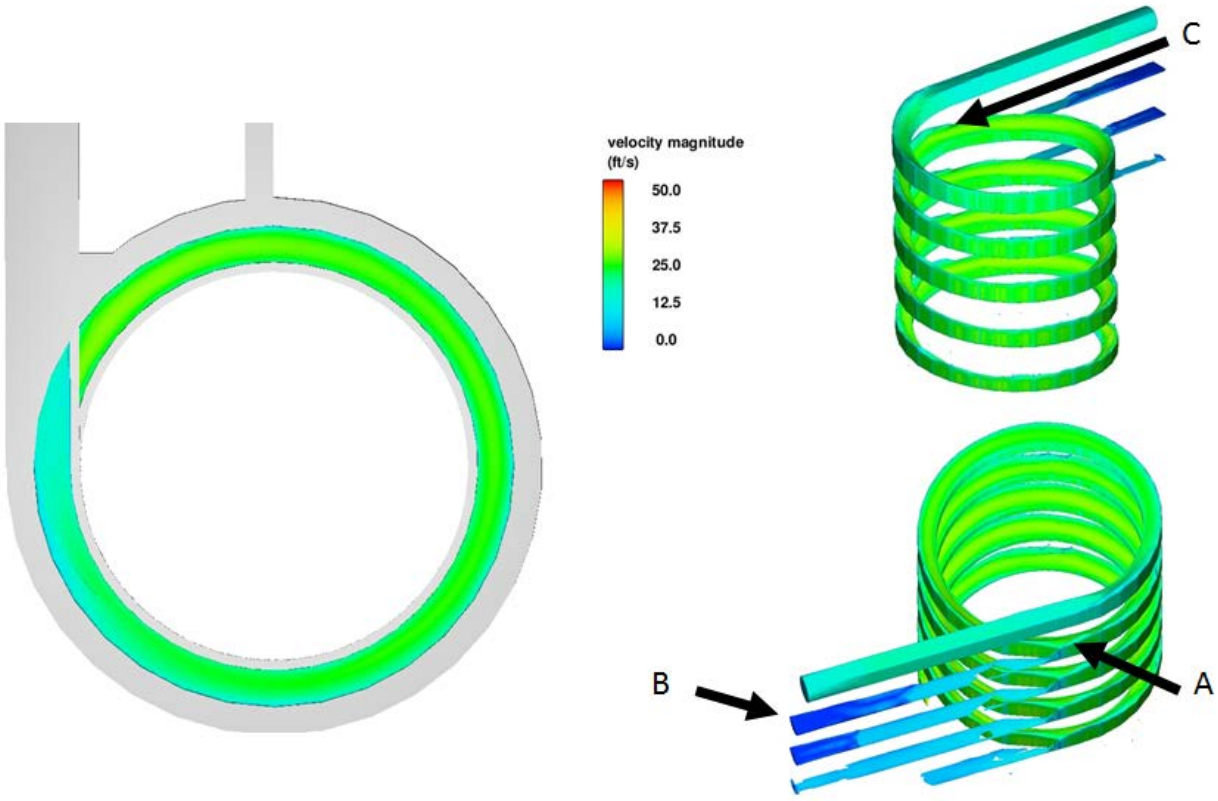

Figure B- 10. Case 5 velocity magnitude color contours. The simulation of Case 5 demonstrated A) significant run up at each end of the straight gate which may cause tumbling roll-over of water that may roll over juvenile fish leading to disorientation. Minor leakage denoted by 'B' was insignificant to the interpretation of the results. Impact with the overhead structure is indicated by 'C'.

Case 6

Case 6 Configuration

For Case 6, the helix inlet transition chute used a warped floor to match the edge of the unmodified helix chute (figure B-11). The warped floor of the helix inlet transition perfectly matched the edge of the unmodified helix chute (Cases 1-4). This caused a very unusual warped shape. To simplify development and construction, the last 3.5 ft (inside) to 10.4 ft (outside) of the warped section did not slope in the downstream direction. The configuration added a curved gate to help merge the flow more smoothly.

At this time it was undecided if the top helix inlet transition should be warped, or if a simple straight inlet would enter the helix at the quadrant. For modeling purposes, a simple straight helix inlet transition was developed and simulated with 200 ft^3/s from the top inlet and 200 ft^3/s from the next inlet with the gate set to 50 percent open.

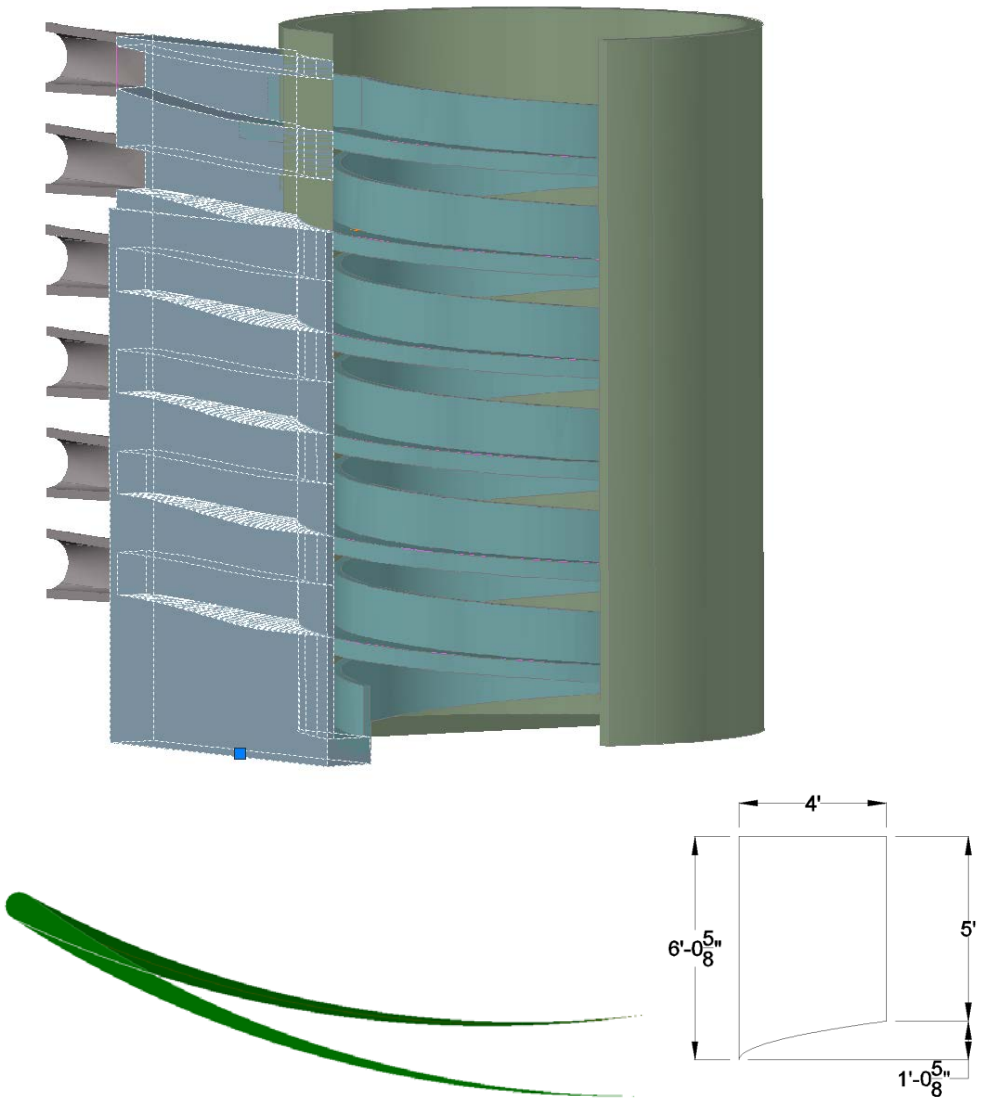

Figure B- 11. Case 6 used a warp floor for the helix inlet transition (bottom right) and a curved gate/guide vane that matched the helix radius (bottom left).

Case 6 Results

The simulation showed the flow jetting up between the gate and the inside wall of the helix (figure B-12). This could cause disorientation or injury for a small percentage of juvenile fish. This also exaggerated banking throughout the helix chute.

The final choice of whether to make the top helix inlet transition warped or straight to the quadrant should be based on cost and constructability, as the results indicated very little difference.

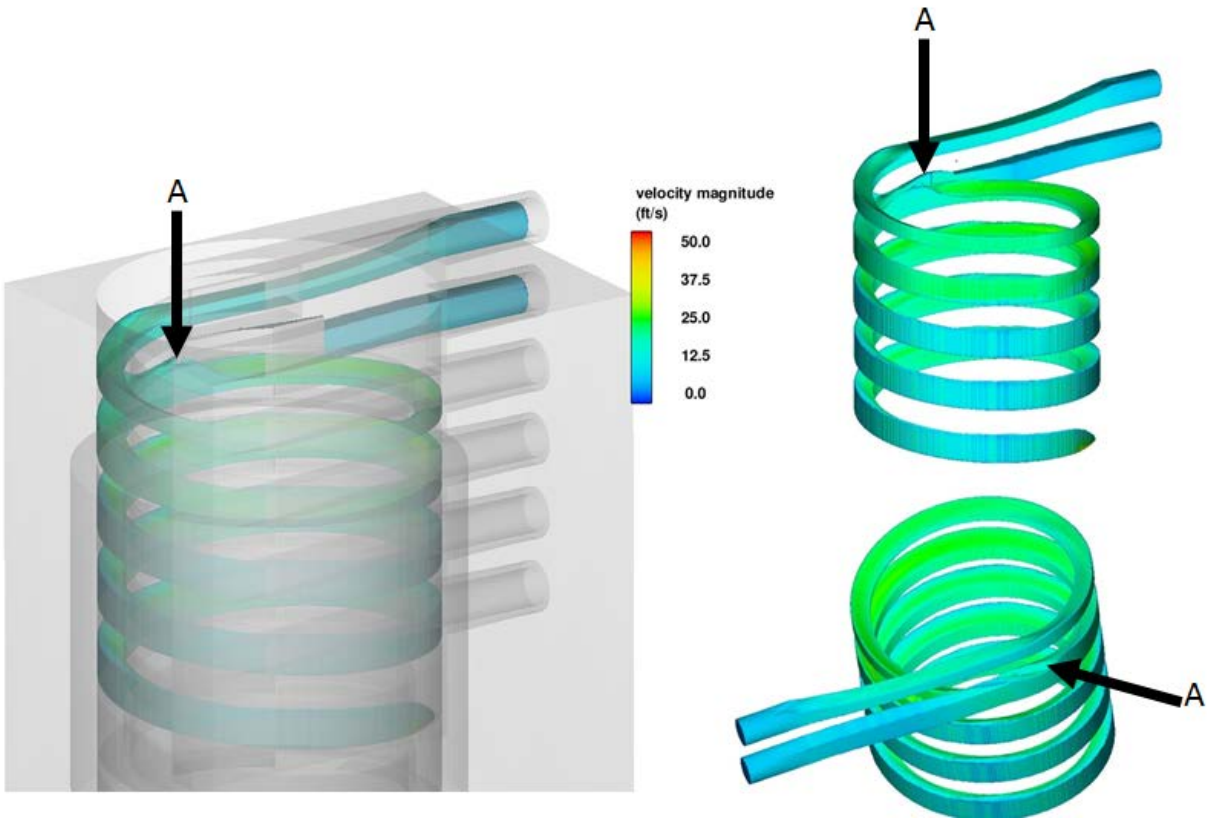

Figure B- 12. For Case 6, flow jetted up between the gate and the inside wall of the helix indicated by A.

Case 7

Case 7 Configuration

To decrease the jetting seen in Case 6, Case 7 used a 1-ft taller helix inlet transition and a 1-ft taller gate in an attempt to reduce jetting. An additional guide vane was placed at the gate hinge to improve flow conditions (figure B-13).

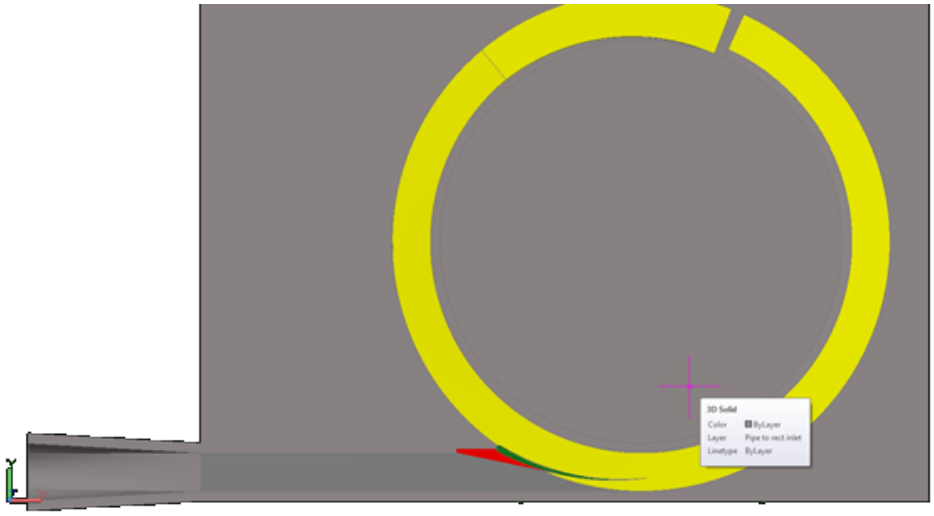

Figure B- 13. Case 7 used a taller gate and an additional guide vane (displayed in red) to improve flow conditions.

Case 7 Results

Flow still jetted up between the gate and the inside wall of the helix (figure B-14) causing the same concerns described in Case 6.

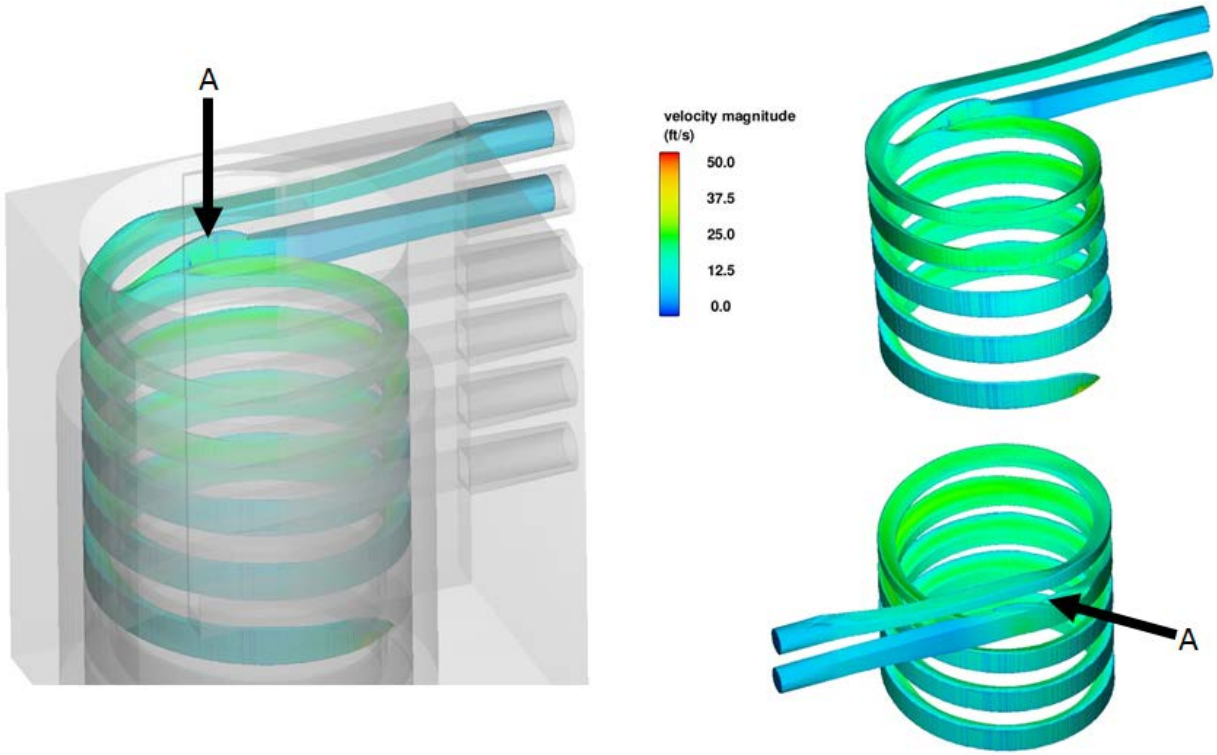

Figure B- 14. For Case 7, flow still jetted up between the gate and the inside wall of the helix indicated by A.

Case 8

Case 8 Configuration

This configuration modified Case 6 with a sliding cover between the top of the gate and the top of the helix inlet transition chute to prevent water from jetting upwards when entering the helix (figure B-15). The same helix inlet transition height was used as in Case 6 (figure B-11).

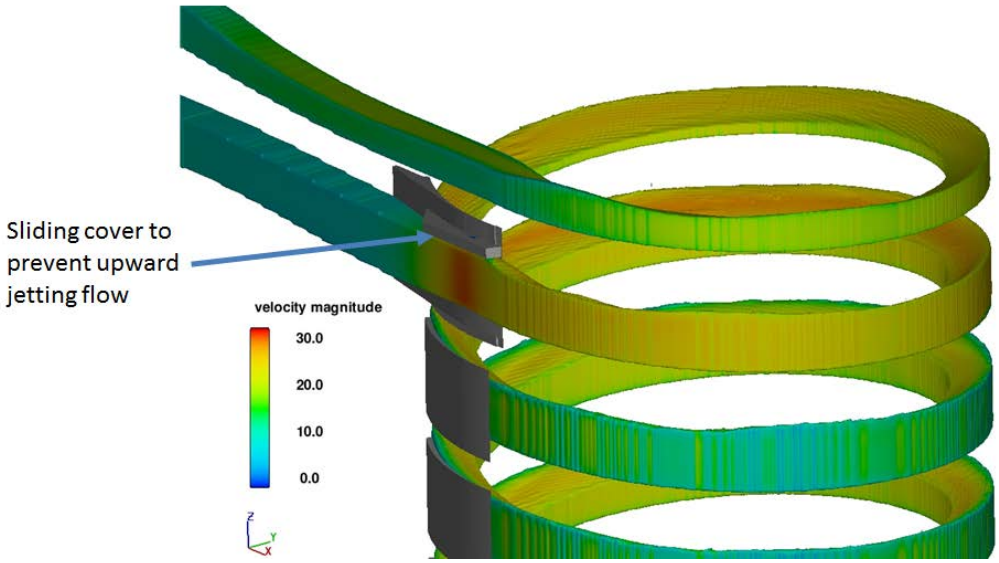

Figure B- 15. Case 8 modified Case 6 by adding a sliding cover.

Case 8 Results

This configuration produced the best results thus far for merging flow conditions. The gate opening of the lower inlet was throttled so that the velocity of the flow closely matched the velocity of the flow coming from the upper inlet to minimize turbulence and shear between the two flows (figure B-16). The throttled gate also caused the banked water surfaces from the two merging flows to more closely match up.

The Case 8 gate and transition design produced acceptable flow conditions for merging flows from two adjacent inlets operating simultaneously, and may be applicable to future sites where this is the desired operating criteria.

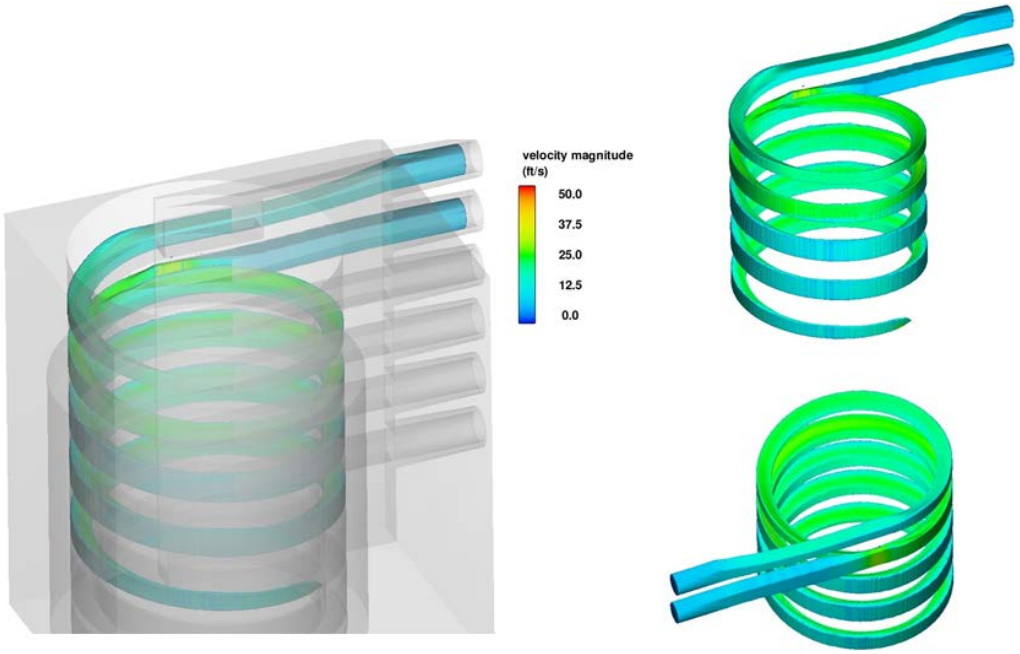

Figure B- 16. Case 8 demonstrated smooth flow and no roll over

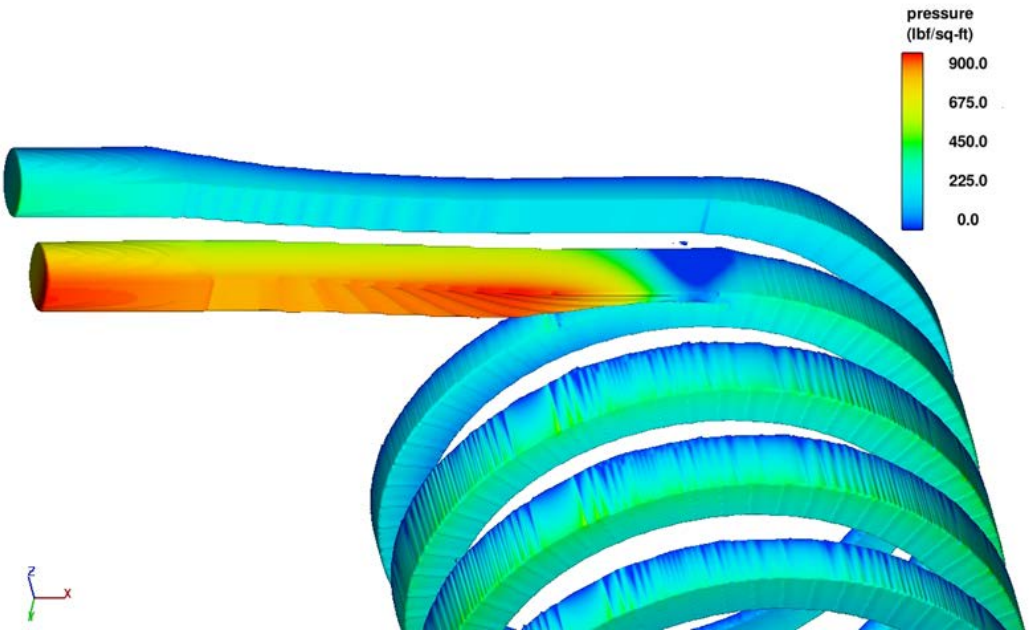

Figure B- 17. Smooth flow is demonstrated in Case 8 by gentle pressure transitions (taking into account the choppy graphical interpolation of the post processor).

Appendix C – Helix to Tunnel Transition

In the initial physical model, the downstream end of the helix merged immediately into a straight chute with the same 4-ft width as the helix chute (figure C-1). While it was not intended to be a first attempt at modeling this transition, it demonstrated an unexpected phenomenon. While significant run-up from sloshing (side to side standing waves) was expected a few chute widths downstream on the inside wall (left wall looking downstream for prototype), sharp run-up was unexpectedly observed on the inside wall beginning immediately at the joint where the channel straightened. It was determined that the immediate sharp run up was caused by the secondary currents from the helix chute (Appendix B). This added to the expected sloshing effect with maximum run up and tumbling roll over (roll over with white water and separation from main flow) occurring about 16-ft downstream from the end of the helix chute. Accordingly, the hydraulic design approach considered both sloshing from straightening the flow and sharp run-up from secondary rotational flow.

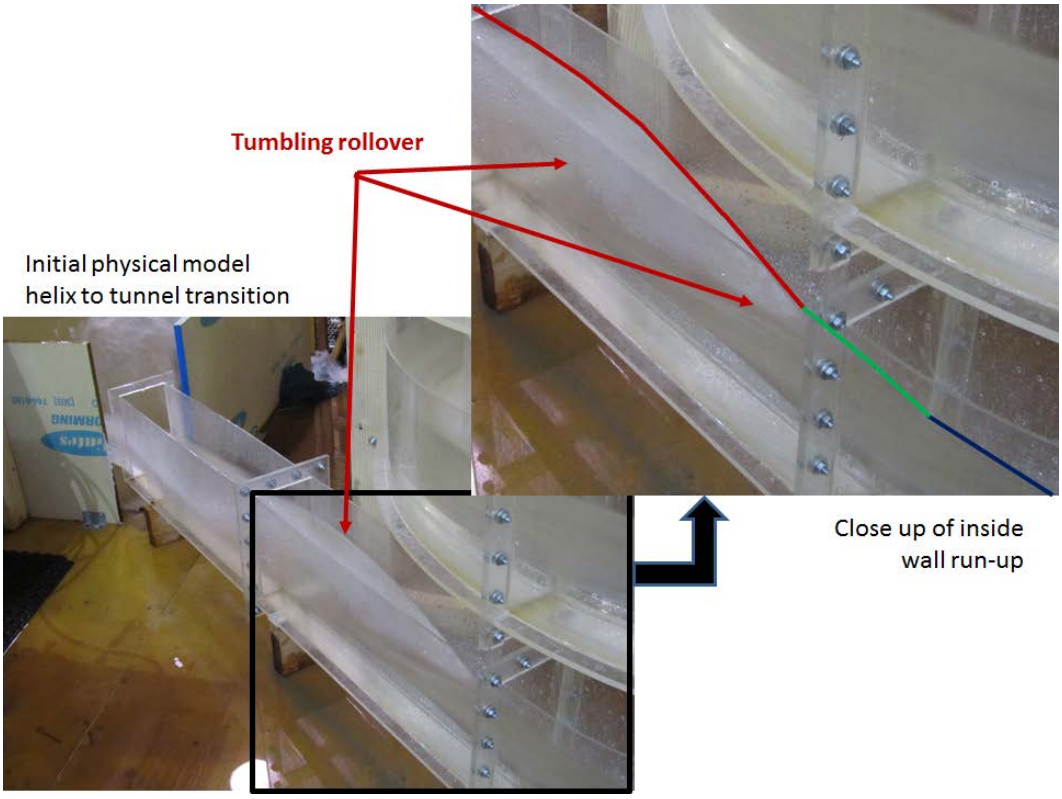

Figure C- 1. Initial transition used for the physical model (mirror image of prototype). While not intended for design purposes, study of this condition demonstrated an unexpected phenomenon. In the close up photo (top-right) the blue line indicates the water surface in the helix chute. The green line designates unexpected run-up. The red line designates run-up mainly caused by sloshing flow that caused tumbling rollover. The unexpected run-up denoted by the green line is caused by rotational flow seen in the cross sectional velocity profiles.

Investigation methods

This investigation used FLOW-3D v 11.0.1.8 by Flow Science Inc., a commercially available Computational Fluid Dynamics (CFD) program. Program variable settings were the same as listed in Appendix B. Since the physical model verified results, a sensitivity analysis was not deemed necessary.

Each proposed transition configuration was studied with a simulated flow of 400 ft^3/s, and the recommended Configuration Q was tested at both 400 and 200 ft^3/s.

All of these simulations used only three-quarters of a helix loop to avoid overlapping (z-direction) flows which can cause presentation difficulties. This also helped reduce simulation time.

These simulations used the Cartesian coordinate systems. Cylindrical coordinate system would better simulate flow in the helix, but the flow in the tunnel would be numerically unstable.

The inflow velocity into the helix was significantly increased to overcome excess energy losses associated with the use of the Cartesian coordinate system for the helix (see Appendix B for the discussion of this issue and how it was addressed in the studies that were focused on helix flow). In addition, 10 percent of the total 400 ft^3/s inflow was introduced near the outside-bottom of the chute and perpendicular to the flow at the flow-entry location to create a rotational flow at the start of the simulated helix section that would be similar to the rotational flow previously observed in the helix simulations described in Appendix B. These boundary condition adjustments were made to accelerate the full development of helix chute flow at the helix exit while using only three-quarters of a helix loop. Increasing the inflow velocity further appeared to create unstable flow and splashing not representative of the prototype.

The first five simulation configurations (A through E) used the design helix drop height (slope) of 11.75 ft per helix loop. The peak velocity only reached 36 ft/s, where nearly 40 ft/s was obtained in the physical model and in the simulations that used cylindrical coordinates. To increase the velocity, the remainder of the simulated configurations used a drop height of 16.0 ft per loop in order to offset the greater energy losses caused by the Cartesian coordinate systems (see Appendix B). A peak velocity of 38 ft/s was observed when using a drop height of 16.0 ft/loop. Consideration of steepening the slope further to achieve a peak velocity of 40 ft/s caused two concerns. First, steepening the slope appeared to have diminishing returns on velocity, such that it appeared the section would need to be significantly steeper to achieve 40 ft/s. Second, the effect of further steepening could cause changes to secondary flow, changes in direction of momentum, or other undesirable changes not accurately representing the prototype. With those concerns in mind, it was decided that 38 ft/s was acceptable.

CFD Investigations

Configuration A (Nov 21, 2014)

Although it was anticipated that additional refinement would be required due to the banked water surface and secondary currents in the helix that would cause sloshing, the first configuration used a simple two-stage transition. First, the inside edge of the helix exit was widened by 1 foot over 7 feet of length (figure C-2), and then over the next 16 feet (which ends inside the secant pile wall) the shape was transitioned from rectangular to round. This simulation used the design helix drop height of 11.75 ft/loop.

The simulation displayed an adverse slope (overhang) at the first standing wave, and tumbling roll-over at the second standing wave inside of the 7 foot diameter tunnel section (figures C-3 and C-4). Peak velocity at the helix exit was approximately 36 ft/s due to the additional headloss produced by modeling the helix section in Cartesian coordinates; the physical model and the cylindrical coordinate CFD models indicated that the helix exit velocity should be about 40 ft/s.

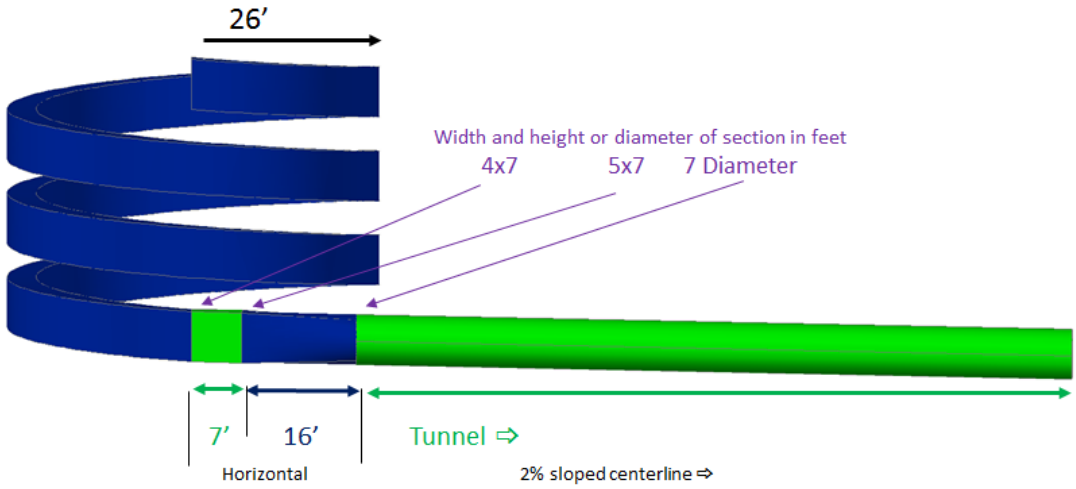

Figure C- 2. Design for Configuration A. The first configuration expanded the left side of the helix exit transition by 1 foot over a 7 foot length (shown in green). The alignment of the right wall in the 7-foot section matched the alignment of the helix chute's exit right wall. Over the next 16 feet (shown in blue), the conduit transitioned from rectangle to round symmetrically, using the AutoCAD Loft Command. Only three-quarters of a helix loop was simulated in FLOW-3D whereas the solids model presented above shows 3 full loops.

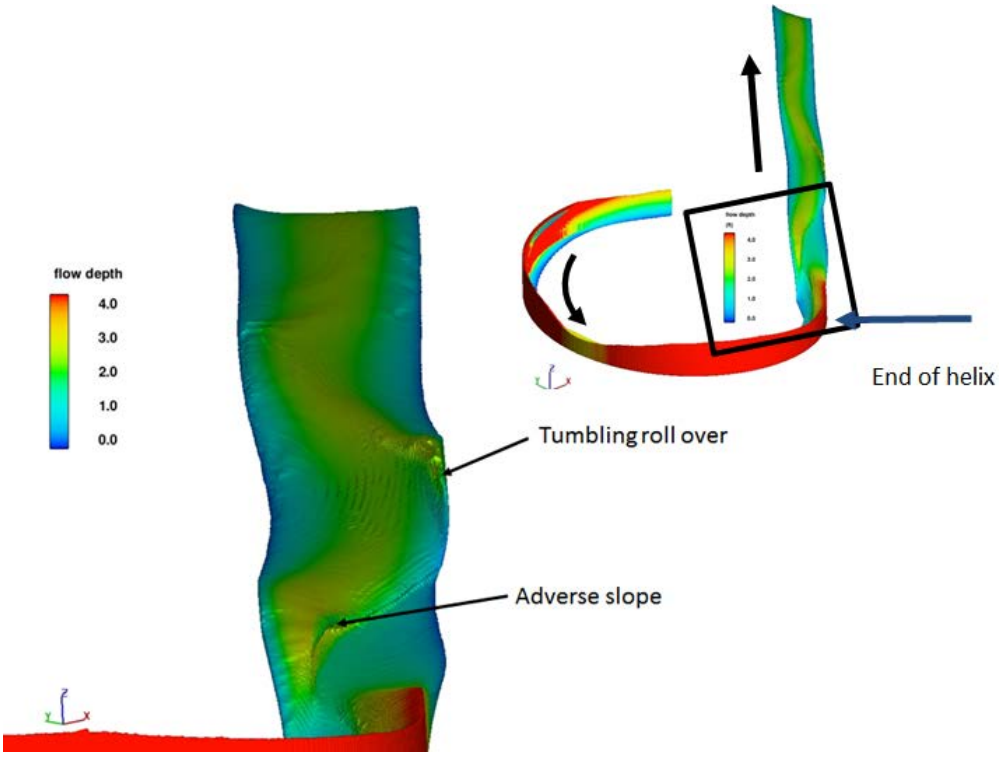

Figure C- 3. View of flow depths looking downstream at the transition flow in Configuration A. The helix chute ends shortly upstream of the red 4+ foot color contour. FLOW-3D may not have displayed tumbling roll over from an adverse slope (over hang) if the water fraction of those cells are below 50 percent water (highly aerated).

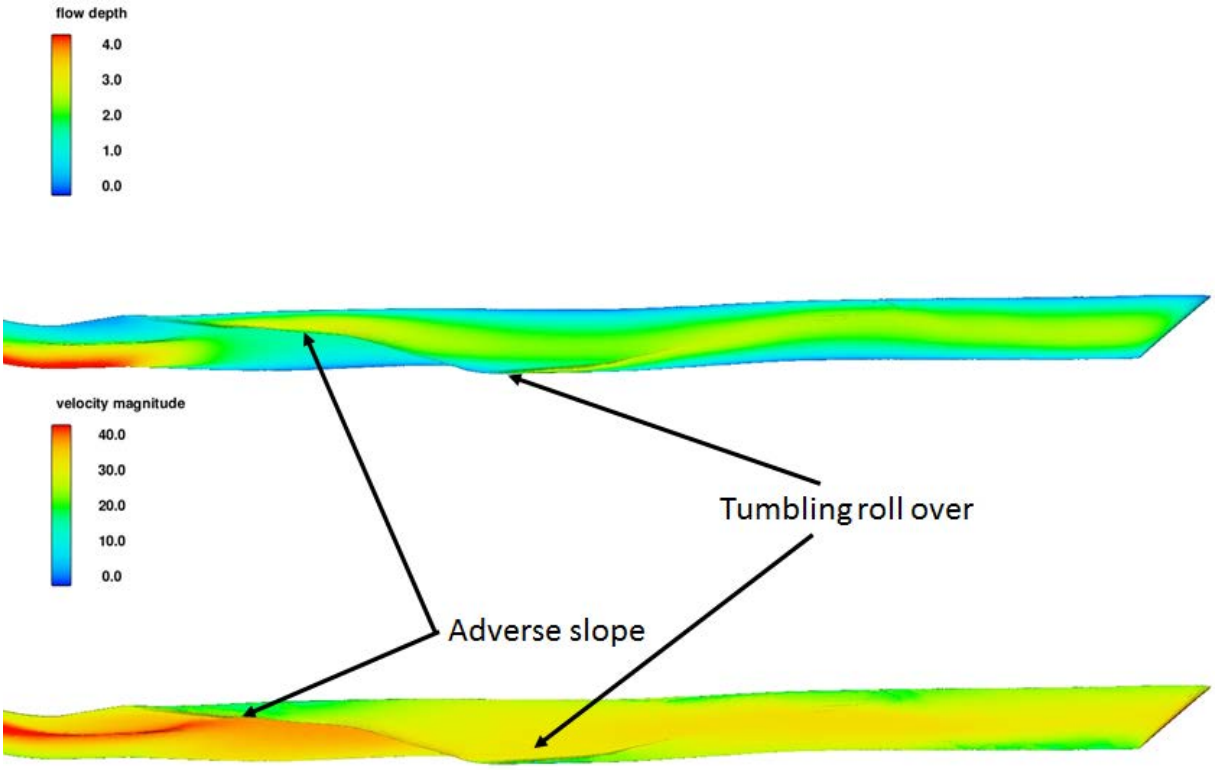

Figure C- 4. Looking down at flow depths (top) and surface velocities (bottom) for Configuration A. Flow is from left to right and the exit of the helix is at the left edge of the image.

Configurations B through D

Results of Configurations B through D are not presented herein; they had little effect on the design process, partly because a change in design direction was made prior to completion of the simulations. In brief:

- Configuration B (Dec 1, 2014): The 7-foot long section was changed to include a minor slope (0.2 ft)
- Configuration C (Dec 2, 2014): Run not completed due to change in direction of investigations.
- Configuration D (Dec 5, 2014): The design included 7-foot x 7-foot sections that would not fit within tunneling design constraints.

Configuration E (Dec 8, 2014)

This configuration used a 23 foot long rectangular to round transition in an attempt to stretch out and reduce the severity of standing waves and sloshing (figure C-5). This was the last simulation that used the helix loop design drop height of 11.75 feet.

While flow conditions improved over previous simulations, adverse water surface slopes were observed in two locations (figure C-6). Peak velocity at the helix exit was again only 36 ft/s (figure C-7). Peak velocity at the helix exit should have been 40 ft/s as demonstrated in previous studies.

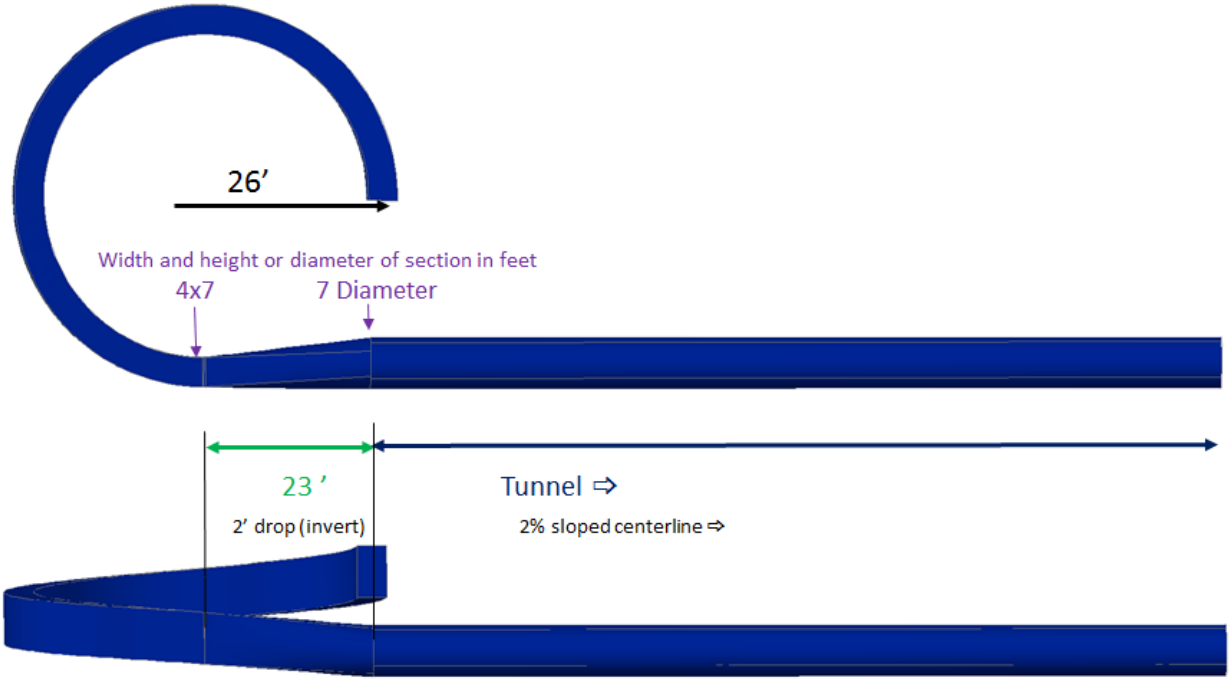

Figure C- 5. Design for Configuration E. This configuration used a single transition section to asymmetrically transition from the 4 by 7 helix exit to a 7 foot diameter tunnel in 23 feet. The right edge of the circular tunnel is tangent to the outside edge of the rectangular helix channel at its exit, and the left edge of the tunnel is offset (expanded) 3 ft to the left of the inside edge of the helix.

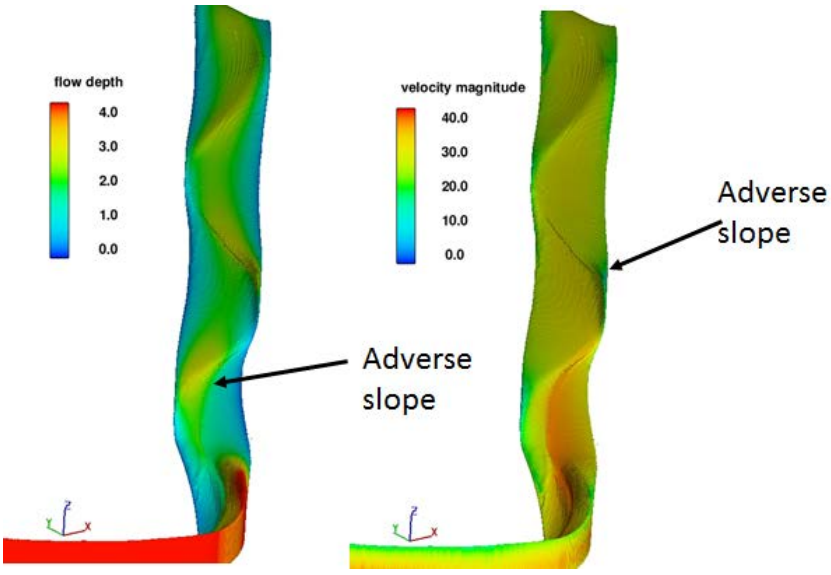

Figure C- 6. View of flow depths looking downstream at the transition flow in Configuration E. The helix chute ends shortly upstream of the red 4+ foot contour.

FLOW-3D may not have displayed tumbling roll over from an adverse slope if the water fraction of those cells are below 50 percent water (highly aerated).

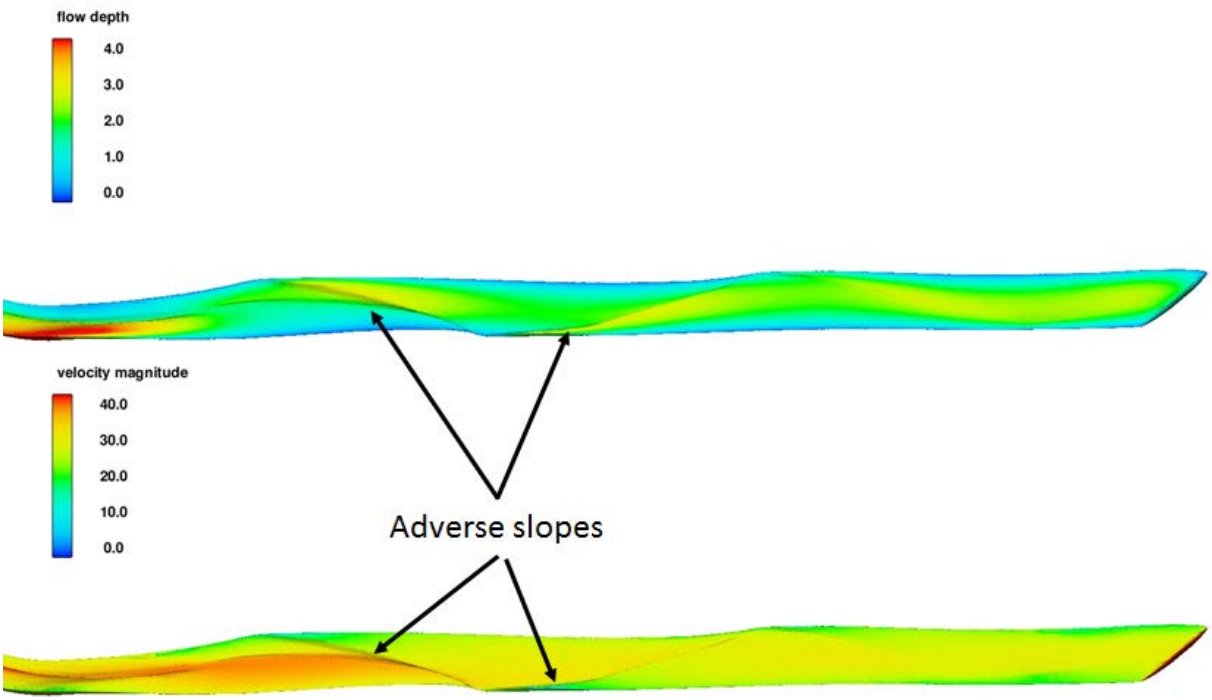

Figure C- 7. Looking down at flow depths (top) and surface velocities (bottom) for Configuration E. Flow is from left to right and the exit of the helix is at the left edge of the image.

Configuration F (Dec 18, 2014)

This configuration was the same as Configuration E except it modified the helix drop height to 16 feet/loop in order to more closely match the true exit velocity (figure C-8). This process is similar to increasing slope in a physical model to accommodate for friction which is too high due to a scale effect. For presentation purposes, the solids model for this simulation and the following simulations was rotated 51 degrees so that the tunnel direction would match the X direction in CFD simulations.

The peak velocity at the exit was 38 ft/s. The differences in flow patterns between Configuration E and configuration F are quite noticeable with obvious tumbling roll over occurring for Configuration F (figures C-9 and C-10). Sloshing also increased in the tunnel for Configuration F compared to Configuration E.

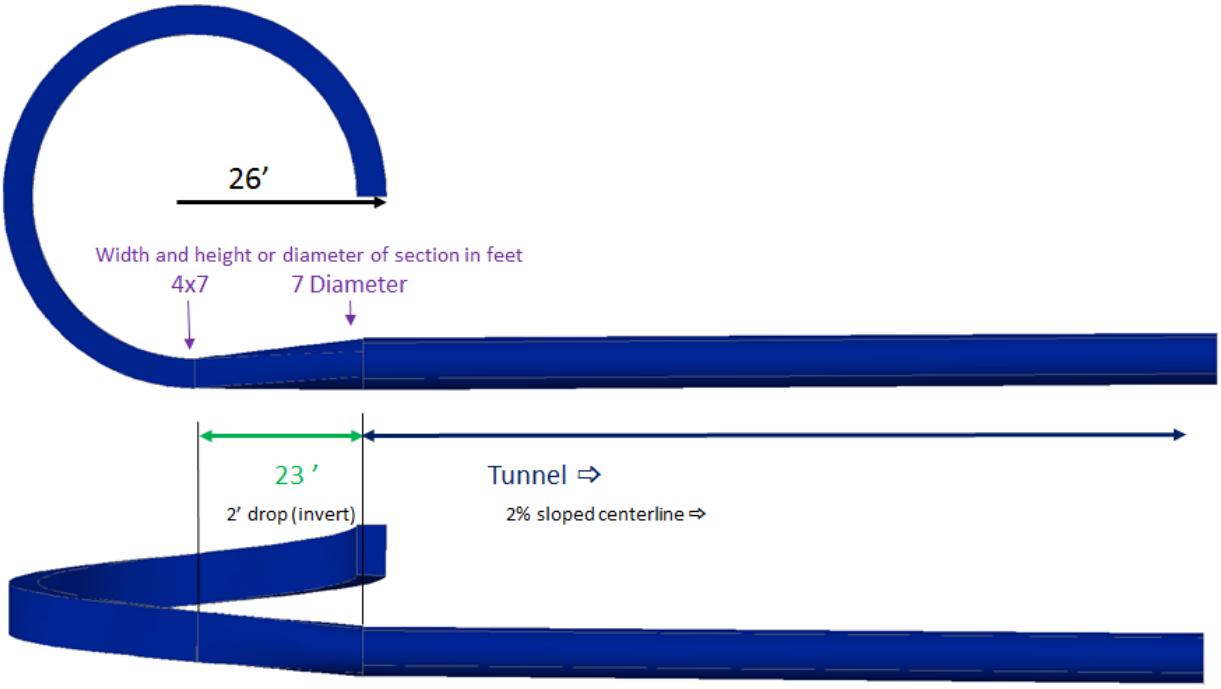

Figure C- 8. Design for Configuration F. This configuration was identical to Configuration E except the helix chute slope was steepened to overcome energy losses caused by the Cartesian coordinate system. The helix drop height was increased from 11.75 feet to 16.0 feet/loop. Configuration F used a single transition section to asymmetrically transition from the 4-ft by 7-ft helix exit to the 7 foot diameter tunnel in 23 feet. The right edge of the tunnel aligns with the right wall of the helix.

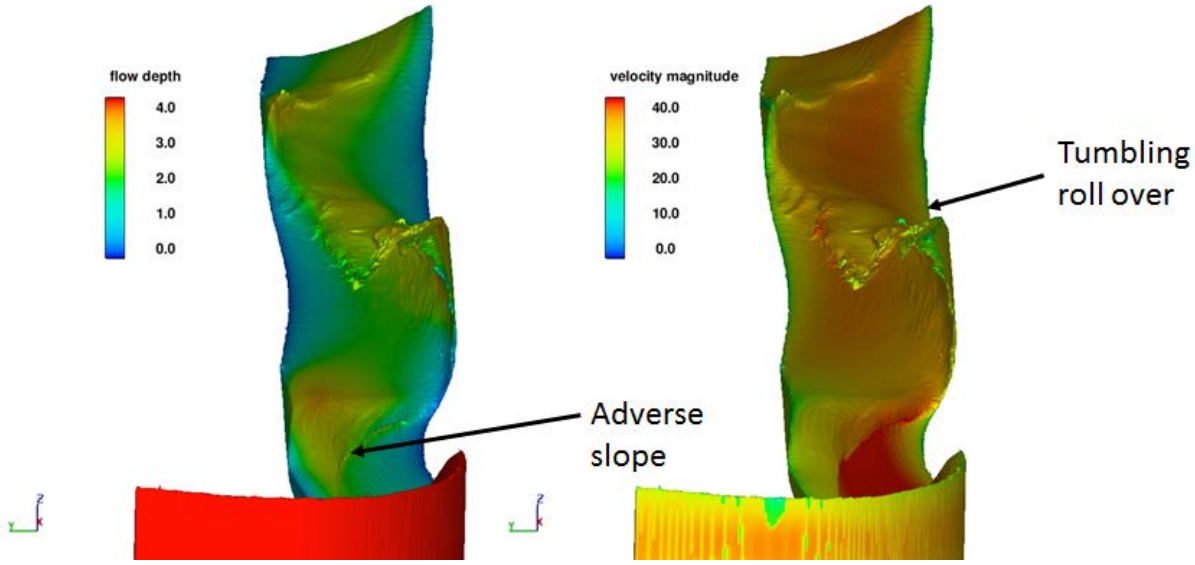

Figure C- 9. View of flow depths (left) and surface velocities (right) looking downstream at the transition flow in Configuration F. The helix chute ends shortly upstream of the red 4+ foot contour. FLOW-3D may not have displayed tumbling roll over from an adverse slope if the water fraction of those cells are below 50 percent water (highly aerated).

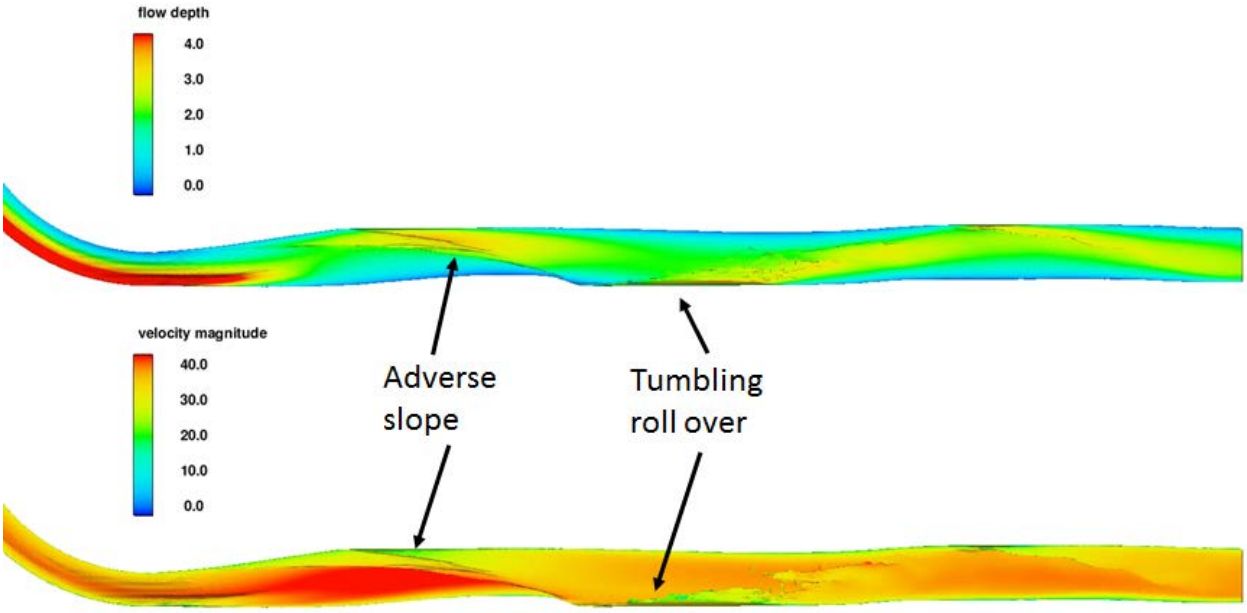

Figure C- 10. Looking down at flow depths (top) and surface velocities (bottom) for Configuration F. Flow is from left to right and the exit of the helix is at the left edge of the image.

Configuration G (Dec 23, 2014)

Configuration G was identical to Configuration F with the exception of a shift in tunnel location to the right by 6 inches which caused the transition section from rectangle to round to asymmetrically shift and changed the shape slightly (figure C-11). This was an attempt to reduce the tumbling rollover observed on the right side of Configuration F.

However, very little change was observed in the tumbling roll over and the sloshing in the tunnel increased (Figures C-12 and C-13).

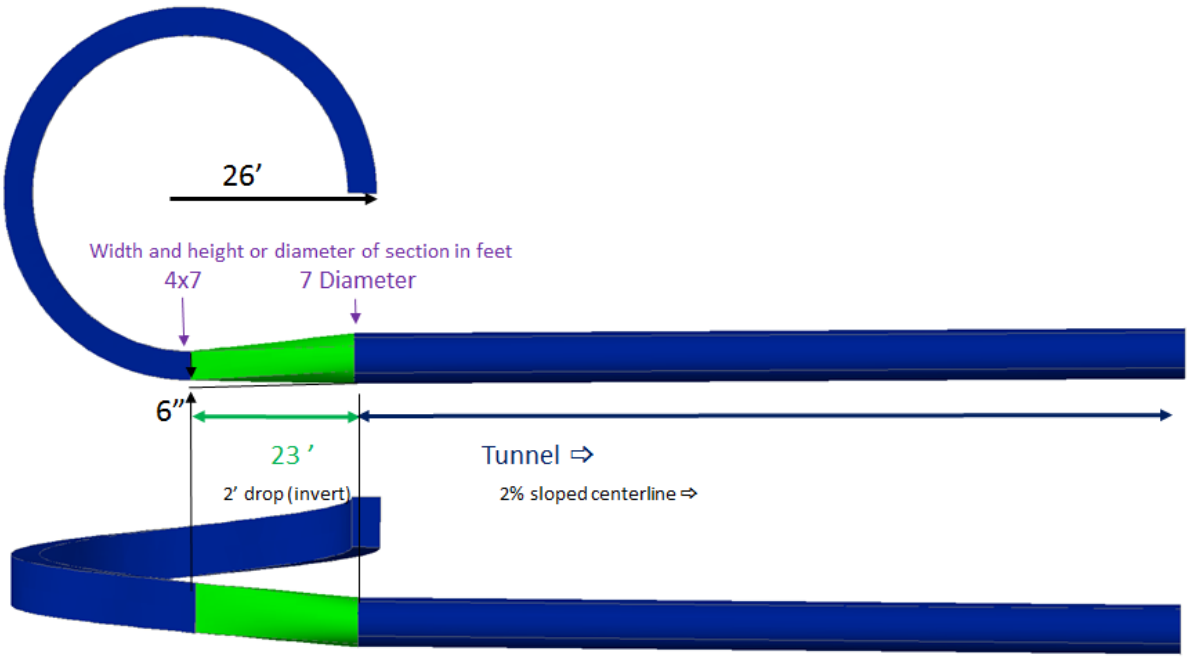

Figure C- 11. Design for Configuration G. This configuration shifted the tunnel in Configuration F 6 inches to the right so that the right edge of the tunnel is offset 6 inches out from the right (outer) edge of the helix channel and the left edge of the tunnel is offset 2.5 ft to the left from the left (inside) edge of the helix channel.

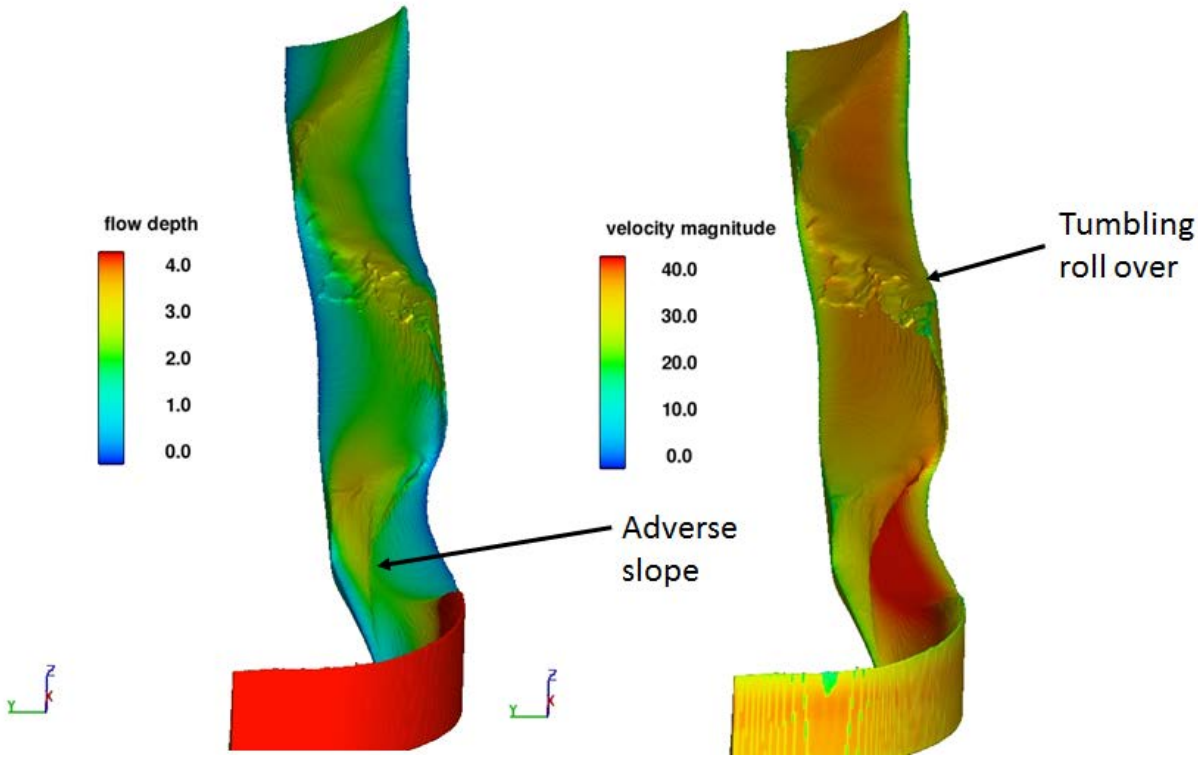

Figure C- 12. View of flow depths (left) and surface velocities (right) looking downstream at the transition flow in Configuration G. The helix chute ends shortly upstream from the downstream end of the red 4+ foot depth contour. FLOW-3D may not have displayed tumbling roll over from an adverse slope if the water fraction of those cells are below 50

percent water (highly aerated). The tumbling roll over appears to be similar to Configuration F.

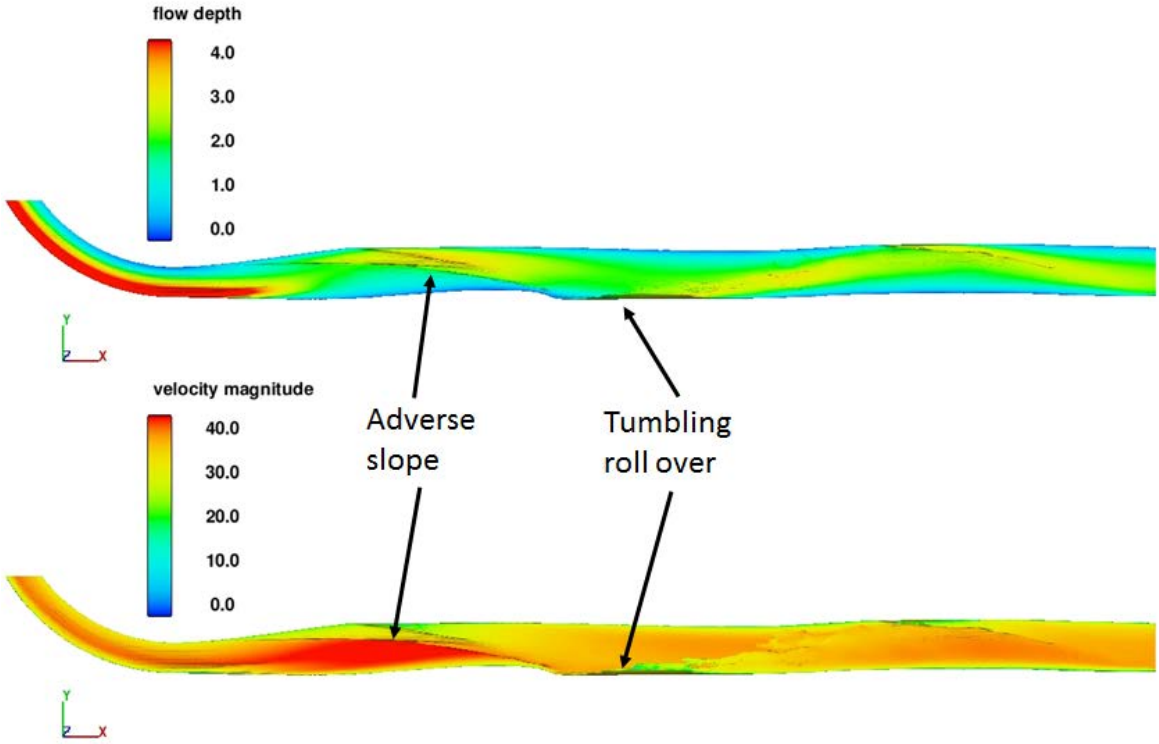

Figure C- 13. Looking down at flow depths (top) and surface velocities (bottom) for Configuration G. Flow is from left to right and the exit of the helix is at the left edge of the image.

Configuration H (Dec 30, 2014)

This Configuration modified Configuration F by gradually reducing the helix chute width from 4 feet to 3 feet for the last quarter turn (figure C-14). This was an attempt to reduce rotational flow in the last quadrant of the helix chute. It also lengthened the rectangular to round transition section to 27.8 feet.

The results show that this change slightly reduced the severity of the first standing wave and tumbling roll over at the second standing wave (figure C-15). Sloshing in the tunnel appeared more pronounced (figure C-16).

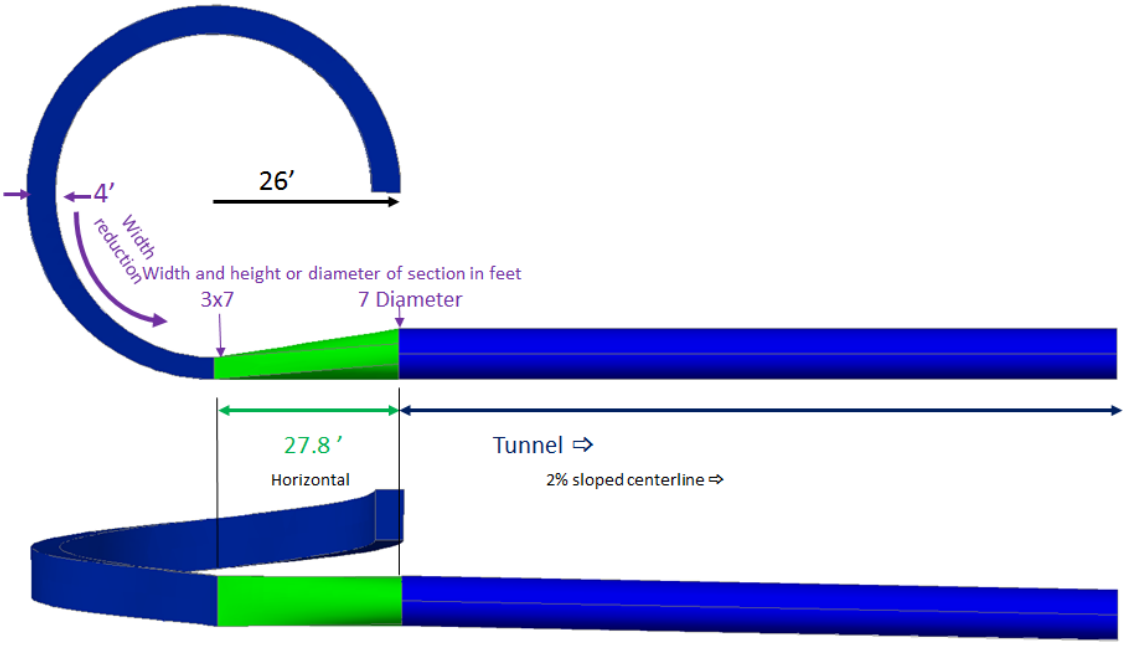

Figure C- 14. Design for Configuration H. This configuration reduced the chute width from 4 feet to 3 feet through the last quarter turn of the helix loop. The 2-ft drop in the rectangular-to-round transition section was also eliminated.

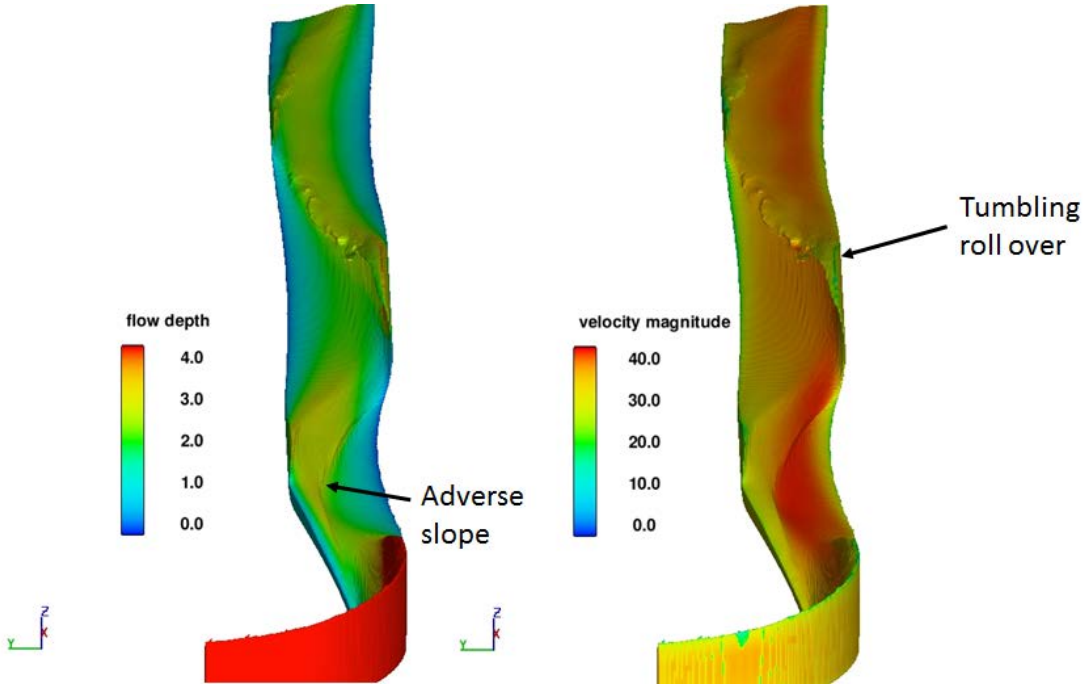

Figure C- 15. View of flow depths (left) and surface velocities (right) looking downstream at the transition flow in Configuration H. The helix chute ends shortly upstream of the red 4+ foot contour. FLOW-3D may not have displayed tumbling roll over from an adverse slope if the water fraction of those cells are below 50 percent water (highly aerated). The initial standing wave and tumbling roll over appears to be a slight improvement to Configuration G.

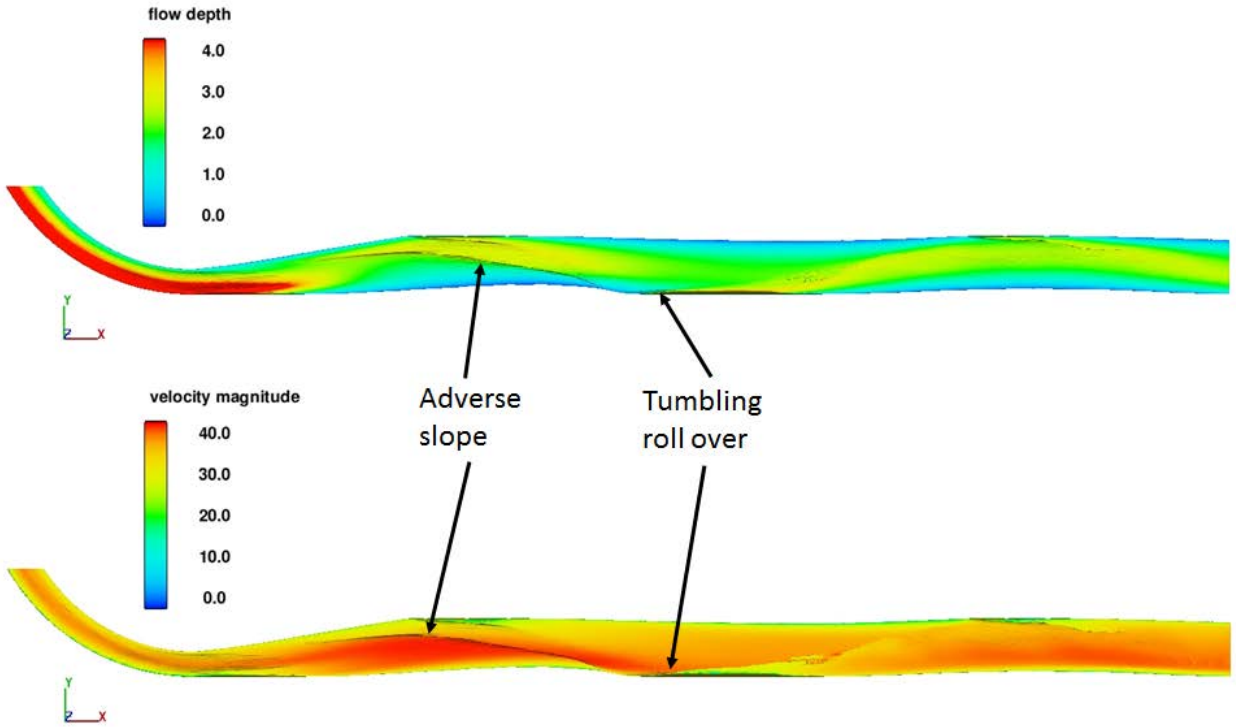

Figure C- 16. Looking down at flow depths (top) and surface velocities (bottom) for Configuration H. Flow is from left to right and the exit of the helix is at the left edge of the image.

Configuration I (Jan 5, 2015)

This configuration modified Configuration H by reducing the 2-foot drop in the 23-foot-long section to a 1-foot drop (figure C-17).

Velocity in the transition and tunnel were slightly reduced, but the initial standing wave and tumbling roll over remained about the same as Configuration H (figure C-18). Sloshing in the tunnel also remained about the same as Configuration H (figure C-19).

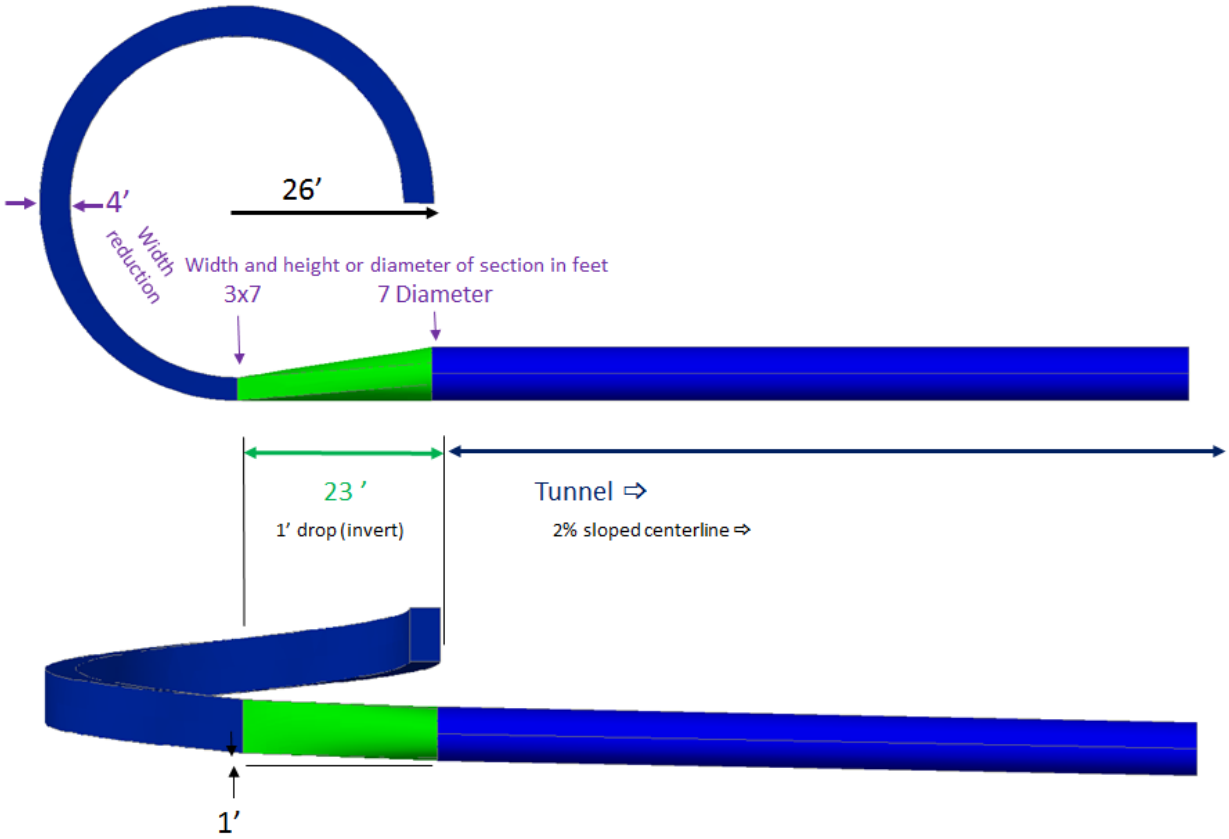

Figure C- 17. Design for Configuration I. This configuration reduced the slope of the 23-foot transition drop from 2 feet to 1 foot.

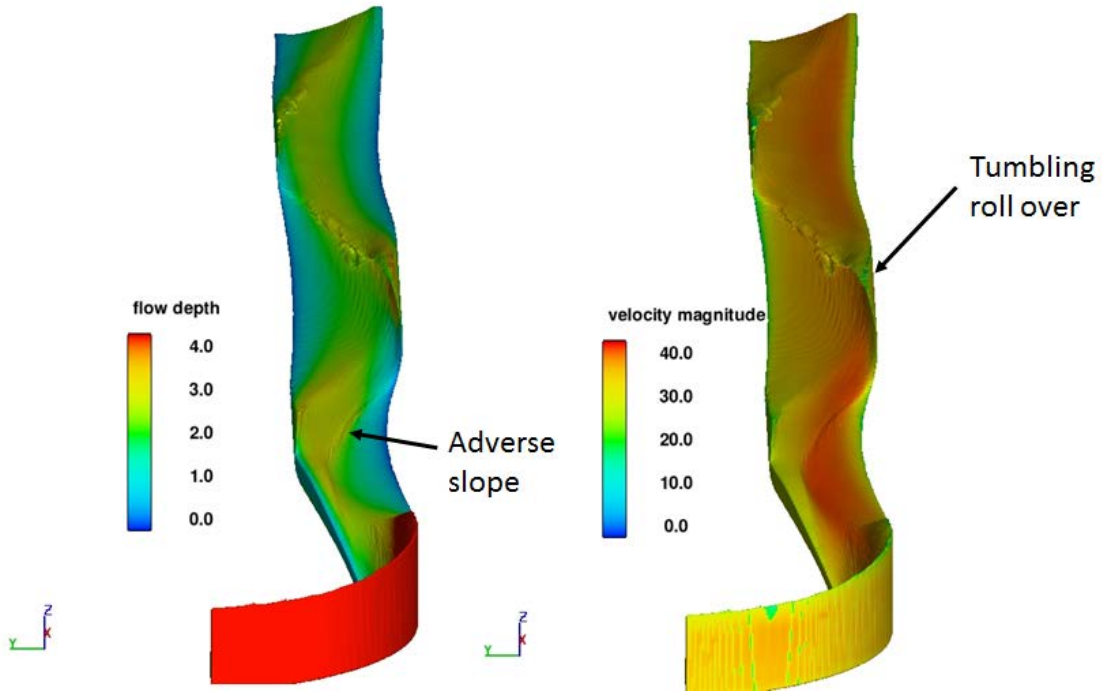

Figure C- 18. View of flow depths (left) and surface velocities (right) looking downstream at the transition flow in Configuration I. The helix chute ends shortly upstream of the red 4+ foot contour. FLOW-3D may not have displayed tumbling roll over from an adverse slope if the water fraction of those cells are below 50 percent water (highly aerated). The tumbling roll over appears to be similar to Configuration H

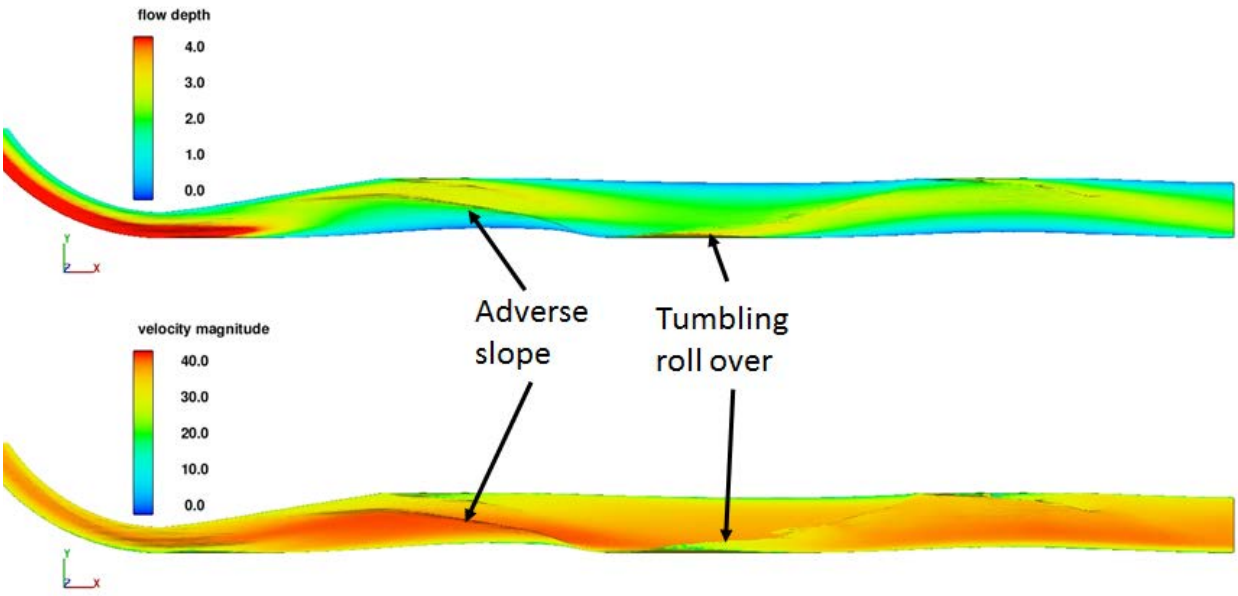

Figure C- 19. Looking down at flow depths (top) and surface velocities (bottom) for Configuration I. Flow is from left to right and the exit of the helix is at the left edge of the image.

Configuration J (Jan 6, 2015)

This configuration lengthened the transition used in Configuration I from 23 feet to 27.8 feet, and the slope was changed to horizontal (figure C-20).

Tumbling roll over was observed behind the first standing wave, and tumbling roll over of the second standing wave appeared about the same as Configuration I (figure C-21). Sloshing in the tunnel remained about the same as Configuration I (figure C-22).

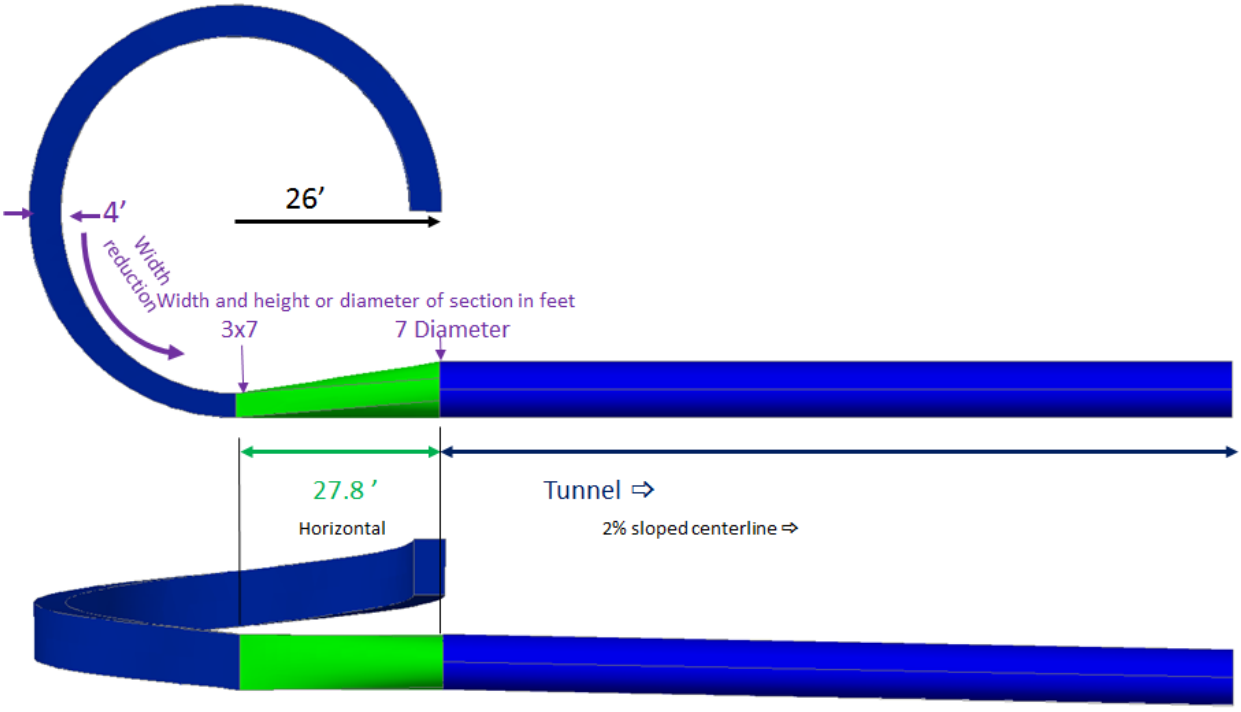

Figure C- 20. Design for Configuration J. For this configuration, the invert of the rectangular-to-round transition was made horizontal and lengthened to 27.8 feet.

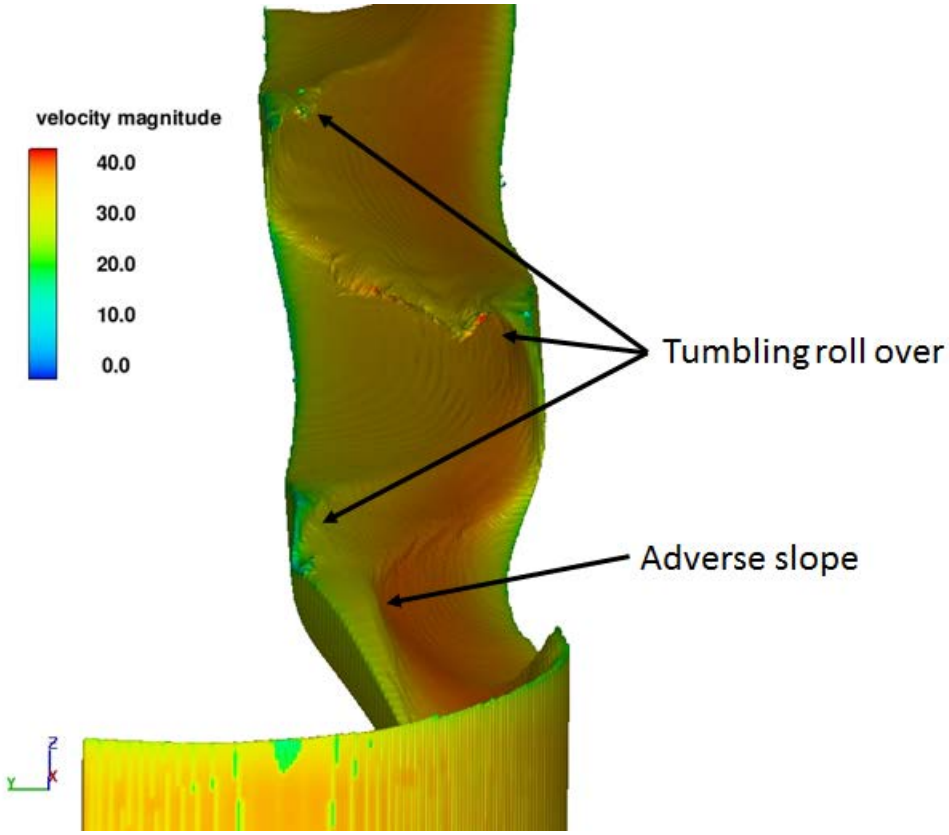

Figure C- 21. View of surface velocities looking downstream at the transition flow in Configuration J. FLOW-3D may not have displayed tumbling roll over from an adverse slope if the water fraction of those cells are below 50 percent water (highly aerated). The tumbling roll over appears to be similar to Configuration I.

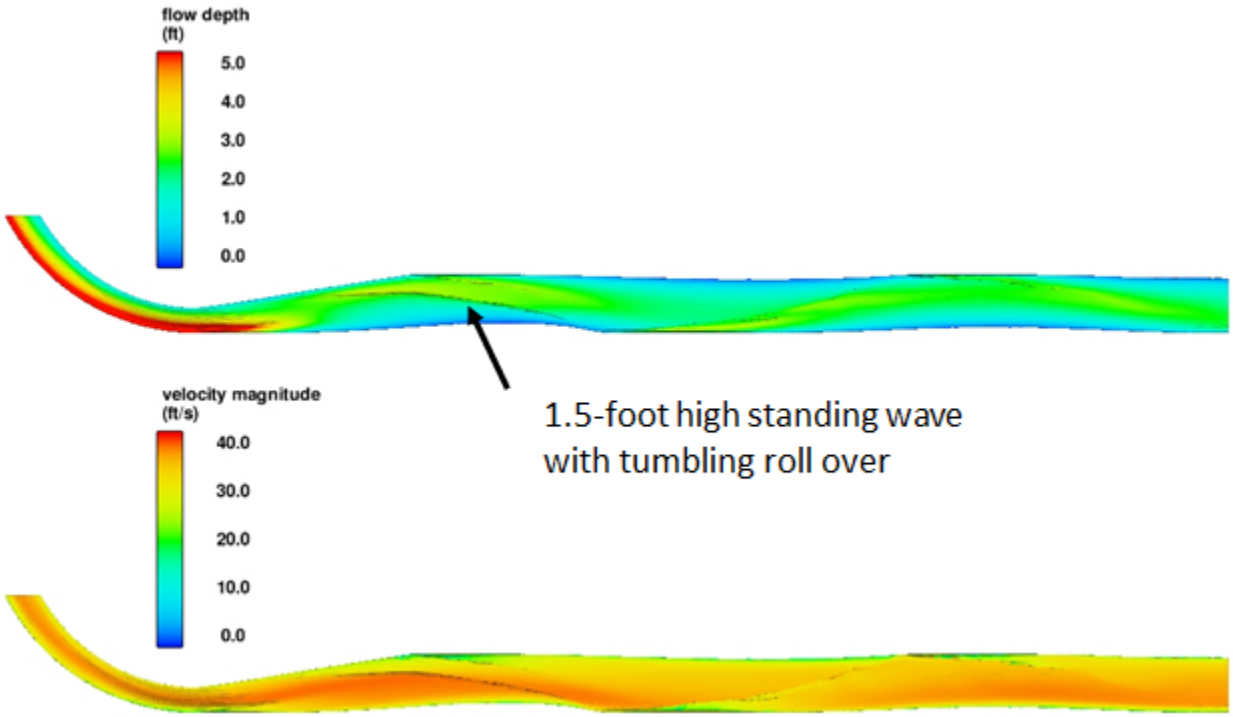

Figure C- 22. Flow depths and surface velocities for Configuration J. The flow may have tumbling roll over at the face of the standing wave since the depth of flow at the base of the wave is only 1 to 3 feet deep. Flow is from left to right and the exit of the helix is at the left edge of the image.

Configuration K (Jan 15, 2015)

Configuration K used a 23-foot long 4-foot x 7-foot rectangle to 6.5-foot x 5-foot rectangle section, then the conduit transitioned over the next 16 feet to the 7-foot diameter tunnel (figure C-23).

The initial standing wave was nearly vertical with some tumbling roll over behind it (figure C-24). The tumbling roll over of the second standing wave appears to be more severe. Sloshing in the tunnel also appeared to be worse (figure C-25).

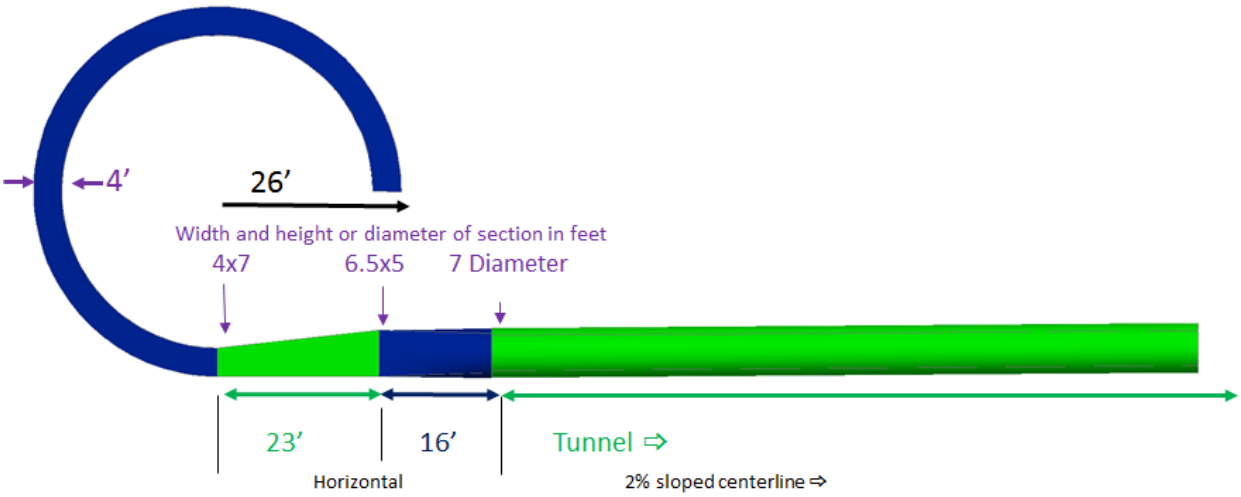

Figure C- 23. Design for Configuration K. The chute width remains 4 feet throughout the helix. The first section transitioned from 4x7 to 6.5 x 5 over 23 feet, while the second transition section remained the same

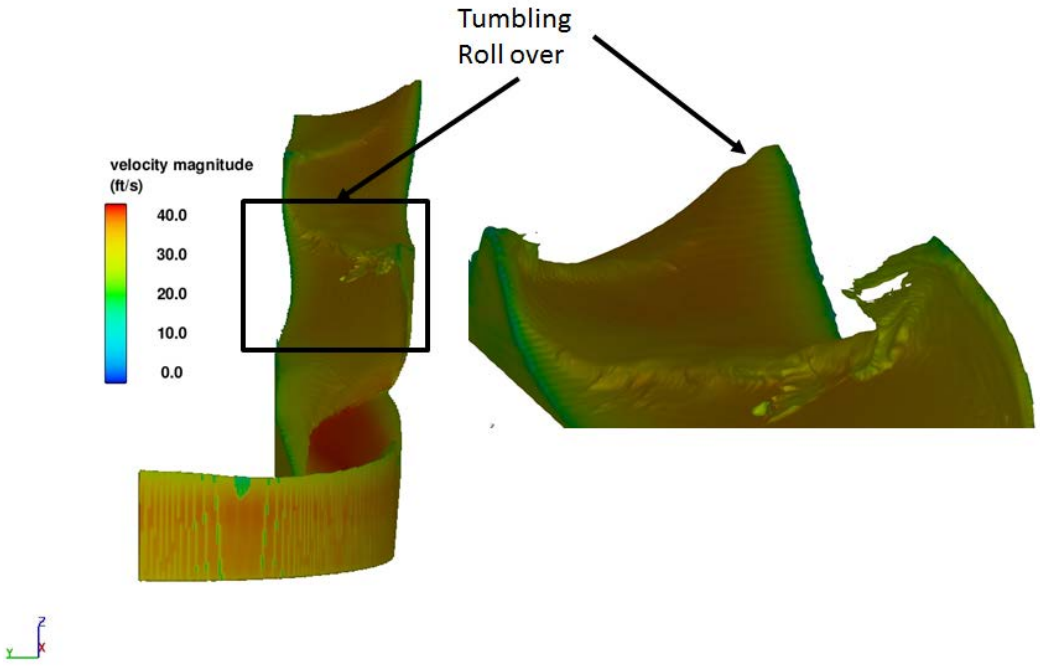

Figure C- 24. View of surface velocities looking downstream at the transition flow in Configuration K. FLOW-3D may not have displayed tumbling roll over from an adverse slope if the water fraction of those cells are below 50 percent water (highly aerated). The tumbling roll over appears to be worse than Configuration J.

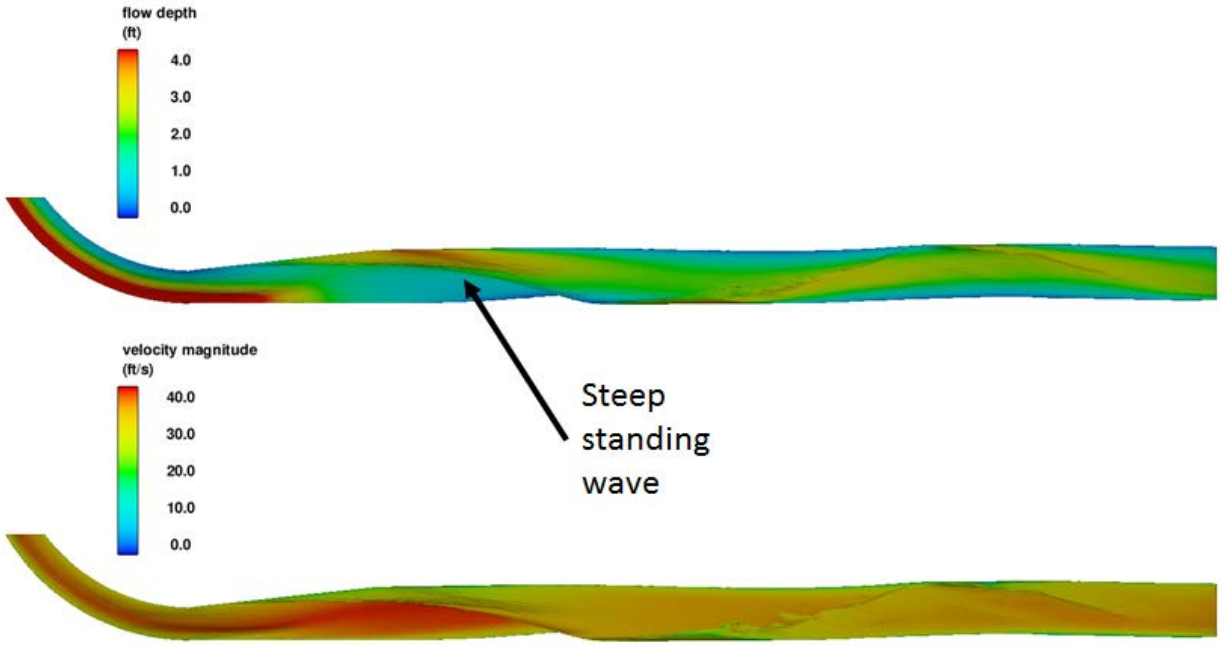

Figure C- 25. Looking down at flow depths (top) and surface velocities (bottom) for Configuration K. Flow is from left to right and the exit of the helix is at the left edge of the image.

Configuration L (Jan 16, 2015)

Configuration L was a combination of Configuration H and Configuration K. The helix chute was gradually reduced from 4 feet wide to 3 feet wide for the last quarter turn (figure C-26). The next 23-foot-long segment transitioned from 3 feet wide to 6.5 feet wide.

The initial standing wave had a favorable surface slope that did not overhang (figure C-27). Downstream velocities were more gradual than previous simulations (C-28). Sloshing in the tunnel still appeared to be excessive (C-29).

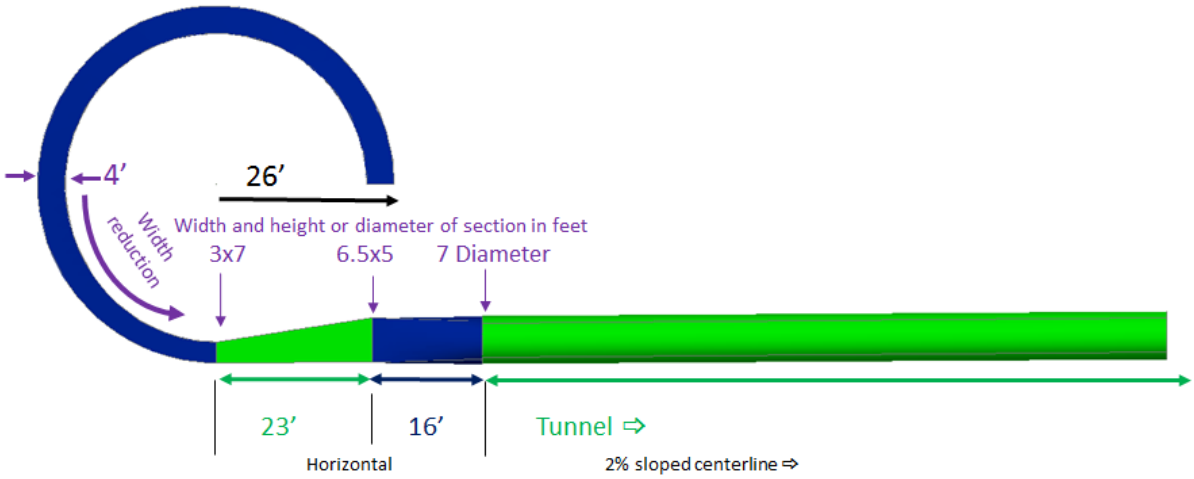

Figure C- 26. Design for Configuration L.

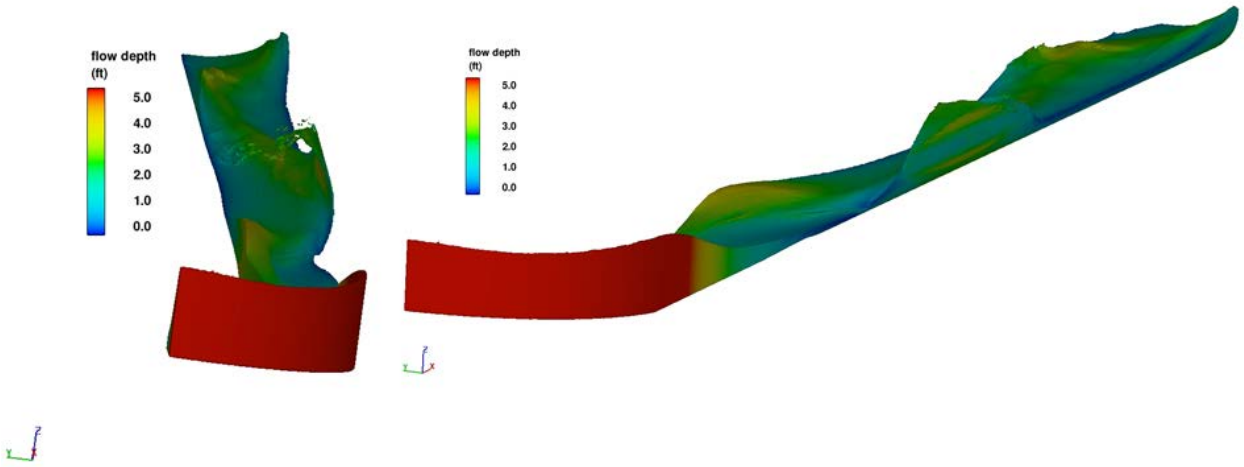

Figure C- 27. View of flow depths looking downstream at the transition flow in Configuration L. The helix chute ends shortly upstream from the downstream end of the red 4+ foot contour.

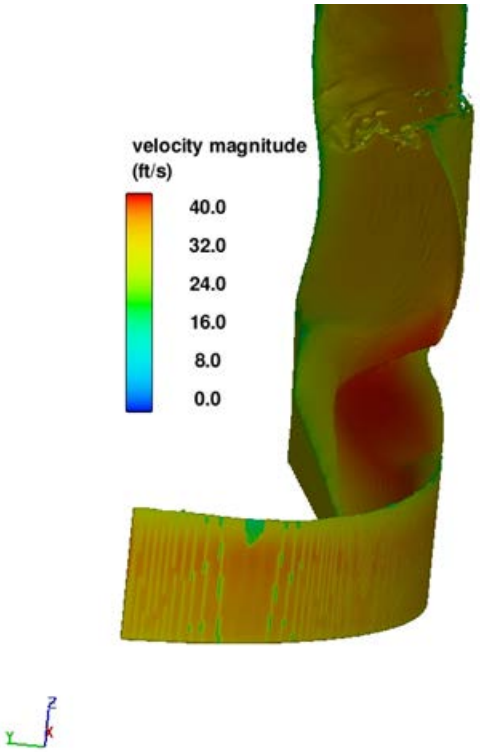

Figure C- 28. View of surface velocities looking downstream at the transition flow in Configuration L. FLOW-3D may not have displayed tumbling roll over from an adverse slope if the water fraction of those cells are below 50 percent water (highly aerated). The tumbling roll over appears to be thin but extreme.

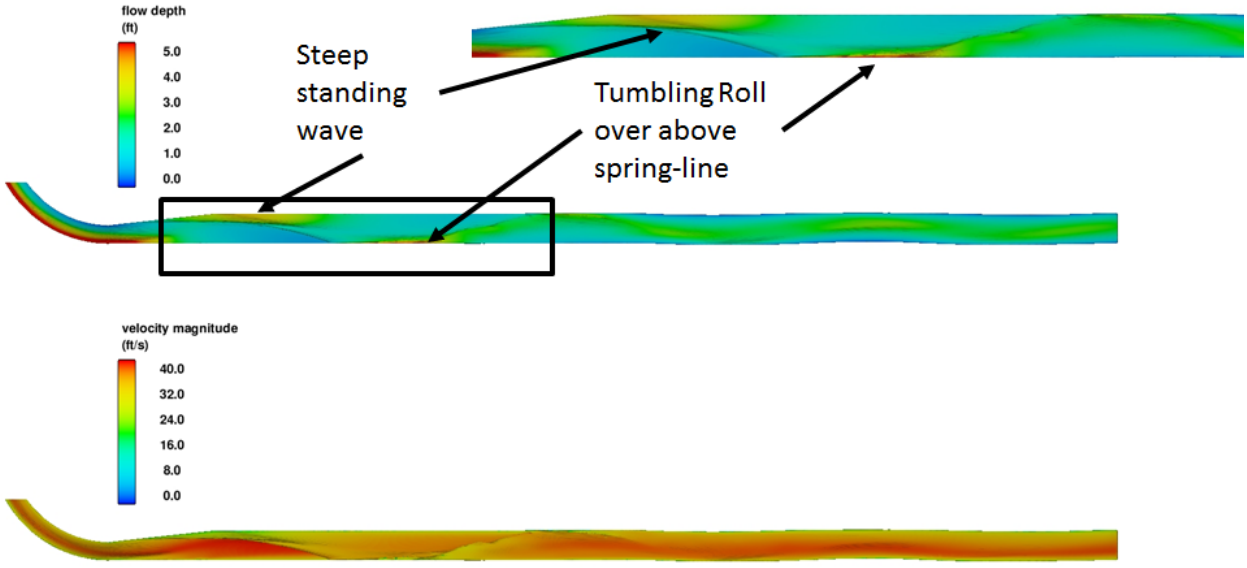

Figure C- 29. Looking down at flow depths (top) and surface velocities (bottom) for Configuration G. Flow is from left to right and the exit of the helix is at the left edge of the image.

Configuration M (Jan 23, 2015)

Configuration M was a modification of Configuration L, where a 50-foot-long 6.5-foot x 5-foot section began at the downstream end of the 23-foot long section. Then the 6.5-foot x 5-foot rectangle lofted into the 7’ diameter tunnel over the next 50 feet (figure C-30). Loft was the AutoCAD command used which created a solid from 2 or more cross section. When two cross sections are used as in this case, generally the resulting shape matches what will be constructed.

The slope of the first standing wave was greatly improved without tumbling roll over. However the second standing wave went to the top of the 5 foot tall conduit causing tumbling roll over to occur at that location (figure C-31). Velocities in the main body of flow approaching the first standing wave were within 10 ft/s of the surface velocities on the standing wave (figures C-32 and C-33).

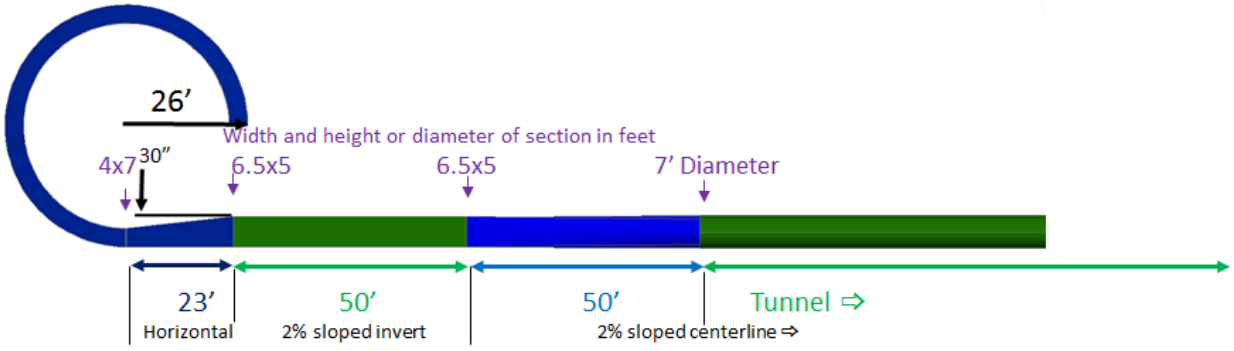

Figure C- 30. Design for Configuration M. This configuration attempted to stretch out the transition to minimize standing waves and tumbling roll over.

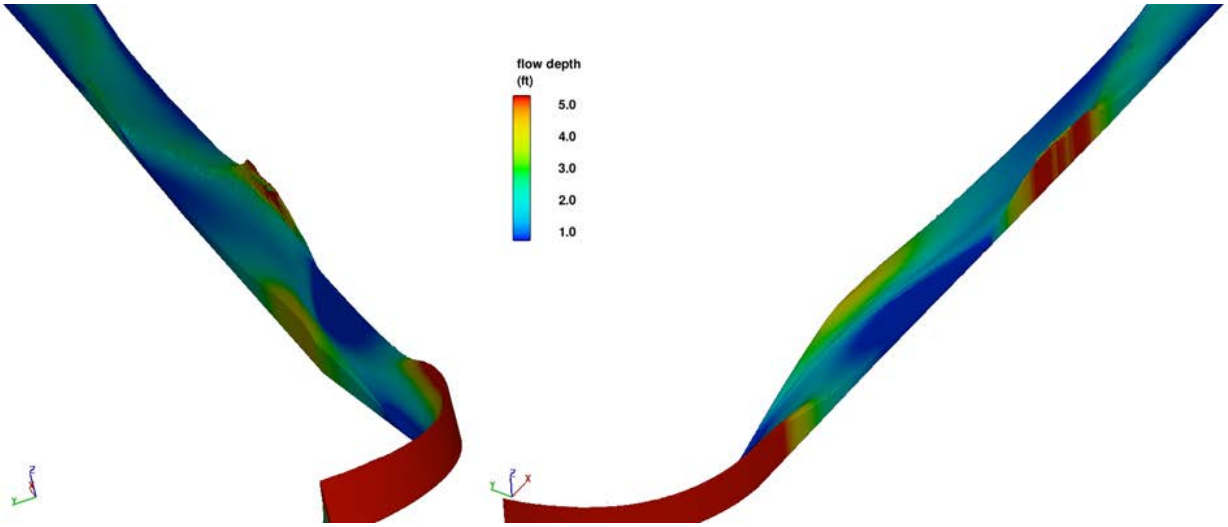

Figure C- 31. View of flow depths looking downstream at the transition flow in Configuration M. The helix chute ends shortly upstream of the red 4+ foot contour. The

tumbling roll over appears to be caused by flow sloshing up to the top of the 5 foot tall conduit.

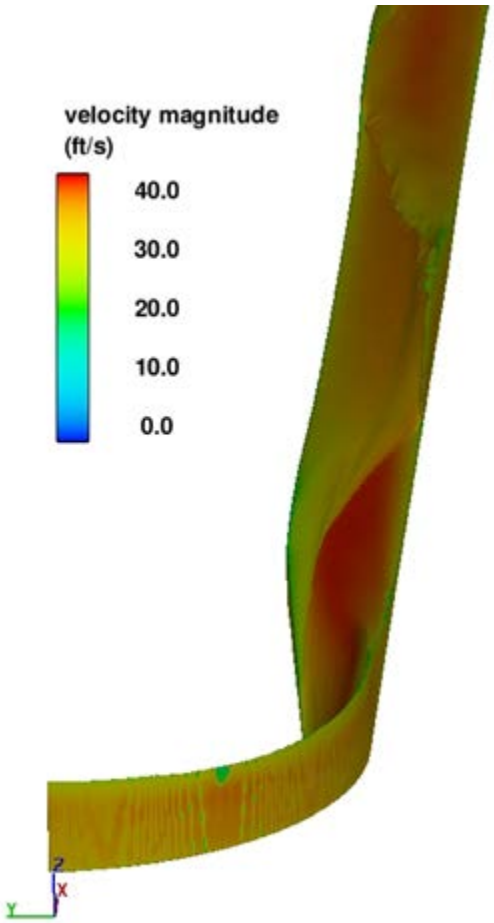

Figure C- 32. View of surface velocities downstream at the transition flow in Configuration M.

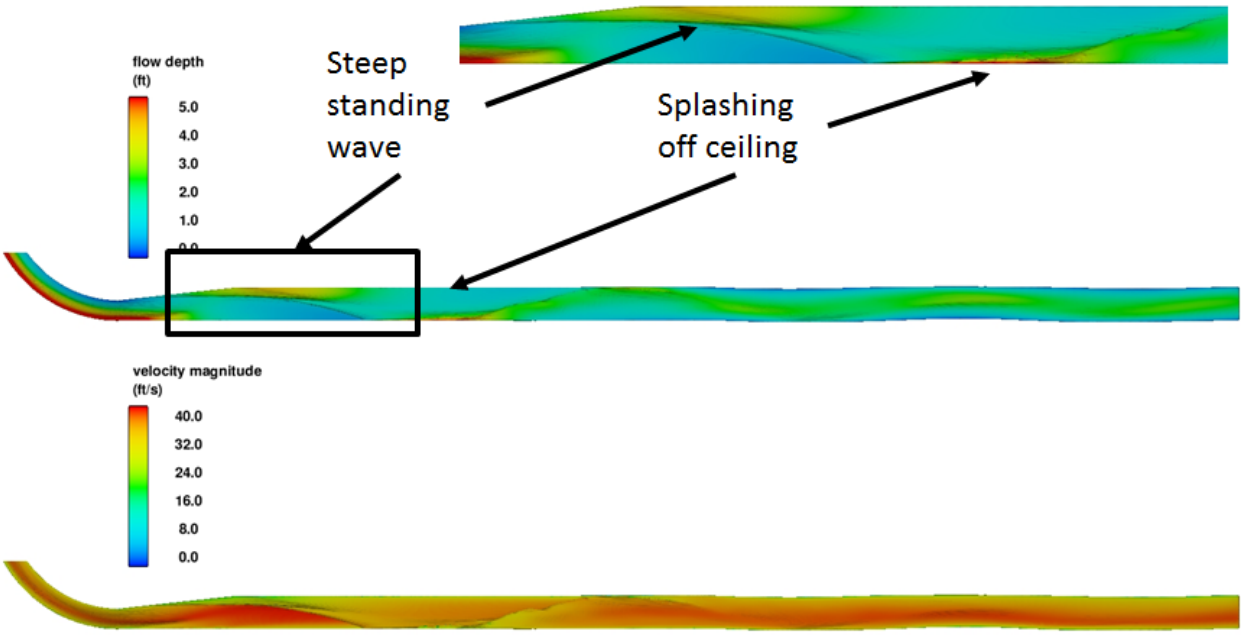

Figure C- 33. Looking down at flow depths (top) and surface velocities (bottom) for Configuration M. Flow is from left to right and the exit of the helix is at the left edge of the image.

Configuration N (Jan 24, 2015)

Configuration N used three 10-foot sections to create a piecewise "S" curve that replaced the 23-foot section used in Configuration M. This was an attempt to reduce the slope of the first standing wave and to spread out the reflection causing the second standing wave (figure C-34).

The piecewise "S" curve appeared to spread out the first standing wave more than Configuration M, reducing splashing off the top of the conduit and also slightly reducing tumbling roll over (figure C-35). Sloshing in the tunnel is also slightly reduced (figures C-36 and C-37).

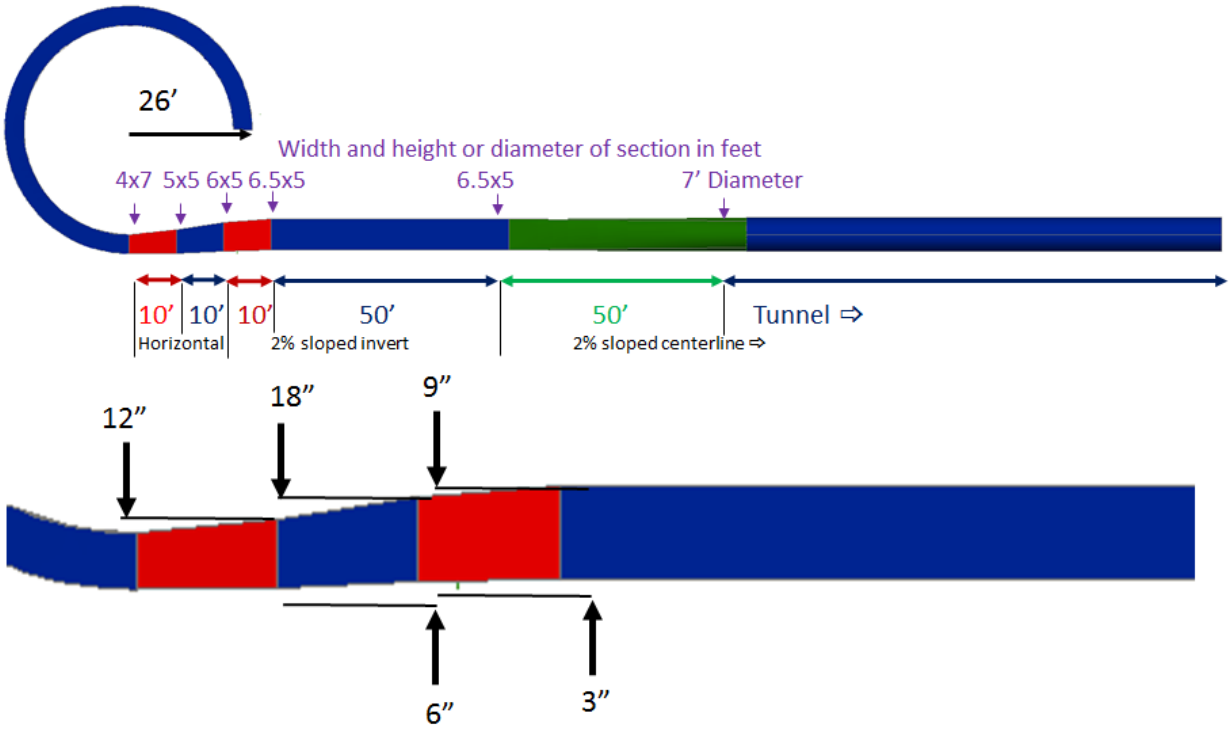

Figure C- 34. Design for Configuration N. Several breaks produce a piecewise "S" curve. The left side expansion of 12 inches was designed to dampen the cross sectional rotational flow from the helix. The next 18-inch offset was designed to dampen much of the sloshing, while the last 9 inch expansion provides more continuous levels of resistance to sloshing (due to water height).

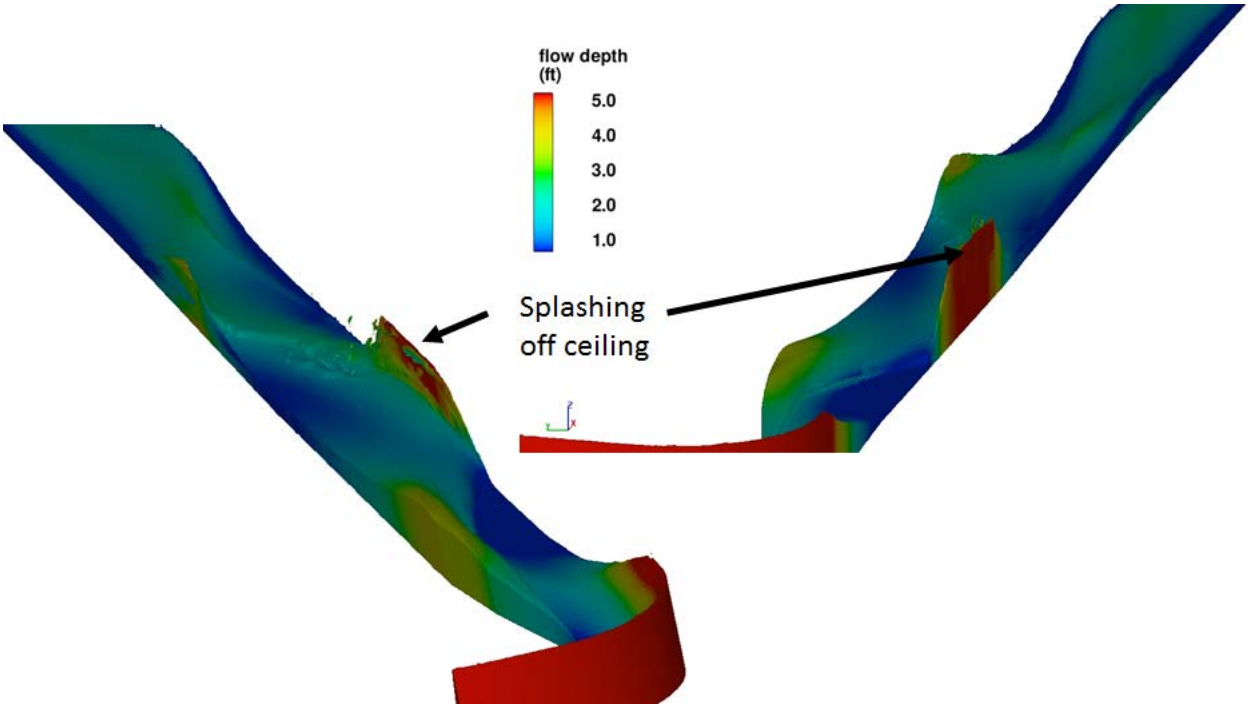

Figure C- 35. View of flow depths looking downstream at the transition flow in Configuration N. The helix chute ends shortly upstream of the red 4+ foot contour.

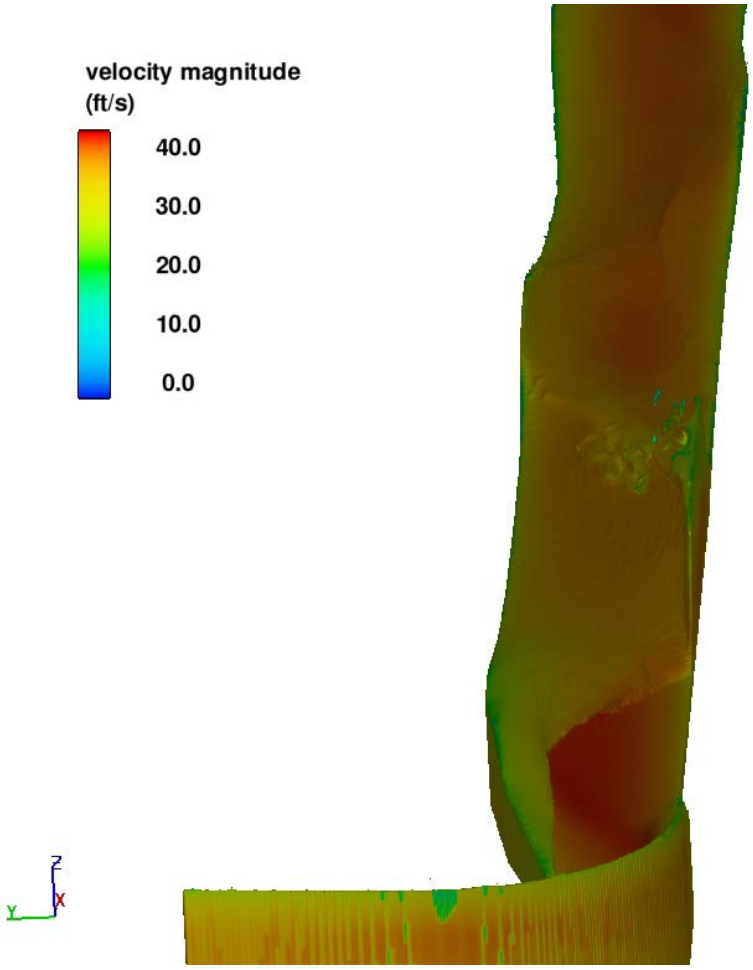

Figure C- 36. View of surface velocities looking downstream at the transition flow in Configuration N.

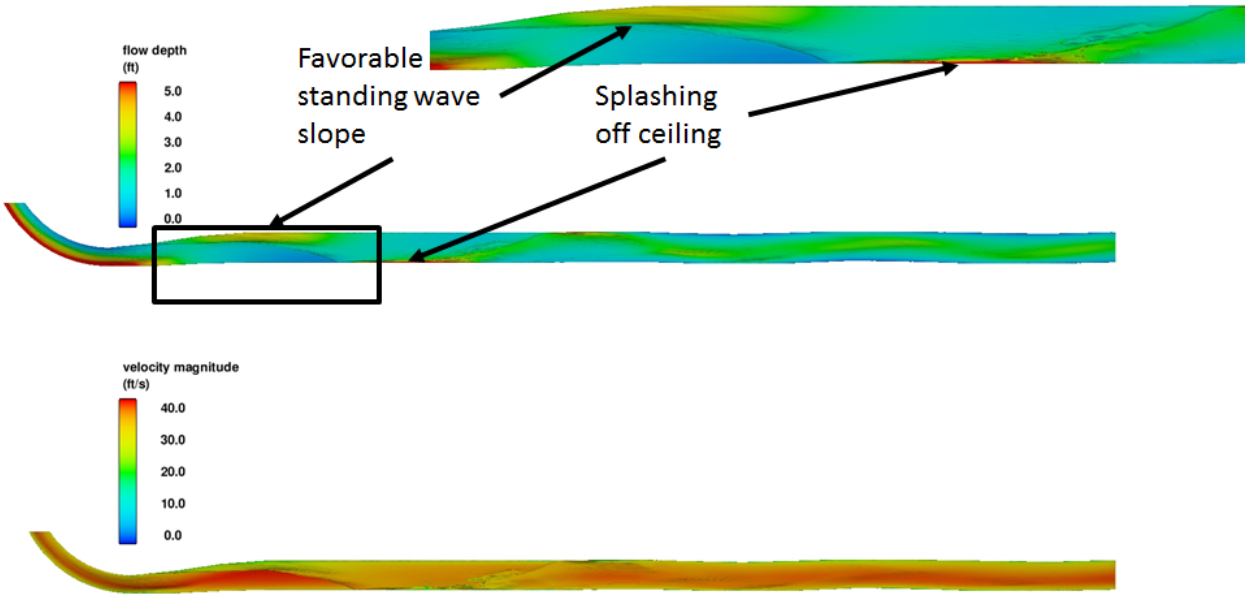

Figure C- 37. Looking down at flow depths (top) and surface velocities (bottom) for Configuration N. Flow is from left to right and the exit of the helix is at the left edge of the image.

Configuration O (Jan 30, 2015)

For Configuration O, an ellipse-shaped guide wall was added to Configuration N (figure C-38). The size and placement of the ellipse was chosen based on the area needed to fill in the shallow-depth zone shown in.

Slight tumbling rollover was observed near the upstream end of the elliptical guide wall (figure C-39). The second standing wave extended 4-feet high and was centered in the channel near the end of the elliptical guide wall. Figure C-40 displays downward vertical velocities up to 8 ft/s in the tumbling rollover of the second standing wave. Surface flow velocities still appear to be acceptable (figures C-41 and C-42).

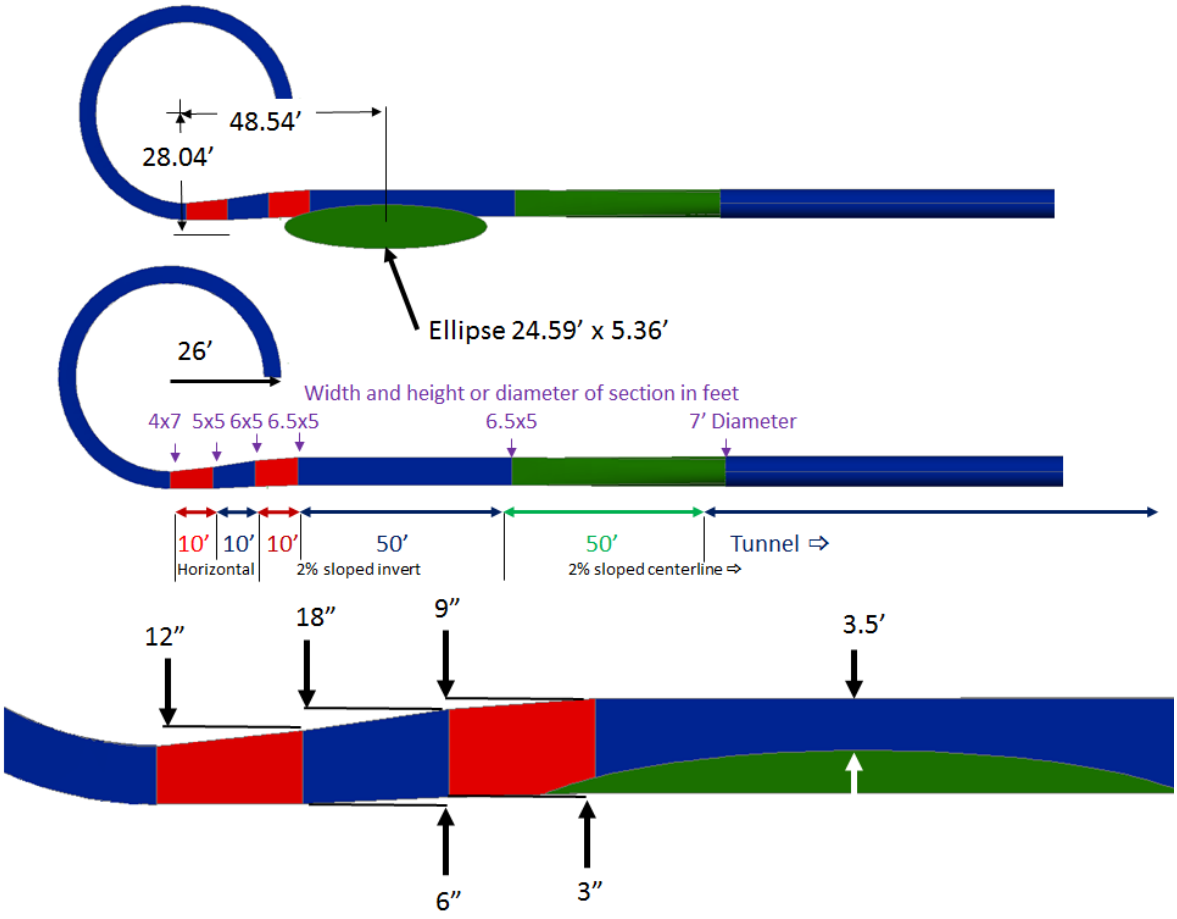

Figure C- 38. Configuration O. This configuration included an ellipse (shown in green) that was positioned to fill in the shallow flow depth area produced with Configuration N.

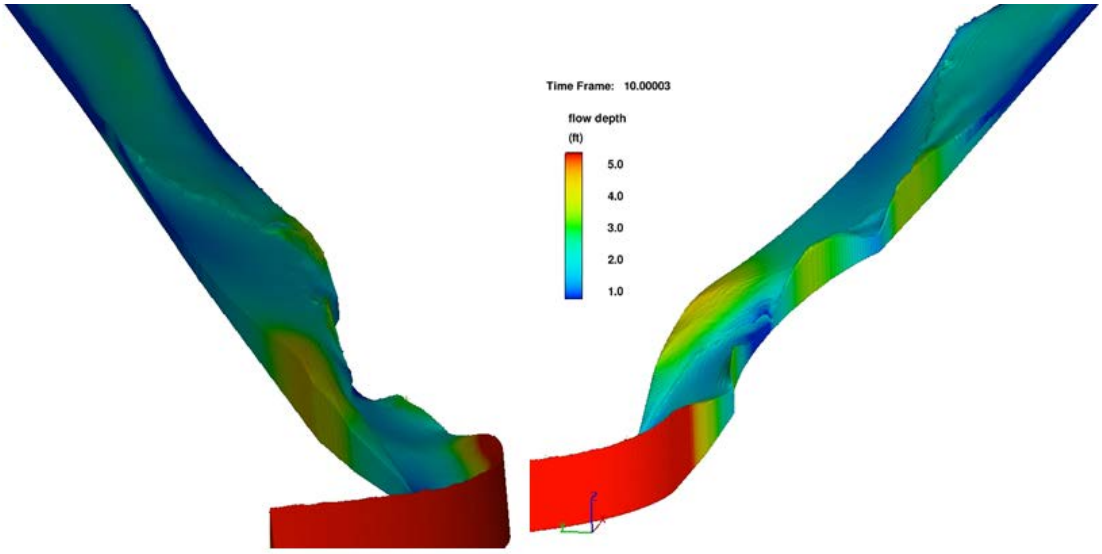

Figure C- 39. View of flow depths looking downstream at the transition flow in Configuration O. The helix chute ends shortly upstream of the downstream end of the red 4+ foot contour.

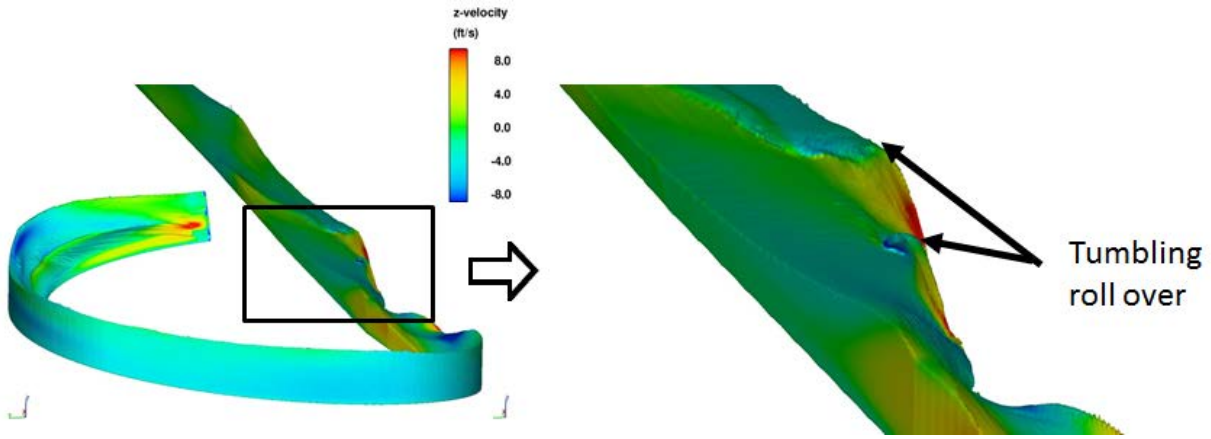

Figure C- 40. View of vertical velocities looking downstream at the transition flow in Configuration O. The helix chute ends shortly upstream of the red 4+ foot contour. Tumbling rollover appears to be slightly improved compared with Configuration N.

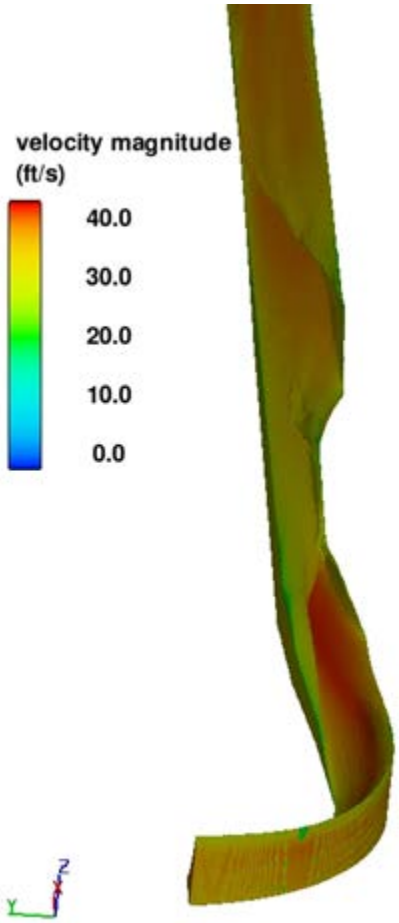

Figure C- 41. View of surface velocities looking downstream at the transition flow depths in Configuration O.

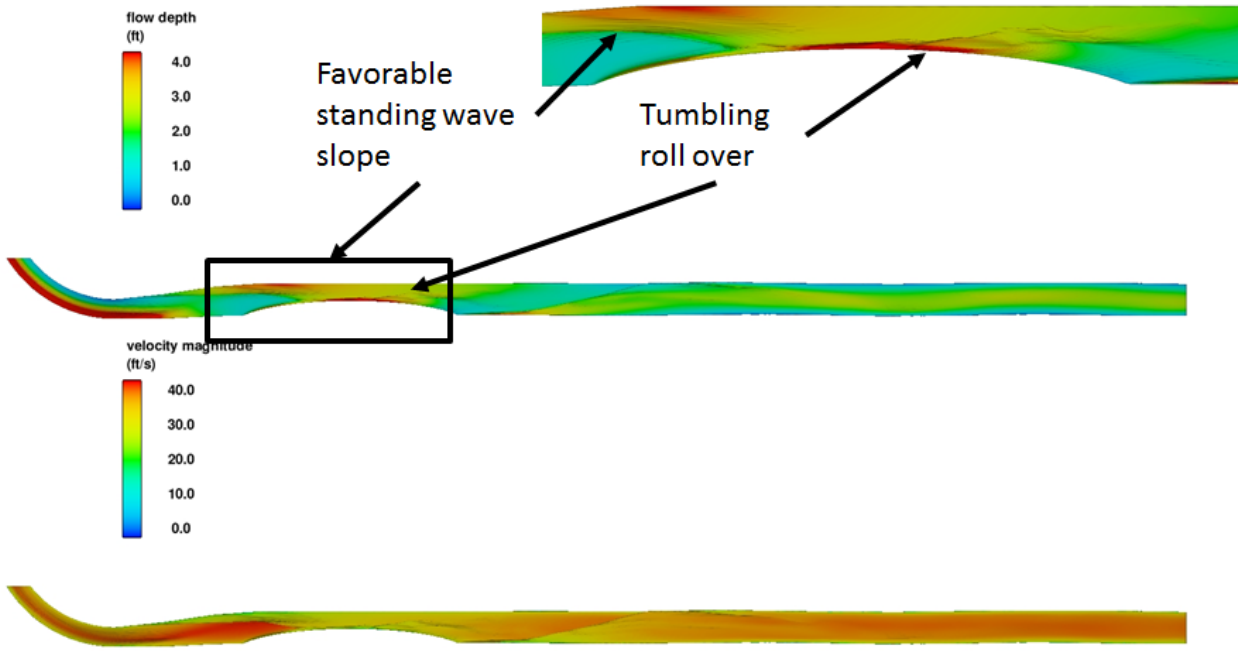

Figure C- 42. View of flow depths (top) and surface velocities (bottom) looking downstream at the transition flow in Configuration O. The helix chute ends shortly upstream of the red 4+ foot contour. The initial standing wave appears favorable. Flow is from left to right and the exit of the helix is at the left edge of the image.

Configuration P (Feb 2, 2015)

For Configuration P, Configuration O was adjusted by moving the ellipse upstream about 6 feet (figure C-43). The ellipse was moved to the right by 6 inches to widen the narrowest part of the conduit to 4 feet. The size of the ellipse was lengthened by a foot. The concept driving these changes was to fill in the shallow areas of Configuration O and to have the first standing wave meet the downstream portion of the elliptical guide wall, to reduce the resistance that causes tumbling rollover.

The initial standing wave appeared to have a favorable slope that was not likely to indicate tumbling roll over (figure C-44). However, some tumbling roll over was shown a few feet downstream from the center of the ellipse. In addition, tumbling roll over was observed a few feet downstream from the ellipse-shaped guide wall (figure C-45).

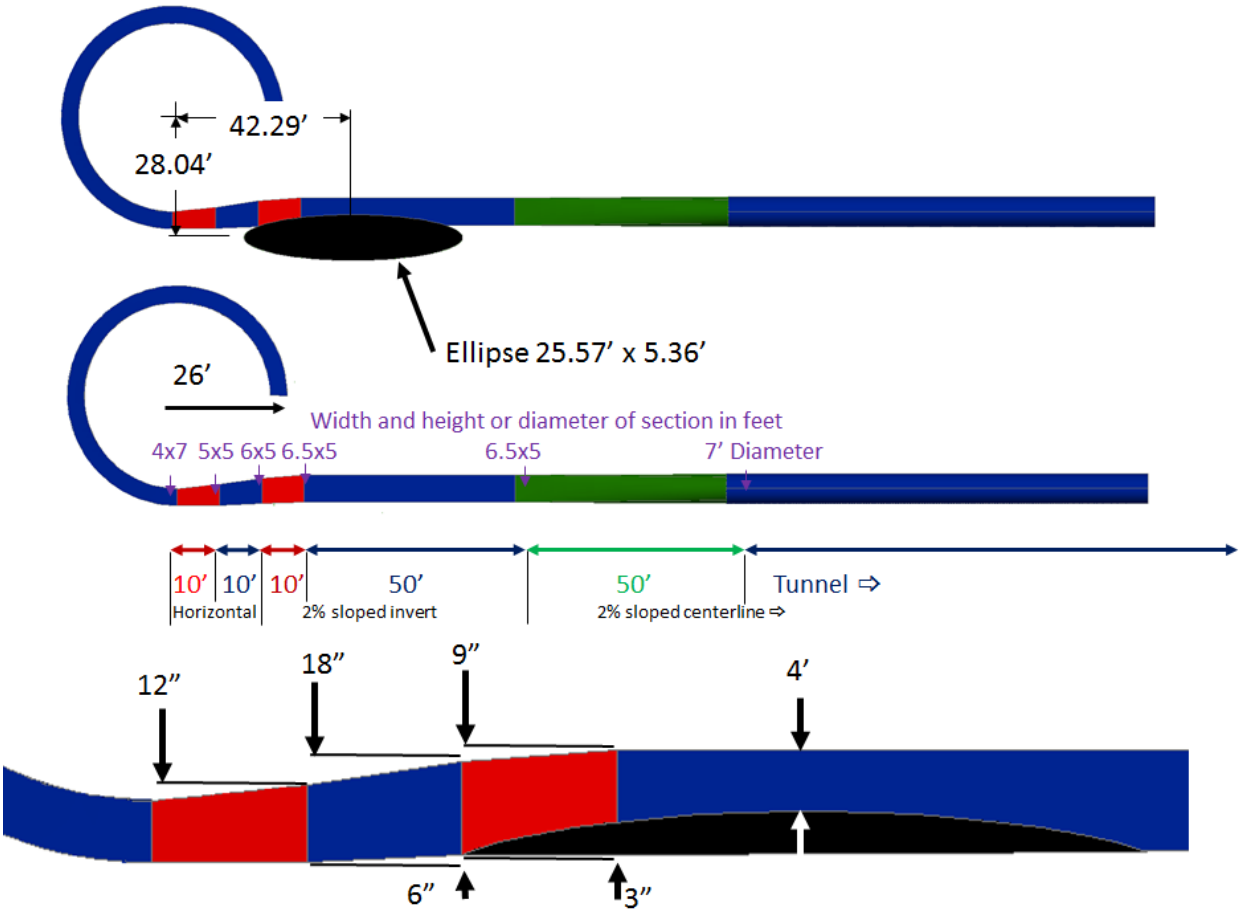

Figure C- 43. Design for Configuration P. The ellipse-shaped guide wall used in Configuration O was moved upstream about 6 feet.

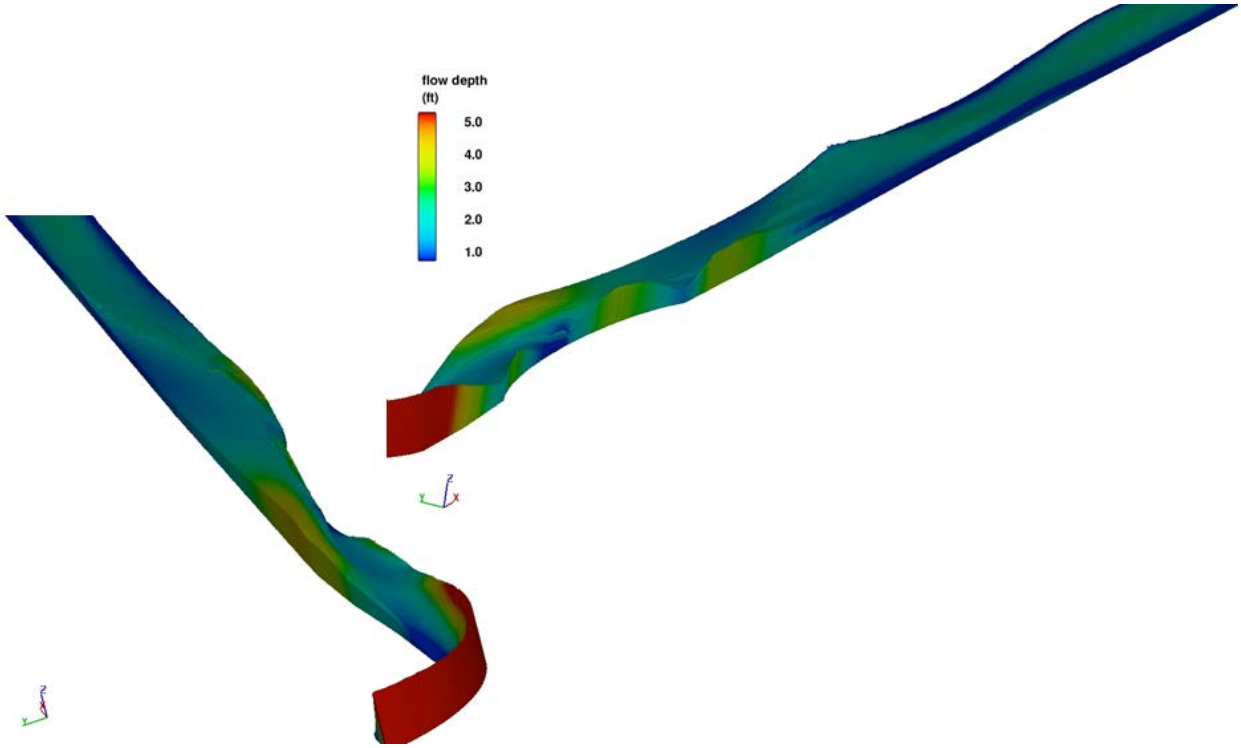

Figure C- 44. Flow depths for Configuration P.

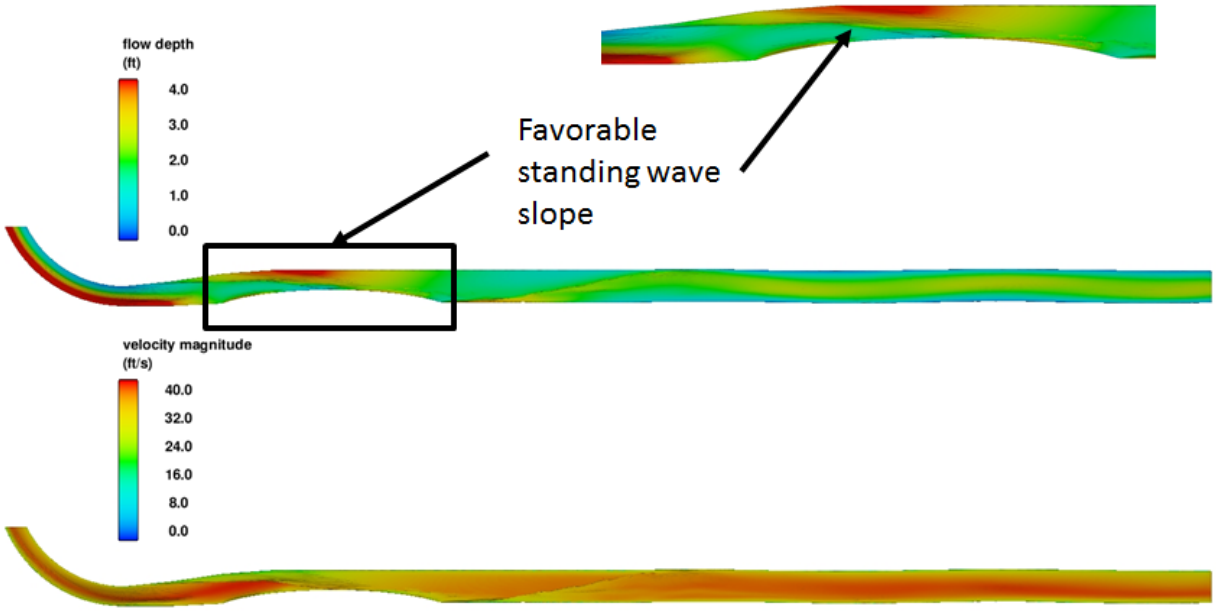

Figure C- 45. Flow depths (top) and surface velocities (bottom) for Configuration P. Flow is from left to right and the exit of the helix is at the left edge of the image.

Configuration Q- Recommended (Feb 6, 2015)

For Configuration Q, Configuration P was modified by adding a straight guide wall on the downstream side of the ellipse to stabilize flow depths along the right wall.

This simulation demonstrated the best flow conditions of all helix to tunnel configurations that were investigated and became the final recommended configuration. Further explanation and a description of this configuration are included in the main body of this report.